



686
2015

Berichte

zur Polar- und Meeresforschung

Reports on Polar and Marine Research

Russian-German Cooperation CARBOPERM: Field campaigns to Bol'shoy Lyakhovsky Island in 2014

Edited by

Georg Schwamborn and Sebastian Wetterich

with contributions of the participants

Die Berichte zur Polar- und Meeresforschung werden vom Alfred-Wegener-Institut, Helmholtz-Zentrum für Polar- und Meeresforschung (AWI) in Bremerhaven, Deutschland, in Fortsetzung der vormaligen Berichte zur Polarforschung herausgegeben. Sie erscheinen in unregelmäßiger Abfolge.

Die Berichte zur Polar- und Meeresforschung enthalten Darstellungen und Ergebnisse der vom AWI selbst oder mit seiner Unterstützung durchgeführten Forschungsarbeiten in den Polargebieten und in den Meeren.

Die Publikationen umfassen Expeditionsberichte der vom AWI betriebenen Schiffe, Flugzeuge und Stationen, Forschungsergebnisse (inkl. Dissertationen) des Instituts und des Archivs für deutsche Polarforschung, sowie Abstracts und Proceedings von nationalen und internationalen Tagungen und Workshops des AWI.

Die Beiträge geben nicht notwendigerweise die Auffassung des AWI wider.

Herausgeber

Dr. Horst Bornemann

Redaktionelle Bearbeitung und Layout

Birgit Chiaventone

Alfred-Wegener-Institut
Helmholtz-Zentrum für Polar- und Meeresforschung
Am Handeshafen 12
27570 Bremerhaven
Germany

www.awi.de

www.reports.awi.de

Der Erstautor bzw. herausgebende Autor eines Bandes der Berichte zur Polar- und Meeresforschung versichert, dass er über alle Rechte am Werk verfügt und überträgt sämtliche Rechte auch im Namen seiner Koautoren an das AWI. Ein einfaches Nutzungsrecht verbleibt, wenn nicht anders angegeben, beim Autor (bei den Autoren). Das AWI beansprucht die Publikation der eingereichten Manuskripte über sein Repositorium ePIC (electronic Publication Information Center, s. Innenseite am Rückdeckel) mit optionalem print-on-demand.

The Reports on Polar and Marine Research are issued by the Alfred Wegener Institute, Helmholtz Centre for Polar and Marine Research (AWI) in Bremerhaven, Germany, succeeding the former Reports on Polar Research. They are published at irregular intervals.

The Reports on Polar and Marine Research contain presentations and results of research activities in polar regions and in the seas either carried out by the AWI or with its support.

Publications comprise expedition reports of the ships, aircrafts, and stations operated by the AWI, research results (incl. dissertations) of the Institute and the Archiv für deutsche Polarforschung, as well as abstracts and proceedings of national and international conferences and workshops of the AWI.

The papers contained in the Reports do not necessarily reflect the opinion of the AWI.

Editor

Dr. Horst Bornemann

Editorial editing and layout

Birgit Chiaventone

Alfred-Wegener-Institut
Helmholtz-Zentrum für Polar- und Meeresforschung
Am Handeshafen 12
27570 Bremerhaven
Germany

www.awi.de

www.reports.awi.de

The first or editing author of an issue of Reports on Polar and Marine Research ensures that he possesses all rights of the opus, and transfers all rights to the AWI, including those associated with the co-authors. The non-exclusive right of use (einfaches Nutzungsrecht) remains with the author unless stated otherwise. The AWI reserves the right to publish the submitted articles in its repository ePIC (electronic Publication Information Center, see inside page of verso) with the option to "print-on-demand".

Titel: Eisreiche Permafrostböden auf Bol'shoy Lyakhovsky in Nordsibirien (Foto von Georg Schwamborn, Alfred-Wegener-Institut, 31. Juli 2014).

Cover: Ice-rich permafrost soil on Bol'shoy Lyakhovsky, Northern Siberia (picture taken by Georg Schwamborn, Alfred Wegener Institute, 31st of July 2014).

Russian-German Cooperation CARBOPERM: Field campaigns to Bol'shoy Lyakhovsky Island in 2014

Edited by

Georg Schwamborn and Sebastian Wetterich

with contributions of the participants

Please cite or link this publication using the identifiers

hdl:10013/epic.44997 or <http://hdl.handle.net/10013/epic.44997> and

doi:10.2312/BzPM_0686_2015 or http://doi.org/10.2312/BzPM_0686_2015

ISSN 1866-3192

Field campaigns to Bol'shoy Lyakhovsky Island in 2014

31 March – 29 April 2014
23 July – 26 August 2014

Lena River Delta and Bol'shoy Lyakhovsky Island



Chief Scientists

Georg Schwamborn and Sebastian Wetterich

Coordinators

Eva-Maria Pfeiffer and Hans-Wolfgang Hubberten

CONTENTS

FOREWORD	3
1 BACKGROUND AND OBJECTIVES	5
2 LOGISTICS AND ITINERARY	8
3 PERMAFROST DRILLING ON BOL'SHOY LYAKHOVSKY	11
3.1 Core L14-02 (Yedoma)	15
3.2 Core L14-03 (thermo terrace)	16
3.3 Core L14-04 (incl. Eemian deposits)	17
3.4 Core L14-05 (Alas deposits)	18
4 PERMAFROST EXPOSURES OF BOL'SHOY LYAKHOVSKY	20
4.1 Introduction	20
4.2 Bedrock and mineralogical studies	21
4.3 Pre-Quaternary	22
4.4 Yukagir Ice Complex	23
4.5 Yukagir Ice Complex to Kuchchugui	24
4.6 Kuchchugui Suite to Molotkov (Yedoma) Ice Complex	26
4.7 Krest Yuryakh (Eemian) deposits	27
4.8 Molotkov (Yedoma) Ice Complex on the thermo terrace	29
4.9 Molotkov (Yedoma) Ice Complex on the thermo terrace (2)	30
4.10 Molotkov (Yedoma) Ice Complex on the thermo terrace (3)	31
4.11 Sartan Ice Complex	32
4.12 Holocene Alas	34
4.13 Modern floodplain of the Zimov'e River	35
5 SOIL ORGANIC MATTER STUDIES ON BOL'SHOY LYAKHOVSKY	37
5.1 Introduction	37
5.2 Yedoma	39
5.3 Thermo-erosional valley / Log deposits	39
5.4 Thermo terrace	40
5.5 Alas	41
5.6 Modern floodplain deposits of the Zimov'e River	43
5.7 Summary	44
6 TACHYMETRY AND KITE AERIAL PHOTOGRAPHY	45
6.1 Tachymetry	45
6.2 Kite aerial photography	46
7 NEAR SURFACE GEOPHYSICS	48
7.1 Employed geophysical techniques	48
7.2 Zimov'e River mouth	51
7.3 Thermo terrace	53
7.4 Yedoma	55
7.5 Thermo-erosional valley	59
7.6 Alas	61

8 REFERENCES	64
APPENDIX	66
Appendix 3-1 to 3-6; drill and log protocols	66
Appendix 4-1; exposure samples	82
Appendix 5-1; soil organic matter samples	90
Appendix 7-1 to 7-5; geophysical datasets	96

FOREWORD

Georg Schwamborn

The German-Russian project CARBOPERM – *Carbon in Permafrost, origin, quality, quantity, and degradation and microbial turnover* - is devoted to studying soil organic matter history, degradation and turnover in coastal lowlands of Northern Siberia. The multidisciplinary project combines research from various German and Russian institutions and runs from 2013 to 2016. The project aims assessing the recent and the ancient trace gas budget over tundra soils in northern Siberia. Studied field sites are placed in the permafrost of the Lena Delta and on Bol'shoy Lyakhovsky, the southernmost island of the New Siberian Archipelago in the eastern Laptev Sea.

Next to the coordination (WP1) the scientific work packages include studies on the origin, properties, and dynamics of fossil carbon (WP2), the age and quality of organic matter (WP3), the modern carbon dynamics in permafrost landscapes (WP4), the microbial transformation of organic carbon in permafrost (WP5), and process-driven modelling of soil carbon dynamics in permafrost areas (WP6). The affiliated institutes from Germany and Russia are listed below and via <http://www.carboperm.net>.

Alfred Wegener Institute, Helmholtz Centre for Polar and Marine Research,
Potsdam and Bremerhaven

Arctic and Antarctic Research Institute, St. Petersburg

GFZ German Research Centre for Geosciences, Helmholtz Centre Potsdam

Lomonosov Moscow State University

Max Planck Institute for Biogeochemistry, Jena

Max Planck Institute for Meteorology, Hamburg

Melnikov Permafrost Institute, Yakutsk

Obukhov Institute of Atmospheric Physics, Moscow

Otto Schmidt Laboratory, St. Petersburg

Sukachev Forest Institute, Krasnojarsk

University of Cologne

University of Hamburg

University of Potsdam

Acknowledgements

The CARBOPERM project is part of the bilateral WTZ (Wissenschaftlich-technische Zusammenarbeit) between Germany and Russia. BMBF (German Ministry for Science and Education) is granting the project (grant no. 03G0836B). The support is greatly acknowledged.

We want to highlight the long-standing and delightful cooperation with the Hydrobase, Tiksi, from Roshydromet, Russia. Particular thanks go to Dmitry Melnichenko, head of the Hydrobase, for his welcoming way and his unfailing local organisation. Colleagues from AARI in St. Petersburg, especially Dmitry Bolshiyarov and Alexander Makarov, covered the permission procedures in the usual reliable way. We thank all of them, and in addition Waldemar Schneider from AWI, for their continuous support.

1 BACKGROUND AND OBJECTIVES

Georg Schwamborn

Bol'shoy Lyakhovsky is the most southern island of the New Siberian Archipelago lying between the Laptev and the East Siberian Seas. It is largely composed of unconsolidated frozen deposits (Figure 1-1), which accumulated during two cold to warm climate periods in the mid to late Quaternary (Andreev et al. 2004, 2009; Wetterich et al. 2009, 2014). Following the palaeoenvironmental and palaeoclimate reconstructions in these studies the area has been identified useful for tracing biogeochemical changes across various climatic and environmental changes. Understanding cycling and recycling of soil organic matter in northern high latitudes underlain by permafrost is one of the key objectives of CARBOPERM. Studying the sediment record from Bol'shoy Lyakhovsky will allow assessing natural degradation processes during a warmer period in the past (i.e. the Eemian) in order to assess possible future degradation processes in an anticipated warmer Arctic.

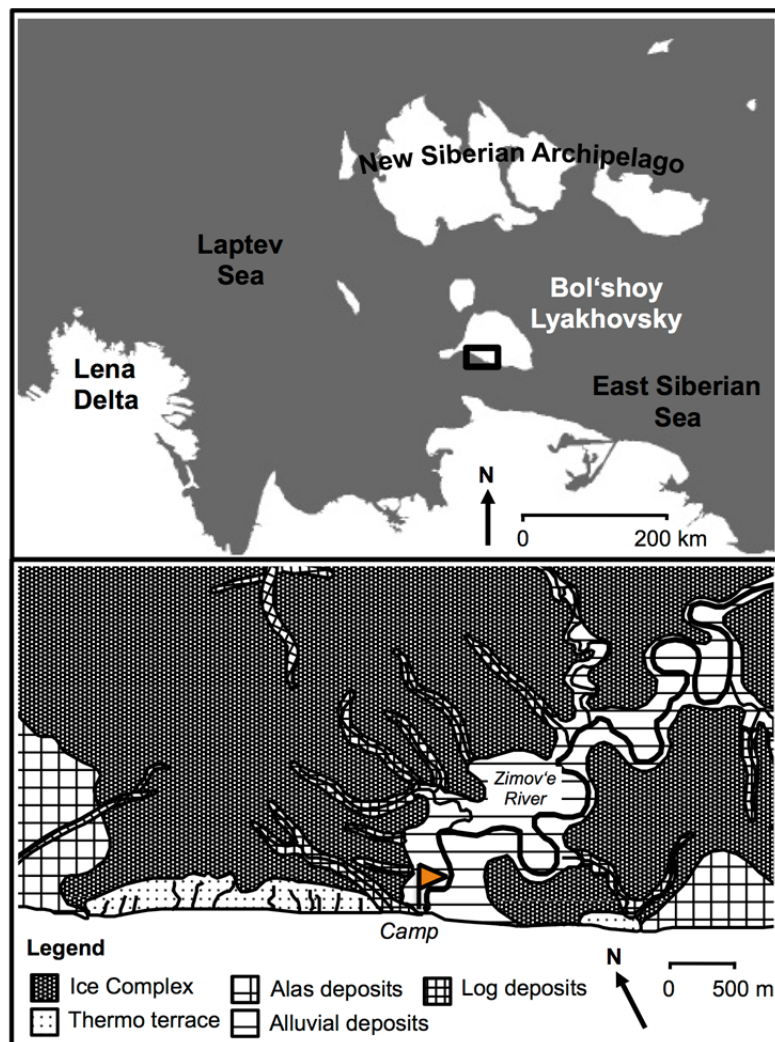


Figure 1-1 Top: Location of Bol'shoy Lyakhovsky in NE Siberia and the study area in the south of the island (black box). Bottom: Scheme of the study area west of Zimov'e River and the main geomorphological units (map modified from H. Meyer and A. Dereviagin, 1999).

Analytical work on past changes of microbial communities, biomarkers and biogeochemical tracers (e.g. ^{14}C) demand recovering drill cores that guarantee sterile material for subsequent analyses in the laboratory. Sites for permafrost coring and manual sampling have been identified based on published papers and field knowledge (Figure 1-2). They are placed in Quaternary strata that stretch along the southern shore and have ages from the Holocene back to pre-Eemian times (~200 ka BP). Partly they are composed of lacustrine deposits containing ice wedge casts (Eemian), partly of Ice Complex deposits from the late Pleistocene including large ice wedges that are several meters in width and height. Partly they consists of Alas deposits that accumulated during the Holocene in thermokarst basins, where they partly formed as limnic sediments (Wetterich et al. 2009). Table 1-1 summarises the prominent Quaternary units exposed in the area.

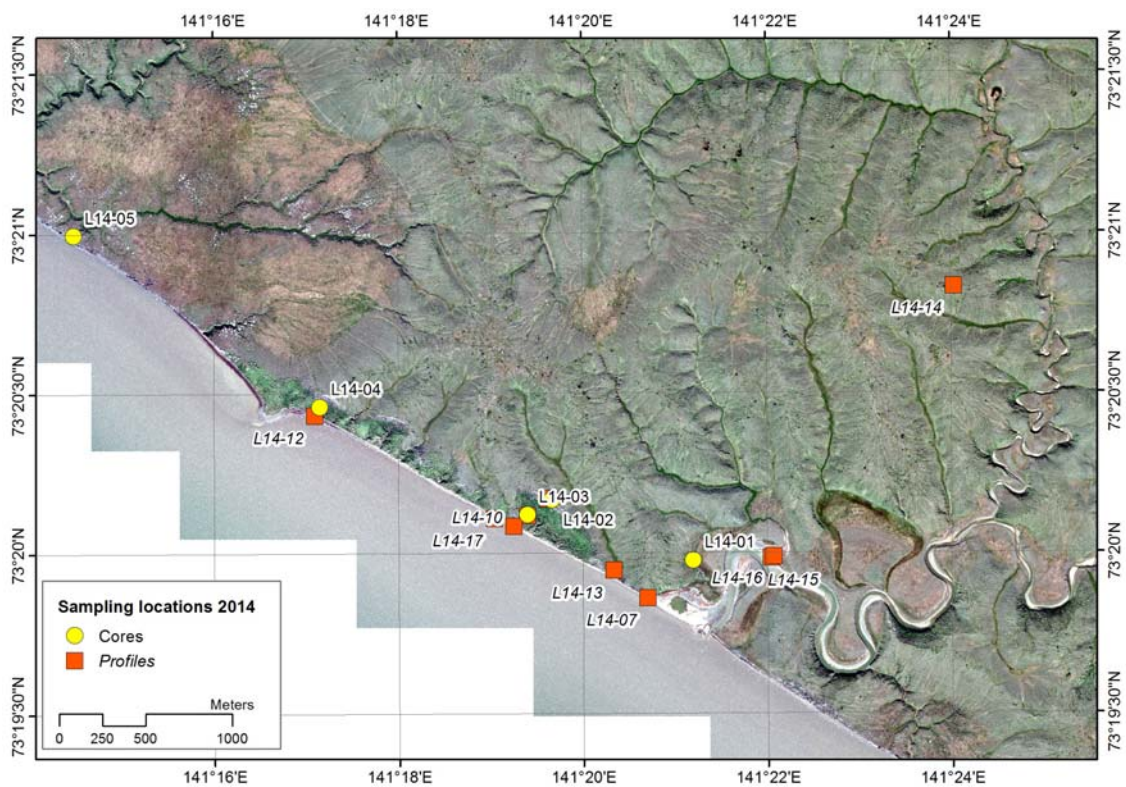


Figure 1-2 Distribution of field sites (cores and profiles), southern coast of Bol'shoy Lyakhovsky. Map compilation: Frank Günther (AWI).

Table 1-1 Quaternary stratigraphic scheme including strata building up southern Bol'shoy Lyakhovsky (Andreev et al. 2004, 2009; Wetterich et al. 2009).

Quaternary epoch (Russian term) (European term)		age range	stratigraphic unit	deposits
	Holocene	<11.5 ka	Alas sequence	boggy and lake deposits, ice wedges
Sartan	Late Weichselian	22-29 ka	Yedoma Suite	Ice Complex formation and paleosol
Kargin	Middle Weichselian	30-55 ka	Yedoma Suite (Molotkov)	Ice Complex formation and paleosol
Zyrian	Early Weichselian	<>120 ka ?	Kuchchugui Suite	flood plain deposits
Kazantsevo	Eemian	~125 ka	Krest Yuryakh Suite	thermokarst and lake deposits
Taz	Late Saalian	~200 ka	Yukagir Suite	Ice Complex formation and peat

In summary the following objectives are linked with the permafrost studies on southern Bol'shoy Lyakhovsky:

- drilling permafrost cores that provide the late Quaternary depositional record of the area,
- measuring ground-penetrating radar and geoelectric lines to set the cores in a spatial depositional context,
- refining the geodetic position and stratigraphy of the Quaternary deposits
- dating selected layers of the local stratigraphy,
- providing modern and ancient soil material for incubation experiments,
- providing modern and ancient soil material for microfossil and sedimentary DNA studies,
- providing modern and ancient soil material for microbial community and biomarker studies.

2 LOGISTICS AND ITINERARY

Georg Schwamborn

One of CARBOPERM's aims is reconstructing the late Quaternary soil organic matter turnover. This may allow for a better assessment of the future greenhouse gas budget from permafrost soils in a warming Arctic. Bol'shoy Lyakhovsky and its landscape units offer the rare opportunity to sample and study deposits back to the pre-Eemian (~200.000 years ago) (**chapter 1**). It is possible to trace back soil organic matter formation, degradation and trace gas release across two climatic cycles. Moreover, the Eemian warm period has been reconstructed to be about 4-5°C warmer than present, this matches the projections of the Arctic by the end of this century and the Eemian could thus hold an analogue of a future warmer arctic environment.

Field campaigns to Bol'shoy Lyakhovsky in 2014 (**chapter 2**) were motivated by research on palaeoenvironmental and palaeoclimate reconstruction, sediment dating, near surface geophysics and microbiological research. In particular the field campaigns focussed on:

- coring Quaternary strata with a ages back to ~200.000 years ago as found along the southern coast; they allow tracing microbial communities and organic tracers (i.e. lipids and biomarkers, sedimentary DNA) in the deposits across two climatic cycles (**chapter 3**),
- instrumenting a borehole with a thermistor chain for measuring permafrost temperatures (**chapter 3**),
- sampling Quaternary strata for dating permafrost formation periods based on the optical stimulated luminescence (OSL) technique (**chapter 4**),
- sampling soil and geologic formations for carbon content in order to highlight potential release of CO₂ and methane based on incubation experiments (**chapter 5**),
- profiling near surface permafrost using ground-penetrating radar and geoelectrics for defining the spatial depositional context, where the cores are located (**chapters 6 + 7**).

The Arctic and Antarctic Research Institute (St. Petersburg) and the Alfred Wegener Institute, Helmholtz Centre for Polar and Marine Research (Potsdam) jointly organized the general logistics of the Bol'shoy Lyakhovsky campaigns in 2014. This includes permission procedures and long distance personnel and freight transfer. The Roshydromet Hydrobase in Tiksi organized local transport, helicopter transfer and housing (see Table 2-1, Figure 2-1).

Table 2-1 Participating institutions

Abbreviation	Institution
AARI	Arctic and Antarctic Research Institute, St. Petersburg
AWI	Alfred Wegener Institute, Helmholtz Centre for Polar and Marine Research, Potsdam
NEFU	North-Eastern Federal University, Yakutsk
TH	Hydrobase of Roshydromet, Tiksi
UHH	University of Hamburg, Institut für Bodenkunde
UP	University of Potsdam, Institut für Erdwissenschaften

Timetable

Field campaigns to Bol'shoy Lyakhovsky in 2014 were realized in two periods:

- 31 March to 29 April (**spring campaign**) and
- 23 July to 26 August (**summer campaign**).

In total 16 participants took part (Tables 2-2 and 2-3).

Table 2-2 Participants of the **spring** campaign, March 31 to April 29, 2014.

Name	E-mail	Institution
Georg Schwamborn	Georg.Schwamborn@awi.de	AWI
Lutz Schirrmeister	Lutz.Schirrmeister@awi.de	AWI
Stephan Schennen	Stephan.Schennen@uni-potsdam.de	UP
Niklas Allroggen	Niklas.Allroggen@uni-potsdam.de	UP
Yuri Kuchanov	Kuchanov@aari.nw.ru	AARI
Stanislav Keltciev (1 st driller)	Sskeltsiev@rambler.ru	NEFU
Vitali Ivanov (2 nd driller)		TH
Vitali Struchkov (camp manager)		TH
Sasha Struchkov (2 nd camp manager)		TH
Viktor Grigoriev (vehicle driver)		TH
Innokenti Struchkov (2 nd vehicle driver)		TH

Table 2-3 Participants of the **summer** campaign, July 23 to August 22, 2014.

Name	E-mail	Institution
Georg Schwamborn	Georg.Schwamborn@awi.de	AWI
Sebastian Wetterich	Sebastian.Wetterich@awi.de	AWI
Margret Fuchs	Margret.Fuchs@awi.de	AWI
Jens Tronicke	jens@uni-potsdam.de	UP
Stephan Schennen	Stephan.Schennen@uni-potsdam.de	UP
Josefine Walz	josefine.walz@uni-hamburg.de	UHH
Viktor Zykov		TH

Tables 2-4 and 2-5 list the itineraries of the spring and summer field parties (see also Figure 2-2).

Table 2-4 Itinerary **spring** campaign.

Date	Activity
30.03.2014	Departure from Berlin and St. Petersburg via Moscow and Yakutsk to Tiksi (Schwamborn, Schirrmeister, Schennen, Allroggen, Kuchanov, Keltciev, Ivanov)
31.03.2014	Tiksi, preparation and arrangements
01.04.2014	Technical group: departure with two all-terrain vehicles (5 days)
05.04.2014	Science group: departure by helicopter from Tiksi to Bol'shoy Lyakhovsky, base camp at Zimov'e river (distance: 500 km, flight time: 150 min), settling in cabins
06.04.2014	Start permafrost drilling
24.04.2014	End permafrost drilling
25.04.2014	Science group: return by helicopter from Bol'shoy Lyakhovsky to Tiksi
26.04.2014	Technical group: return by all-terrain vehicles to Tiksi (takes 4 days)
26.04.2014	Tiksi, packaging and arrangements
28.04.2014	Return from Tiksi to Yakutsk and via Moscow to St. Petersburg and Berlin
29.04.2014	Arrival

Table 2-5 Itinerary **summer** campaign

Date	Activity
23.07.2014	Departure from Berlin via Moscow to Tiksi (Schwamborn, Wetterich, Fuchs, Tronicke, Schennen, Walz*, *from Samoylov)
25.07.2014	Tiksi, preparation and arrangements

28.07.2014 Science group by helicopter to Bol'shoy Lyakhovsky, base camp at Zimov'e River (distance: 500 km, flight time: 150 min)
29.07.2014 Start fieldwork
21.08.2014 End fieldwork
22.08.2014 Return by helicopter to Tiksi
25.08.2014 Return via Yakutsk, Moscow to Berlin
26.08.2014 Arrival



Figure 2-1 Cabins for housing in April (top) and August (bottom), Zimov'e River mouth, south coast of Bol'shoy Lyakhovsky.



Figure 2-2 Left: Spring campaign field team. Right: Summer campaign field team.

3 PERMAFROST DRILLING ON BOL'SHOY LYAKHOVSKY

Georg Schwamborn, Lutz Schirrmeister

The study sites for permafrost coring are placed west of Zimov'e River on the southern coast of the island (Figures 3-1 and 4-1). Geographic positions and recovery of five cores in total are listed in Table 3-1 (and Appendix 3-1). An overview of core positions and the stratigraphical context is given in Figure 3-2. Basic core descriptions and photographic examples are found in the chapters below. Detailed core descriptions are listed in Appendix 3-2 to 3-6.

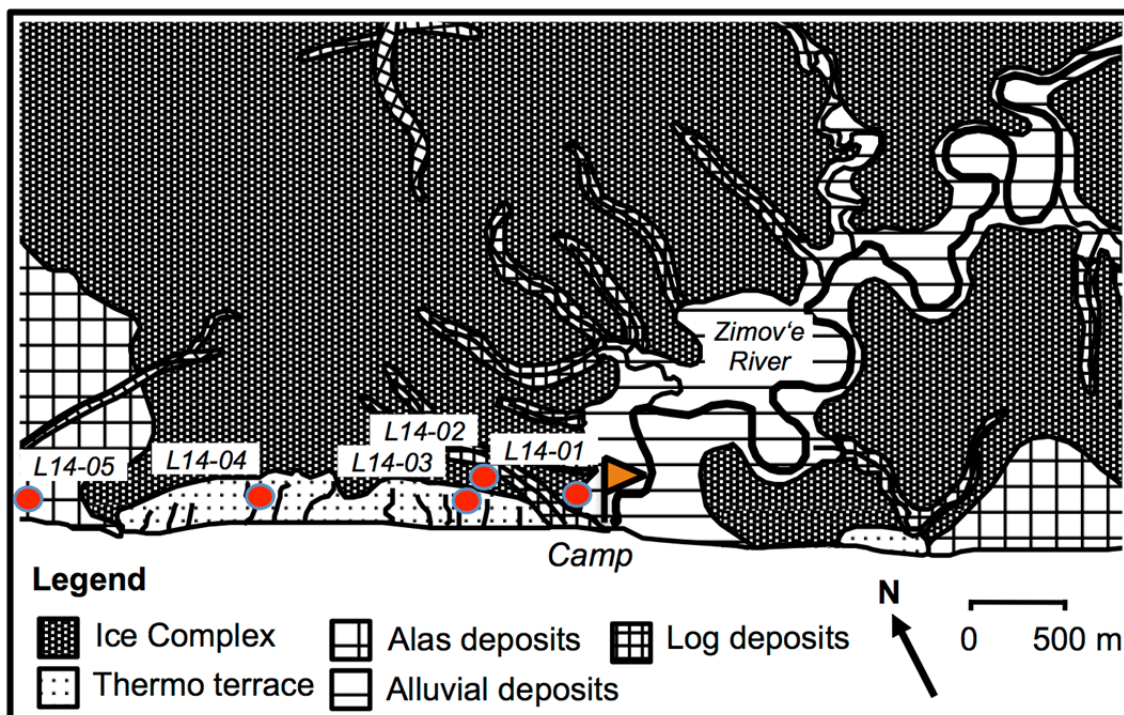


Figure 3-1 Scheme with permafrost drilling sites on southern Bol'shoi Lyakhovskiy.

Table 3-1 Specification of cores and core recovery (a.s.l. = above sea level).

Label	Recovery (m)	Lat	Long	Height a.s.l. (m)		Sediment Record
L14-01	00.82	73.33297°N	141.35325°E			test (river terrace)
L14-02	20.02	73.33616°N	141.32776°E	32.3 (top)	12.2 (bottom)	mid Weichselian - Ice Complex
L14-03	15.49	73.33538°N	141.32337°E	17.0 (top)	1.5 (bottom)	early Weichselian
L14-04	08.10	73.34100°N	141.28586°E	12.0 (top)	3.9 (bottom)	supposed incl. Eemian
L14-05	07.89	73.34994°N	141.24139°E	11.5 (top)	3.6 (bottom)	Alas (Holocene)
total	52.32					

The used drilling machine for retrieving cores was a mobile Russian KMB3-15M rig mounted on an all-terrain vehicle (Figure 3-3). It has been specifically designed for shallow permafrost coring using a rotary mechanism in dry holes.

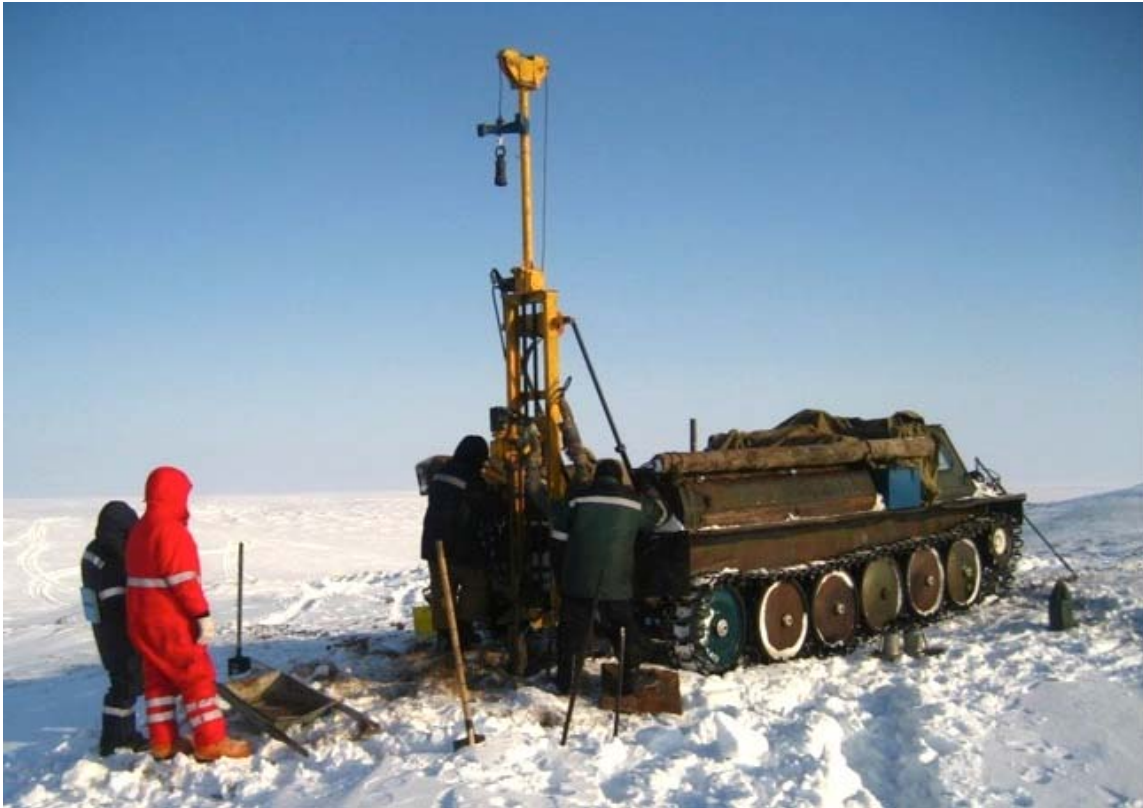


Figure 3-3 Drill rig KMB-15M mounted on a vehicle.

Outer drill diameters were 132 mm, 112 mm, 93 mm, and 76 mm (Appendix 3-1 to 3-6). Drilling was done during dayshifts. The Yedoma borehole (L14-02) has been cased using a tube of 132 mm in diameter and 2 m in length. All other holes remained uncased.

After extracting individual core runs of up to 1.5 m in length, the borehole depth was confirmed with a measuring tape. Open-air core processing was as follows (see photo panels on next page):

1. cleaning from drill cuttings,
2. describing the cores, filling in the protocol,
3. taking photographs from whole core and close-ups,
4. wrapping up the core sections into plastic foil, close them, annotating them, storing them in thermo-boxes.

After the field campaign cores were transported frozen by helicopter to Tiksi for intermediate storage in a freezing container at -20 °C.

Final usage of borehole L14-02 was devoted to record the permafrost **temperature profile**. A 10 m long thermistor chain including a digital logger has been lowered into the borehole after drilling was completed.

Temperatures are logged four times a day and have the following depths (m): +0.3, 0.0, -0.4, -0.8, -1.2, -1.6, -2, -2.5, -3, -3.5, -4, -4.5, -5, -5.5, -6, -6.5, -7, -8, -9, -10.

First readings were collected two days after drilling. More readings were collected during summer. Data storage and download is accessible via the *Global Terrestrial Network for Permafrost* web site (gtnp.org). To stabilize the upper borehole against hill creep and active layer drainage a casing of 2.0 m was installed with 1.5 m underground.

The ground thermal regime at borehole L14-02 is displayed in Figure 3-4. It indicates maximum and minimum temperatures of the available readings, the beginning of the thaw season (July-02), the depth of zero-annual amplitude at 7.8 m, and the depth of seasonal thaw (the active layer) at 0.6 m.

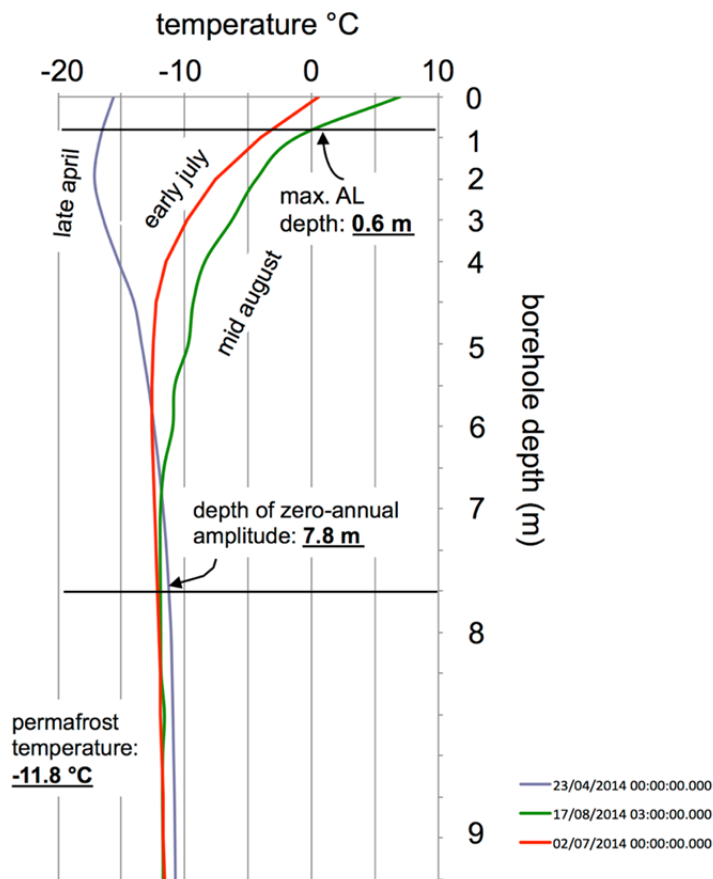


Figure 3-4 Ground thermal regime at borehole L14-02. Note the temperature offset below 7.8 m depth between the April reading (shortly after drilling termination) and the July and August readings, when the permafrost temperature is back to equilibrium.

3.1 Core L14-02 (Yedoma)

Drilling at site L14-02 on the Yedoma hill began at the ground surface on top of a baidzerakh (thaw mound that exposes a polygon centre with soil horizons) and continued down to the maximum borehole depth of 20.02 m (Figure 3-5). In this core ice-rich silt containing scattered plant remains and peaty inclusions is underlain by ice wedge ice that was encountered between 11.10 m and 20.02 m. We stopped drilling due to the slow speed of progress. The borehole has been instrumented with a thermistor string for measuring permafrost temperatures (see Figure 3-4).

Based on the field descriptions the core can be subdivided into two main units:
 00.00 - 10.92 m core depth: ice-rich silt, grey to brown and olive, scattered mm-sized plant remains, partly with peat inclusions, mainly coarse lense-like cryotexture, partly with cm-thick ice bands; preliminary interpretation: Yedoma deposits consisting of a succession of palaeosol horizons,
 10.92 - 20.02 m core depth: ground ice with air bubbles, silty streaks; preliminary interpretation: ice wedge ice. For more core description see Appendix 3-3.

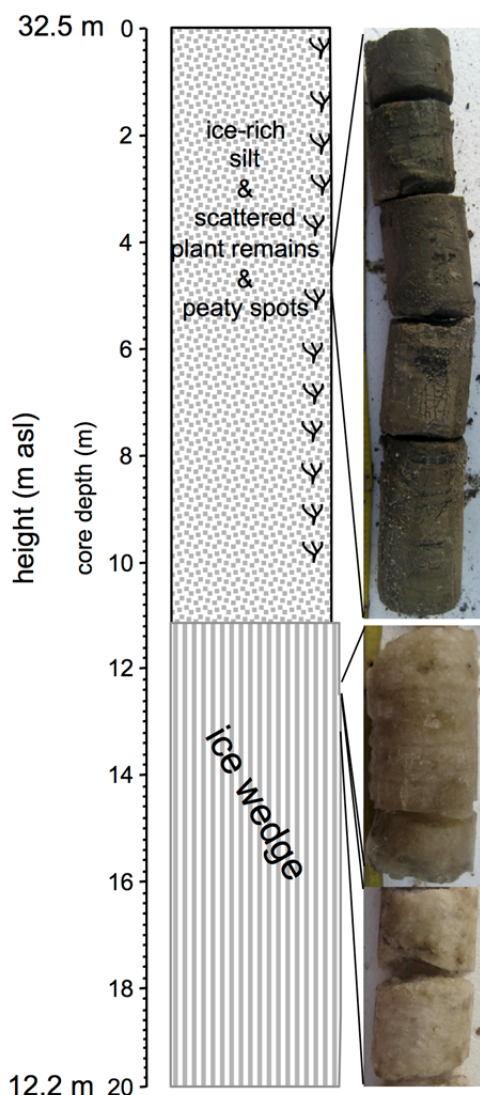


Figure 3-5 Left: Core recovery of site L14-02 with a photographic example from 4.77-5.03 m (ice-rich silt incl. plant remains) and 12.20-12.35 and 12.70-12.80 m depth (ice wedge ice). Core diameter is 132 mm and 93 mm. Right: Core site on the Yedoma hill (see arrow).



3.2 Core L14-03 (thermo terrace)

Drilling at site L14-03 took place in the thermo terrace from 17.0 m a.s.l. down to 1.5 m a.s.l. (Figure 3-6). Total length of the core is 15.49 m. Stony deposits stopped further progress in the borehole. There is an additional 1.18 m core available at the top, after re-arranging the drilling site for a second run (Appendix 3-4). L14-03 extends the L14-02 record from a lower topographic position.

Based on the field descriptions the core is generally composed as follows:

00.00 - 06.02 m: silt, grey to brown, rarely with plant remains, lense-like cryotexture, partly with cm-thick ice bands

06.02 - 08.62 m: rich in vertical ice bands, which are interpreted as composite ice wedges (in Russian: polosatiki)

08.62 - 09.59 m core depth: ice-rich sand and pebble layers

09.59 - 11.95 m core depth: polosatiki-type of ice wedge ice continued

11.95 - 13.70 m core depth: ice-supported pebble, partly clear ice

13.70 - 15.49 m core depth: sand and gravel layers, gravel with subangular components, clast-supported.

Overall the material in the core is linked with a floodplain environment. For more core description see Appendix 3-4.

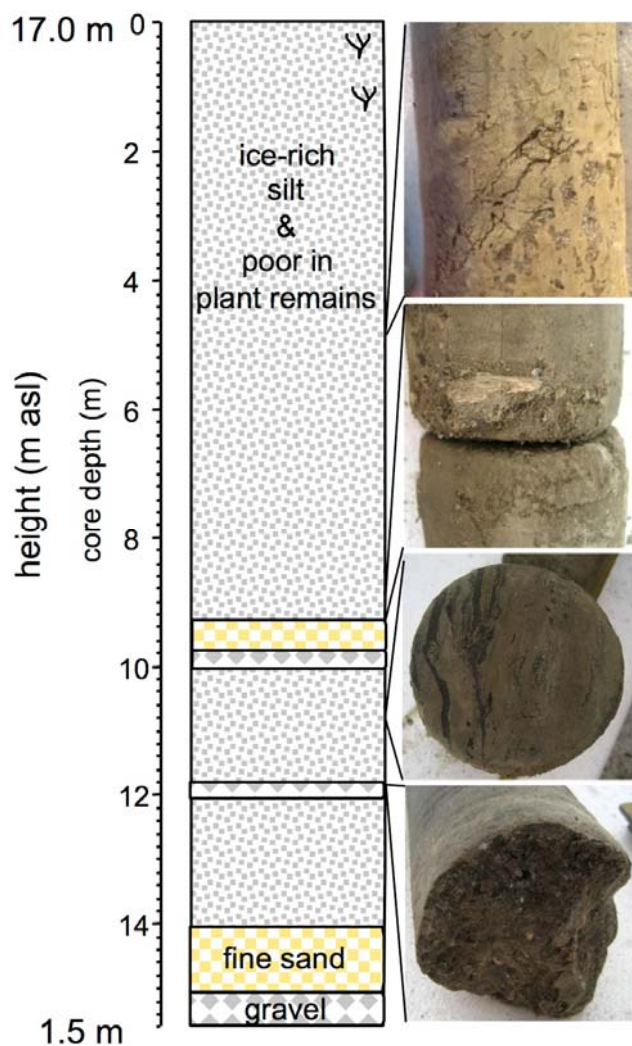


Figure 3-6 Core recovery of site L14-03 with photographic examples from 4.9 m (ice-rich silt, upper panel), from 9.10 m (note the angular cm-sized clast), from 10.90 m (note the vertical ice veins), and from 11.70 m depth (note the white gravel, lower panel). Core diameter is 112 mm.

3.3 Core L14-04 (incl. Eemian deposits)

Drilling at site L14-04 took place in the thermo terrace 2.5 km west of Zimov'e River mouth. The borehole is from 12.0 m a.s.l. down to 3.9 m a.s.l. (Figure 3-7). In contrast to L14-03, which is placed at a similar altitudinal level, this core is supposed to contain interglacial, i.e. Eemian, deposits from the Krest Yuryakh formation as known from previous outcrop studies around the site (Wetterich et al. 2009).

Based on the field descriptions the core is generally composed as follows:

00.00 - 06.43 m core depth: ice-rich silt, grey to brown, rarely plant remains and spots with peaty inclusions, mostly with lense-like to blocky cryotexture, partly ice from ice wedge ice containing mm-sized air bubbles

06.43 - 08.10 m core depth: ice-poor silt, grey to brown, faintly laminated and containing distinct black spots of reduced organic material, micro lense-like cryotexture (Figure 3-7). For more core description see Appendix 3-5.

Due to core barrel loss in the borehole the site was abandoned at 8.10 m depth. From a coastal bluff near the borehole, we added nine samples from between 9.6 m a.s.l. to 2.5 m a.s.l. (Figure 3-8). The upper four samples have been taken from ice-rich peaty layers, which resemble sediment characteristics from the upper core part of L14-04. The lower five samples originate from ice wedge casts that resemble the sediment characteristics from the lower core part of L14-04 as described above and displayed in Figure 3-7. They consist of silt that is typically faintly layered and can contain ostracods and mollusc fragments. The deposits are partly rich in plant detritus and can have twig remains. The cryotexture is predominantly massive (i.e. ice cement) with only individual mm-thin ice veins that are visible parallel to the bedding. The material is interpreted to represent interglacial deposits that likely accumulated under subaquatic conditions in a thermokarst basin (Wetterich et al. 2009). For more sample description see Appendix 3-5.

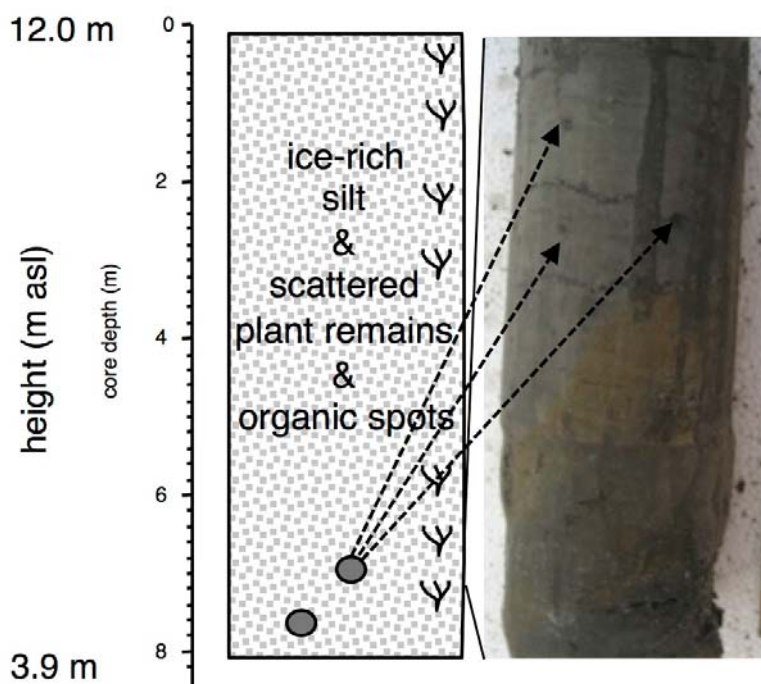


Figure 3-7 Scheme of core recovery of site L14-04 with a photographic example from 7.30 to 7.40 m depth. Note the dark spots (see arrows) stemming from organic inclusions preserved in an anoxic depositional environment. Core diameter is 112 mm.



Figure 3-8 Positions of core L14-04 and additional samples that were taken from the coastal bluff near the coring site (person for scale).

3.4 Core L14-05 (Alas deposits)

Drilling at site L14-05 took place in an alas 4 km west of the Zimov'e River mouth. The borehole is from 11.5 m a.s.l. down to 3.6 m a.s.l. with a total core length of 7.89 m (Figure 3-9). A broken joint stopped further progress.

Based on the field descriptions the core is generally composed as follows:
 00.00 - 07.89 m core depth: silt, grey to brown, scattered plant remains and spots and thin layers of peaty material, occasionally orange mottles of Fe-oxides, mostly with lattice- to lense-like cryotexture, the ice content decreases from the top to the bottom. The preliminary interpretation is that the material has accumulated in a thermokarst basin. For more core description see Appendix 3-6.

From a coastal bluff near the borehole we added 12 samples from between 10.9 m a.s.l. to 3.6 m a.s.l. (Figure 3-10). The samples were taken from sediment layers that were deposited in ice wedge casts. In addition to the core material these samples partly have shells from ostracods, can contain wood remains and have distinct layers with plant fragments. For more sample description see Appendix 3-6.

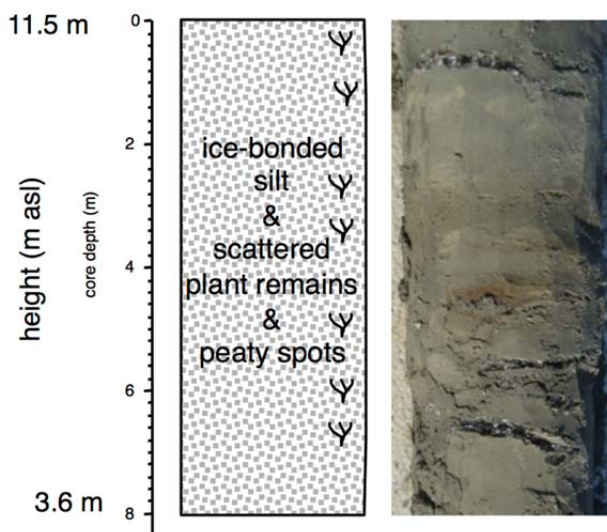


Figure 3-9 Core recovery of site L14-05 with a photographic example from 5.70 to 5.80 m depth. This core has visibly less ground ice than all other cores.

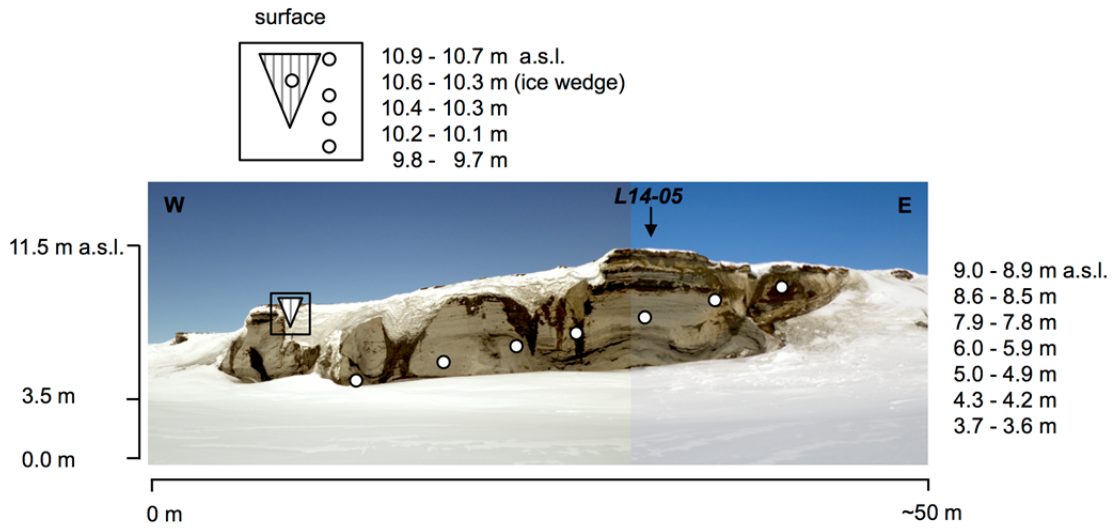


Figure 3-10 Position of core L14-05 and additional samples that were taken from the coastal bluff below the coring site.

4 PERMAFROST EXPOSURES OF BOL'SHOY LYAKHOVSKY

Margret Fuchs, Georg Schwamborn, Josefine Walz, Sebastian Wetterich

4.1 Introduction

The investigations of permafrost exposures on Bol'shoy Lyakhovsky Island addressed the project scope of CARBOPERM: the dynamics of fossil organic matter (OM) and its distribution in permafrost sequences with respect to Quaternary climate changes. Therefore, fieldwork during the 2014 summer campaign focussed on representative exposures of the main glacial and interglacial deposits of the island. Sampling aimed at extending the sample set of frozen material available for further geochronological and biogeochemical analyses. The sampled profiles were chosen in close relation to the drill positions from spring 2014 (see chapter 3) or to exposures studied during earlier field campaigns in 1999 (Schirrmeister et al. 2000) and 2007 (Schirrmeister et al. 2008). The publications of Andreev et al. (2004, 2009, 2011), Ilyashuk et al. (2006), Kienast et al. (2008), Meyer et al. (2002), Schirrmeister et al. (2002), Tumskey (2012) and Wetterich et al. (2009, 2011, 2014) provide a comprehensive understanding of the palaeoenvironmental background. The newly undertaken efforts focus on the dynamics of fossil organic matter (OM) during late Quaternary climate changes, and on its distribution in permafrost sequences. Local stratigraphic terms refer to Tumskey (2012) and are used in the following profile descriptions which include the pre-Eemian Yukagir Ice Complex, the Kuchchugui Suite, the Krest Yuryakh Suite, the Yedomia Ice Complex, the Sartan Ice Complex, the Holocene thermokarst Alas and modern floodplain deposits.

Sample material was obtained in frozen state for the following applications using spade, axe, hammer, a HILTI TE6 - A36 cordless rotary hammer or a Stihl chain saw, and kept frozen in an ice cellar (lednik - ледник in Russian) next to the camp at -4 °C:

- Luminescence dating of quartz and feldspar (sample code: OSL)
- Th/U dating of frozen peat (sample code: Th/U)
- Accelerator mass spectrometry (AMS) radiocarbon (¹⁴C) dating (sample code: 14C)
- Bedrock mineralogy
- Palaeogenetics of plant macro-remains (sample code: palaeogenetics - PG)
- Dissolved organic carbon of ice-wedge ice (sample code: DOC)
- Chlorine-36 (³⁶Cl) of ice-wedge ice (sample code: 36Cl)
- Carbon stock and degradation (sample code: Bodenkunde - BK)

An overview of all samples is given in Appendix 4-1 including position parameters, a brief cryolithological description, and intended analytical methods. Additionally, the gravimetric ice content was determined for all samples. Values in Appendix 4-1 represent the normalised weight difference between frozen and dry subsamples based on the wet (absolute) and dry (gravimetric) subsample mass.

The absolute altitude of the sampled profiles was measured in meter above sea level (m a.s.l.) using a Leica TCP 1203+ Total Station (see chapter 6) while

sampling positions were estimated as relative depth in meter below surface (m b.s.) using measurement tape, and transferred later into m a.s.l.

In total, eleven locations have been studied (Figure 4-1), including bedrock exposures, modern deposits and relevant pre- to late Quaternary stratigraphic units. All profiles and sampling positions are shortly described in the following chapters according to their stratigraphic order.

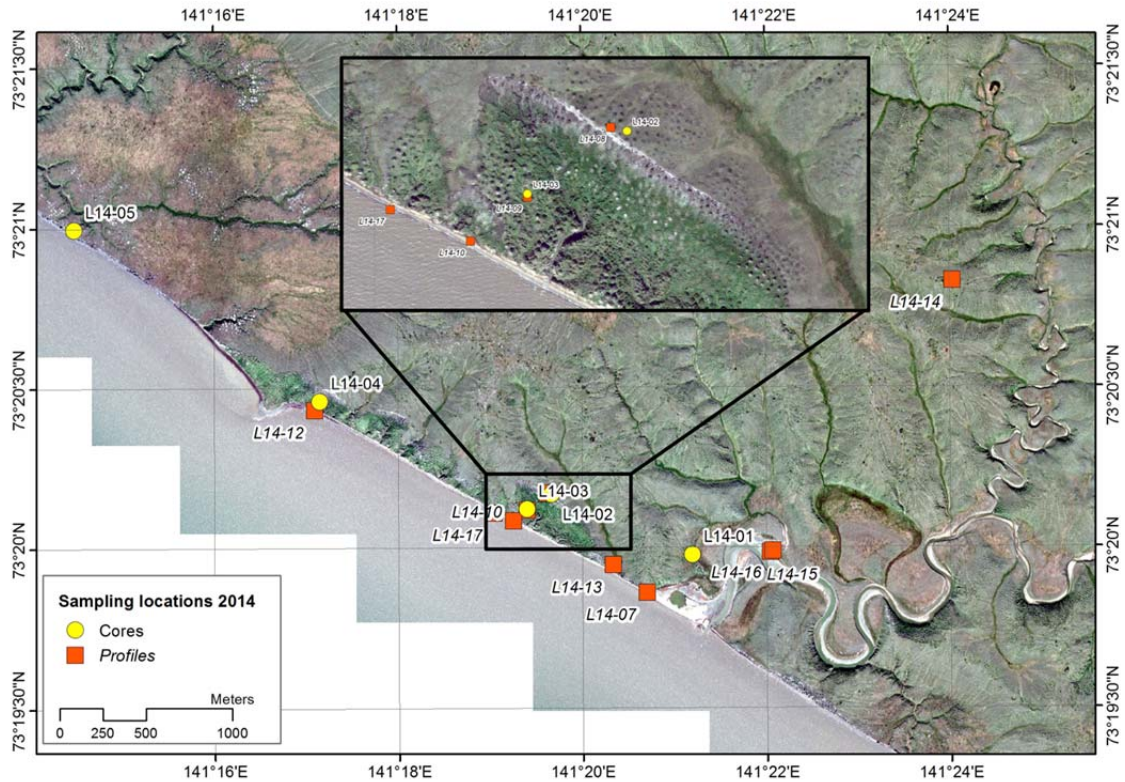


Figure 4-1 Pansharpended GeoEye satellite image (true color composite), acquired on 11 Aug. 2013, of the southern coast of Bol'shoy Lyakhovsky, west of the Zimov'e River mouth with positions of the coastal exposures sampled in summer 2014 and the drilling performed in spring 2014 (see also Figure 1-2). Map compilation: Frank Günther (AWI).

4.2 Bedrock and mineralogical studies

The bedrock below the unconsolidated Quaternary Strata of Bol'shoy Lyakhovsky is largely composed of a Mesozoic flyschoid sequence of sandstones, siltstones, and shales. The most extensive rock outcrops are located in the south and southeastern part of the island (the Khaptagai-Tas, Cape Burus-Tas and nearby areas). Small exposures are also known in the western (Cape Kigilyakh) and northern parts (Usuk-Yuryakh Rise) of the island (Figure 4-2). The siliclastica on Bol'shoy Lyakhovsky are related to the Siberian mainland such as at Svyatoi Nos, where Palaeozoic basaltic bedrock eroded and the debris filled foreland basins.

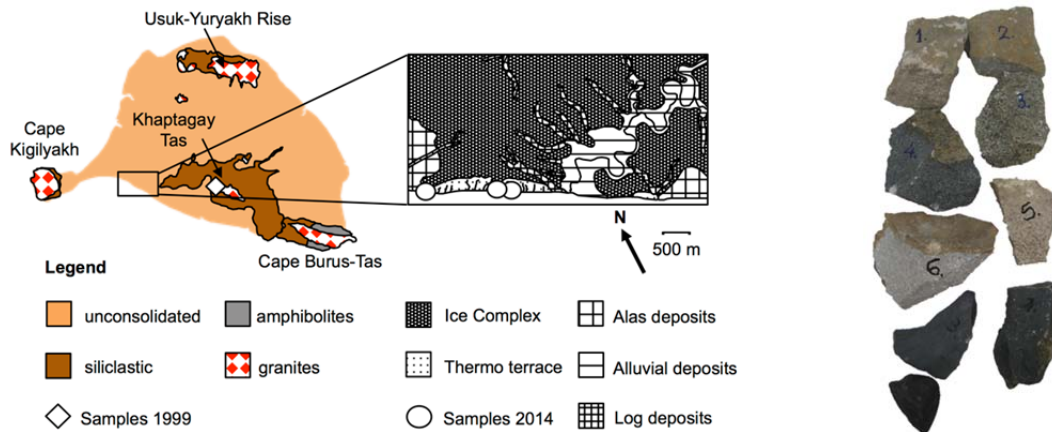


Figure 4-2 Left: Geological map of Bol'shoy Lyakhovsky (simplified from Kyz'michev et al., 2006) and sample sites of outcropping hard rock on the beach. Right: Sampled bedrock comprises crystalline (granitic) rocks and sandstones.

Today Cretaceous granites and diorites and ophiolitic basalts and amphibolites are found next to the siliclastica. The crystalline bodies likely intruded into the siliclastic complex after the terrane collision of the New Siberian platform with the Siberian continent (Kyz'michev et al. 2006). Bedrock outcrops can be observed in our study area. We collected various rock types from exposures on the beach west of Zimov'e River. Rock types resemble those described above (Figure 4-2).

Future rock analysis includes (i) thin section microscopy, (ii) X-ray diffraction measurements, and (iii) X-ray fluorescence measurements to determine the mineralogical composition of the main bedrock units in the southern part of the island. This will allow tracing the provenance of the overlying Quaternary Strata that were recovered in cores L14-02 to -05. Hypothetically, growth and shrinking of Quaternary ice sheets may have deflected transport ways across the island at least temporarily during glacial drainage.

4.3 Pre-Quaternary (profile L14-14)

An exposure of probably pre-Quaternary deposits was found inland at the riverbank of the Vetvisty River (tributary of the Zimov'e River). The material exposed at about 0.5 and 1.5 m above river level (Figure 4-3a, b) resembles the profile L7-17 studied in 2007 (Schirrmeister et al. 2008). The unfrozen deposits consisted of alternating light-grey sand layers and black organic layers (each 5 to 10 cm thick) that are overlain by a loose layer of pebble with diameters of up to 5 cm and more or less rounded shape. The organic-rich zones contained charcoal and wood remains (up to 10 cm in diameter and up to 10 cm long). Reddish iron-oxidation spots were common in the light-grey sands as well as quartzitic less-rounded gravels. Large wood remains and pebbles, comparable to those in the profile, were also found along the river (Figure 4-3c). The permafrost table was reached at about 0.5 m above the river level. Profile L14-14 was not sampled.

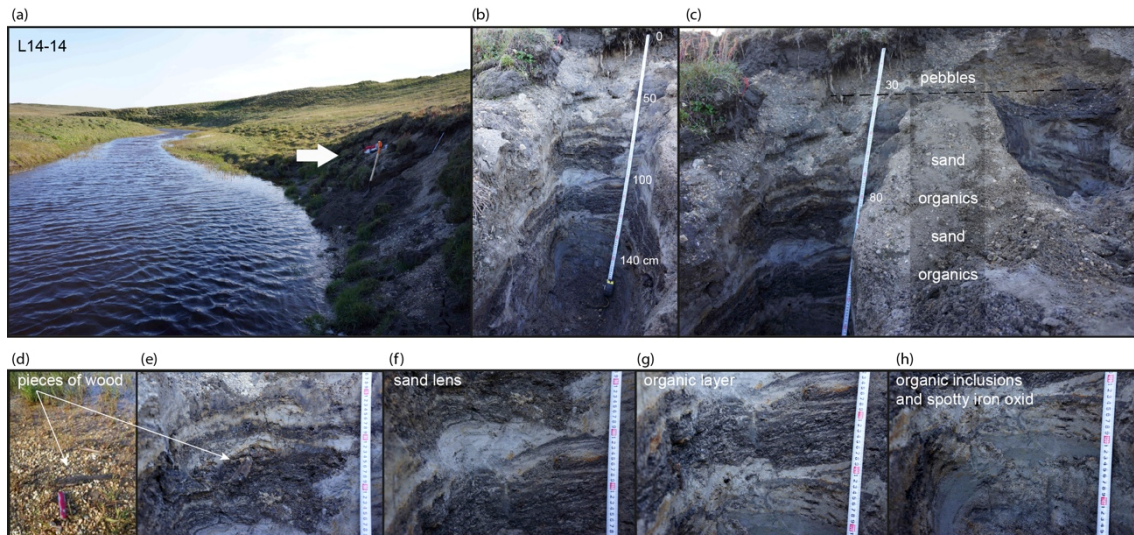


Figure 4-3 Profile L14-14 of pre-Quaternary deposits in (a) landscape overview, (b) the profile itself and (c) pebbles and large wood remains on the Vetvistyi River bank.

4.4 Yukagir Ice Complex (profile L14-11)

The cryolithological inventory of the Yukagir Ice Complex comprises ice-rich greenish-grey fine-grained sands with coarse reticulated ice lenses (2 mm thick and 20 to 50 mm long) and ice bands (up to 20 mm thick). Large syngenetic ice wedges (up to 5 m wide in their upper part) intersected the sediment polygon fillings. The Yukagir ice wedge was rich in unregular air bubbles (1 to 2 mm in diameter) and exhibited single sand veins. Pebbles and peat lenses (50x50 to 100x100 mm) occurred at the cryoturbated contact of the greyish sediments with the overlying peat at about 2.6 m a.s.l. The overlying peat of about one meter thickness was exposed at several, similar outcrops within a distance of about 550 m along the beach between the Zimov'e River mouth and Cape Kammenyi Mys' (Figure 4-4a). The peat contained fine ice lenses and rather coarse vertical and subvertical ice veins (20 mm thick and 200 to 300 mm long). The peat itself is represented by rather fresh (sometimes green) mosses in the inner frozen parts and by degraded dark-brown material in the thawed outer parts (Figure 4-4b). Previous dating of the Yukagir peat based on Th/U radioisotope disequilibria revealed an accumulation about 200 kyr ago (Schirrneister et al. 2002). In 2007, similar material was sampled at the profile L7-01 (Schirrneister et al. 2008). For further analyses, the profile L14-11 was sampled for palaeogenetics, Th/U dating and soil carbon studies.



Figure 4-4 Profile L14-11 of Yukagir Ice Complex deposits located along the coast (a). The profile exposed the ice-rich greyish silt to find sand overlain by the ice-rich peat as shown in the photo (b) and scheme (c), respectively.

4.5 Yukagir Ice Complex to Kuchchugui Suite (profile L14-10)

Profile L14-10 represents the vertical contact of the Yukagir Ice Complex with overlying deposits of the Zimov'e Strata and the Kuchchugui Suite (Figure 4-5a-d). Parts of the Yukagir Ice Complex are exposed in the lowermost profile section, visible as a huge ice wedge and moss peat (as described in profile L14-11). The Zimov'e Strata directly above the syngenetic Yukagir ice wedge is about 0.5 m thick and is characterised by frozen yellowish-brown silt and fine-grained sand. The sediment itself showed only fine ice lenses or lacks any visible (massive) cryostructures. Andreev et al. (2004) summarised previous work on deposits of the Zimov'e Strata and gave an age of 134 ± 22 ka according to Infrared-Stimulated Luminescence (IRSL) dating. Less-rounded yellowish and reddish pebbles were numerous and varied in size (>2 mm up to 20 mm in diameter; Figure 4-5d). The pebbles clustered in yellowish-orange sandy pockets that documented cryoturbation. Black organic spots and vertical grass roots were rare. Epigenetic sand-ice wedges of the Kuchchugui (up to 0.5 m wide) penetrated the Zimov'e Strata and reached into the Yukagir ice wedge.

The Kuchchugui Suite was composed of predominantly yellowish-brown silt and a minor portion of fine-grained sand. The frozen, relatively homogeneous material indicated horizontal layering (visible in thawed surface), only some parts were medium-scale waved (0.5 m length). The deposits contained only fine ice lenses or lacked any visible cryostructures. Vertical grass roots, organic lenses (ca. 20x50 mm) and single black spots (ca. 2x2 mm) were common. Both, the Zimov'e Strata as well as the Kuchchugui have been sampled for luminescence dating (Figure 4-5a, b, d).

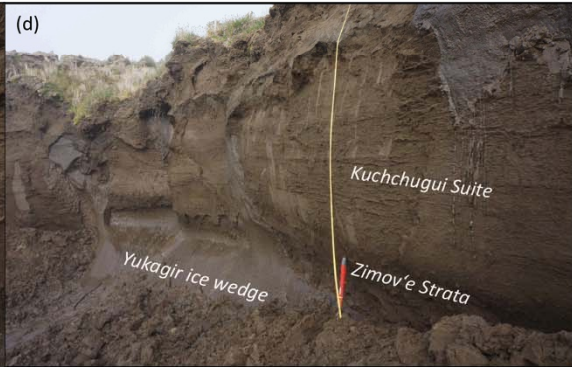
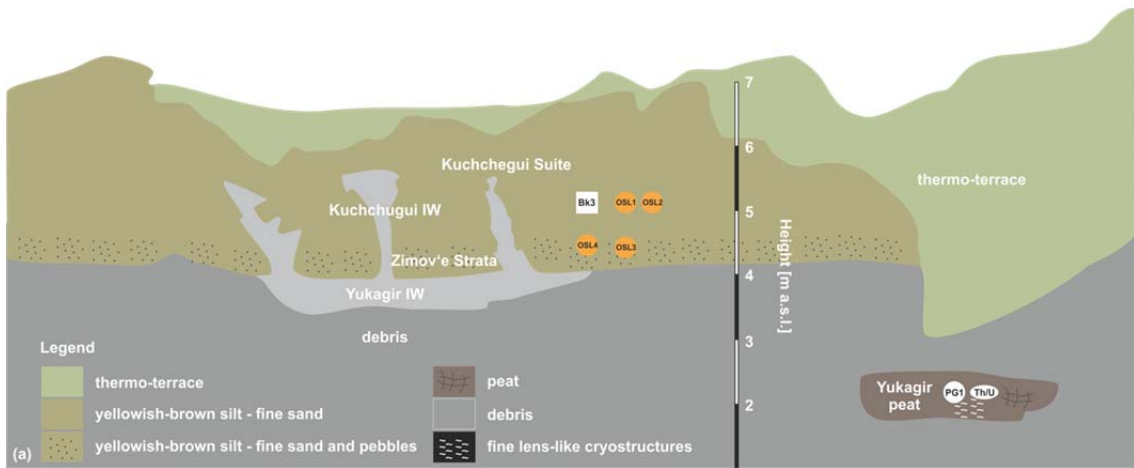


Figure 4-5 Profile L14-10 of the Yukagir Ice Complex and Kuchchugui Suite in (a) scheme of the sampled exposure, (b) corresponding overview image of the whole exposure, (c-g) detailed images of sampled sediment units.

An additional sample for soil carbon analyses was obtained from the Kuchchugui Suite. The described stratigraphy and contacts correspond to the

previously studied profile L7-01 of the field campaign in 2007 (Schirrmeister et al. 2008).

4.6 Kuchchugui Suite to Molotkov Ice Complex (profile L14-17)

While the lower contact of the Kuchchugui to the Yukagir Ice Complex has been found and described in profile L14-10 (chapter 4.5), its upper contact is described in profile L14-17 (Figure 4-6). The rather typical composition of the Kuchchugui Suite (see chapter 4.5) was found again in profile L14-17 between about 4 and 6 m a.s.l. A likely syngenetic ice wedge reached into the Kuchchugui. In the very top of the Kuchchugui about 0.7 m b.s. of the thermo terrace and in contact to the syngenetic ice wedge, the deposits resembled typical polygon fillings (about 0.5 m thick) of the Yedoma Ice Complex (Figure 4-6b) with distinct up-bent ice bands. The sediment structures and the position at the coastal end of a thermo terrace suggested the unit to display the onset of polygon formation of the Molotkov (Yedoma) Ice Complex above the Kuchchugui. However, the exposure was not sampled to safety reasons. Previous studies on Bol'shoy Lyakhovsky in 1999 and 2007 mention the contradicting stratigraphic position and the unclear age of the Kuchchugui Suite (Schirrmeister et al. 2000, 2008). This typical formation of layered brownish silt and fine-grained sands with low ice content, small epigenetic ice wedges, and grass roots was found overlying the Yukagir Ice Complex (profiles L7-01, L7-02 and L7-05 from 2007, profile L14-10 from 2014) (see chapter 4.5). The formation was further described underlying the Krest Yuryakh (Eemian) as taberite in profile L7-14 from 2007, underlying the Buchchagy Ice Complex in profile L7-15 from 2007. Kuchchugui deposits without determinable upper or lower stratigraphic contact were found in in profile L7-12 from 2007. The current understanding of the stratigraphic position of the Kuchchugui Suite is summarised by Andreev et al. (2004, 2009; unit IV *ibidem*). Radiocarbon dating of the subaerial Kuchchugui Suite given in Andreev et al. (2004) show ages close to the limits of the method with infinite ages and ages between 42 and 53 ka BP (Table 4-1). IRSL yielded ages between 57 and 79 ka (Table 4-1). Andreev et al. (2004) attributed the Kuchchugui Suite to floodplain deposition of the Early Weichselian (Zyryan) Stadial younger than 120 ka, while Andreev et al. (2009) refined the age of this facies to about 100 to 50 ka.

Table 4-1 Dating results of the Kuchchugui Suite (summarised in Andreev et al. 2004, 2009)

Profile ID in 1999	Radiocarbon ages	IRSL ages
R6	infinite	
R18+50	infinite 44.00 +3.43/-2.39 ka BP	57 ± 10 ka
R8+50	49.81 +3.15/-2.26 ka BP	
R14+40	50.11 +2.95/-2.15 ka BP	
R9+85	49.20 +2.40/-1.85 ka BP	68 ± 14 ka 77 ± 12 ka
R17		79 ± 14 ka



Figure 4-6 Profile L14-17 of Kuchchugui and Molotkov (Yedoma) Ice Complex deposits in (a) coastal exposure overview and (b) detailed image of the sediment units.

4.7 Krest Yuryakh (Eemian) deposits (profile L14-12)

Lake sediments near Cape Kammenyi Mys' were studied in the exposure L14-12 about 8 m a.s.l. (Figure 4-7a-c) and in close relation to the L14-04 drill core obtained in spring 2014 (see chapter 3). The lowermost exposed deposits at about 3 m a.s.l. exhibited slightly layered bluish-grey silt and fine-grained sand without any visible cryostructures. Black spots (2 to 5 mm in diameter) of degraded organics occurred in clusters. Whitish fine-grained sand layers (ca. 1

mm thick and 20 to 50 mm long) as well as pebbles (>2 mm up to 30 mm in diameter) were present. The slightly layered bluish-grey silt prevailed between 4.8 and 5.5 m a.s.l. The cryostructure was lens-like reticulated with 1 mm thick and 10 to 20 mm long ice lenses. Yellowish-brown material surrounded ice bands in contact with the sediment. Black spots (2 to 10 mm in diameter) of degraded organics occurred in clusters (Figure 4-7c), and whitish fine-grained sand was found in several layers. Between 5.5 and 6.2 m a.s.l., the cryostructure of the slightly layered bluish-grey silt changed to horizontal ice lenses (1 mm thick and 10 to 20 mm long). Black spots (2 mm in diameter) became rare. The uppermost part of the profile was characterised by an increasing content of brown peat lenses (10 mm thick and 20 to 50 mm long) and ended upwards in a thick layer of thawed peat with wood remains. Mollusc remains have also been found. The cryostructure was lens-like layered (1 mm thick and 10 to 20 mm long) until about 7 m a.s.l. and not visible above. The L14-12 exposure has been sampled for OSL and soil carbon analyses as shown in Figure 4-7.

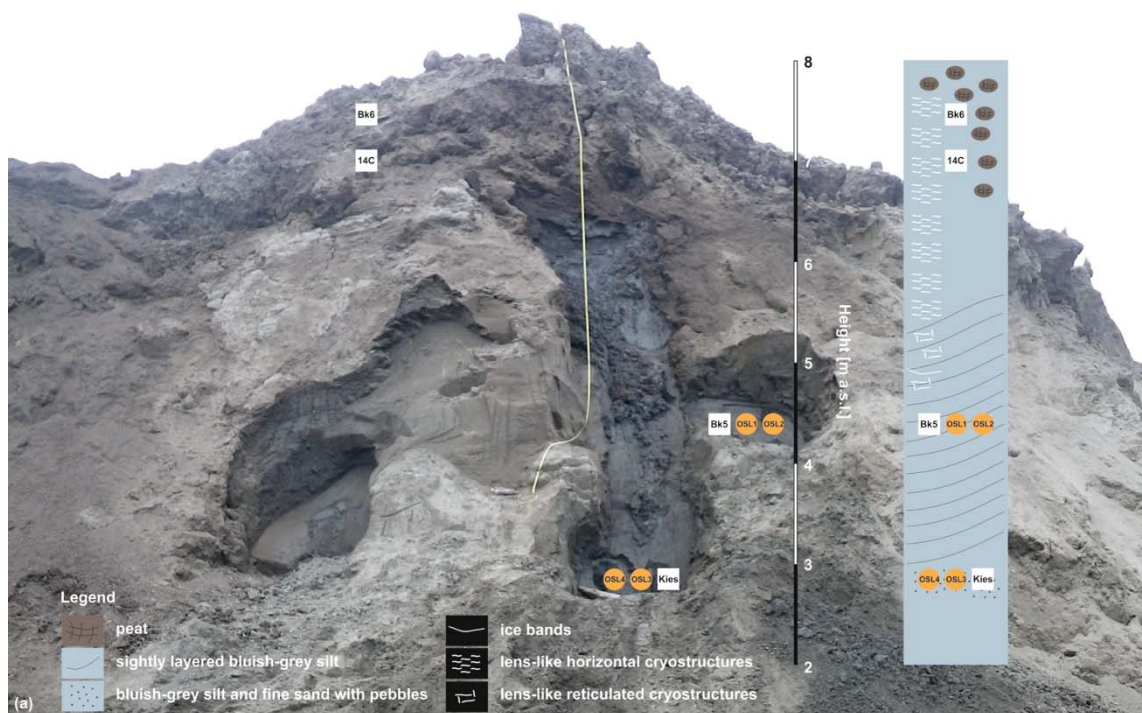


Figure 4-7 Profile L14-12 of Krest Yuryakh (Eemian) deposits in (a) overview of the studied exposure including a scheme of the described sediment units, (b) beach life and (c-g) detailed images of the sediment (continued on next page).

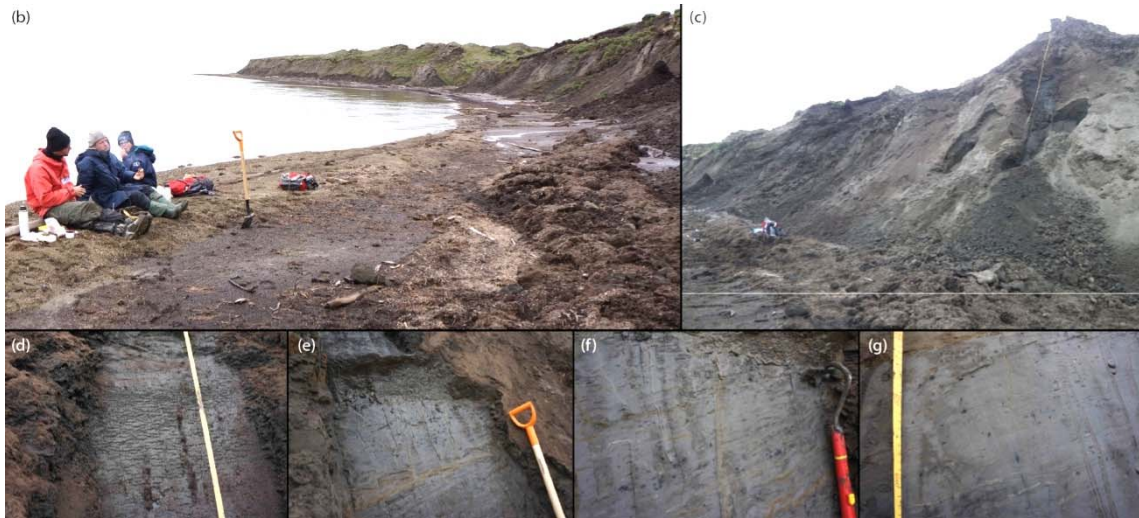


Figure 4-7 continued.

4.8 Molotkov Ice Complex on thermo terrace (profile L14-09)

In addition to the L14-03 core from spring 2014, the drilled baidzherakh (thaw mound) was sampled for OSL analyses about 1 m b.s. (Figure 4-8).

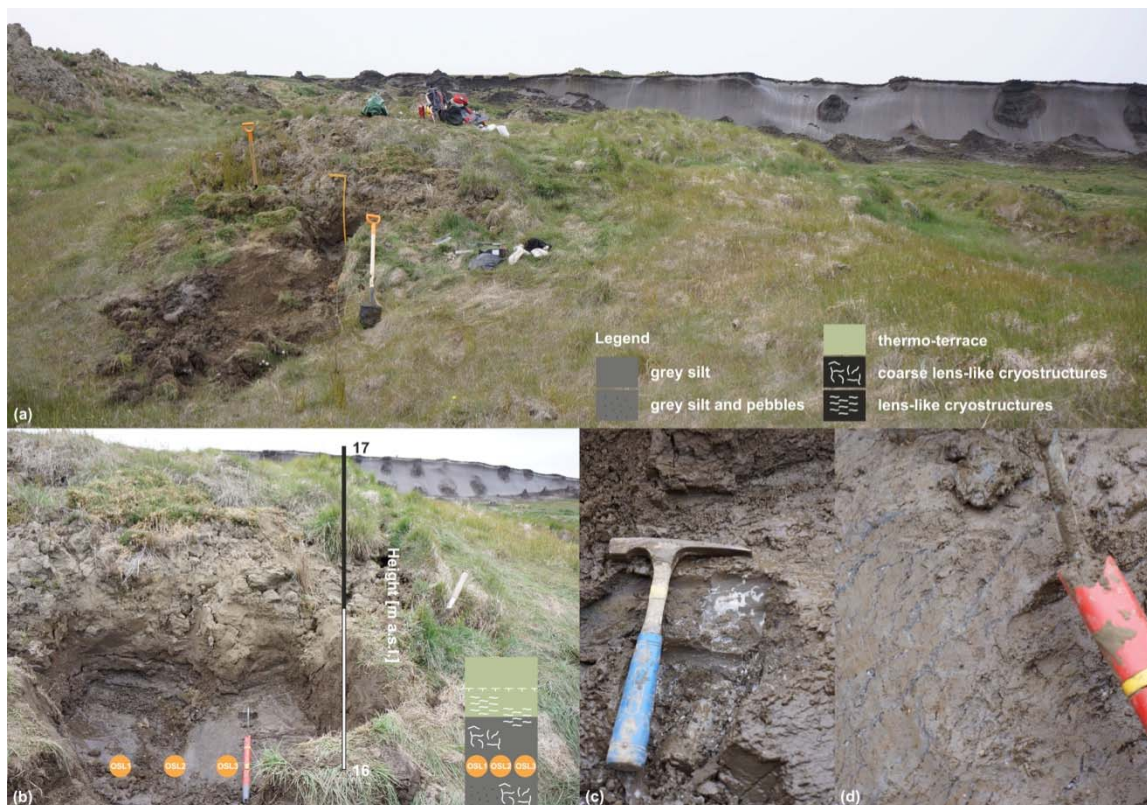


Figure 4-8 Profile L14-09 of Molotkov Ice Complex deposits showing (a) the baidzherakh position at the thermo terrace in front of the Ice Complex's wall, (b) scheme and image of the sampled profile, (c) and (d) detailed images of the exposed sediment.

The baidzherakh surface height was estimated to be 17 m a.s.l. The pit at the distal (southern) slope of the baidzherakh revealed ice-rich grey silt with single pebbles and organic lenses (50 x 50 mm) between about 15.7 and 16.3 m a.s.l.

The horizontal, lens-like cryostructure was composed of coarse lenses (1 to >1 mm thick and 10 to 50 mm long) and in places blocky ice (Figure 4-8c). Reddish-brown spots occurred. The overlying deposits were attributed to re-worked material of the thermo terrace, which was re-frozen below about 16.5 m a.s.l. and consisted of light-brown (spotty grey) silt with fine lens-like (<1 mm thick) and lens-like (about 1 mm thick) cryostructures (Figure 4-8d). The deeply fissured baidzherakh had an active layer depth of about 0.5 m.

4.9 Molotkov Ice Complex on thermo terrace (profile L14-08)

A baidzherakh was sampled for OSL and soil carbon analyses (Figure 4-9) directly at the Ice Complex wall, corresponding to the drilling position of L14-02 (see chapter 3). The baidzherakh formed a steep wall of about 4 m height with a foot height of 22 m a.s.l. The lowermost part was still connected to the Ice Complex wall. OSL samples were taken at 23.5 m a.s.l. and a soil carbon sample was taken at 23 m a.s.l.



Figure 4-9 Profile L14-08 of Molotkov Ice Complex deposits showing (a) the sampled baidzherakh and (b) its position directly in front of the Ice Complex wall, and (c) an detailed image of the exposure's sediment.

The light grey-brown silt between 22 to 25 m a.s.l. contained grass-roots concentrated in irregular small patches and single dark-brown organic spots (10x10 mm). A single pebble was found at 23.5 m a.s.l. The cryostructure was fine lens-like (<1 mm thick and 2 to 10 mm long) of different orientation (mainly horizontal, partly reticulated, partly ataxic) or did not exhibit any visible ice structures.

4.10 Molotkov Ice Complex on thermo terrace (profile L14-13)

A syngenetic, about 5 m wide ice wedge exposed at a smaller thermo-cirque was sampled for analyses of chlorine-36 (^{36}Cl) and dissolved organic carbon content (DOC). The exposed uppermost part of the ice wedge was 2 m high above the thermo terrace surface (Figure 4-10).



Figure 4-10 Profile L14-13 of Molotkov Ice Complex deposits on the thermo terrace with (a) a detailed image of the sampled ice wedge and (b) an overview image of the small thermo-cirque.

The bottom part was buried beneath the thermo terrace deposits. The wedge ice consisted of dirty transparent ice with single, 2 to 5 mm thick veins and rather non-oriented air bubbles. At about 1 m below the land surface, the ice wedge was cut using a chainsaw into three blocks that were labelled as L14-13-36CI-A, -B and -C.

4.11 Sartan Ice Complex (profile L14-07)

A stadial Ice Complex younger than the Molotkov (Yedoma) interstadial was studied in profile L7-07 (sampled in 2007 and described by Wetterich et al., 2011). Its deposits at the slopes of the Zimov'e River valley were exposed at the coast (Figure 4-11a). The location was sampled to retrieve additional material for OSL, palaeogenetic, soil carbon, ice-wedge DOC and ^{36}Cl analyses. The profile L14-07 was characterised by two stacked generations of ice wedges. Stable water isotope data revealed cold winter climate for both wedges by low mean values of about -37 ‰ for $\delta^{18}\text{O}$ and -290 for δD (Wetterich et al. 2011). The upper (2nd generation) ice wedge was exposed for about 3 m width and over 3 m height. The lower (1st generation) ice wedge is of unknown extent because it was mainly buried. The sampled sediment profile started at about 6 m a.s.l. (3 m b.s.; Figure 4-11b) above the lower ice wedge. A brown peat was exposed at both sides of the upper ice wedge between 6 and 6.7 m a.s.l. A silty grey matrix with reddish spots included numerous coarse plant remains. Samples for soil carbon were taken from the peat at 6.5 m a.s.l. and for palaeogenetics at 6.7 m a.s.l. (Figure 4-11b, d). Its cryostructure was fine lens-like with horizontal and subhorizontal single lenses (<1 mm thick and 2 to 5 mm long). A wavy-layered grey-brown silt was exposed between 6.7 and 7.2 m a.s.l. (Figure 4-11c). The silt included plant roots, larger organic lenses (5 to 10 mm in diameter) and black spots (1 to 2 mm in diameter). A fine lens-like ataxitic cryostructure occurred directly below an ice band, but most parts were frozen without visible (massive) ice structures. Two samples were taken for radiocarbon dating at 7 m a.s.l., one represented the plant material and a second one *in-situ* bone fragments (Figure 4-12). Between 7.2 and 7.4 m a.s.l. the grey brown silt contained numerous root remains and organic lenses (5 to 10 mm in diameter). Above 7.4 up to 8.4 m a.s.l., the silt color changed to light brown and the organic content (roots and lenses) decreased. A slight layering of the light brown silt appeared between 7.85 and 8.4 m a.s.l. Fine horizontal and subhorizontal ice lenses (<1mm thick and 2 to 5 mm long) were visible between ice bands (every 5 to 10 cm), which were oriented towards the ice wedge. In places, single vertical ice veins (1 to 2 mm thick and 50 to 100 mm long) were found. The boundary of the covering thermo terrace at about 8.4 m a.s.l. coincided with a distinct boundary that highlights the depth of the modern active layer. The unfrozen, 0.4 to 0.6 m thick layer consisted of light brown silt with roots and plant remains. Samples were taken for OSL and soil carbon analyses at 7.5 m a.s.l. and for DOC and ^{36}Cl analyses from the upper ice wedge at 7 m a.s.l.



Figure 4-11 Profile L14-07 of Sartan Ice Complex deposits west of the Zimov'e River mouth with (a) overview image of the coastal exposure, (b) image of the sampled profile, (c-i) detailed images of the exposed material.



Figure 4-12
Bone fragments found in-situ in profile L14-07.

4.12 Holocene Alas

The thermokarst basin (Alas) west of Cape Kammenyi Mys' has already been studied in 1999 (e.g. profile R33-A1, Andreev et al. 2009), 2007 (profile L7-08, Wetterich et al. 2009) and drilled in spring 2014 (L14-05, see chapter 3). Therefore, no additional sampling of sediments was performed in summer 2014. The surface features (e.g., high-centre polygons, thermo-erosion valleys) and coastal exposures were inspected visually (Figure 4-13). Surface samples were taken for soil carbon studies (see chapter 5). The coastal exposures exhibited the typical sediment sequence of the lateglacial lacustrine facies covered by Holocene thermokarst deposits as previously described by Andreev et al. (2009) and Wetterich et al. (2009). The lower lacustrine unit showed striking features including fine-layered and partly ripple-bedded lake deposits (Figure 4-13b, f), ice-wedge pseudomorphs (Figure 4-13d), vivianite minerals (hydrated iron phosphate; Figure 4-13e), mollusc and wood findings (Figure 4-13e, f, g), and epigenetic roots from syngenetic ice wedges penetrating from above. Deposits of boggy polygon tundra cover the lacustrine facies.

Syngenetic ice wedges (3 to 4 m top-wide) with contact to the surface polygon pattern separated the characteristic polygon fillings of layered sediment units and intercalated thick peat layers (Figure 4-13b). At the surface, the ice wedge pattern was characterised by thermo-erosional valleys draining the modern Alas. The resulting high-centre polygons point at on-going ice-wedge thaw (Figure 4-13c). The general structure of the deposits underlying the Alas were observed over several hundred meters between Cape Kammenyi Mys' and the mouth of the Maly Zimov'e River.



Figure 4-13 Images of the Holocene Alas surface (a, c) and the coastal exposure of its characteristic underlying sediments (b, d-g) including the lower lacustrine facies and the upper polygon facies.

4.13 Modern floodplain of the Zimov'e River (profiles L14-15, -16)

Sampling of modern floodplain deposits intended to obtain additional material of known age (i.e. modern) for OSL studies. Such material allows independent tests of the material-specific luminescence properties and the residual signals and may serve as an equivalent for palaeo-floodplain sediments (e.g. deposits of the Kuchchugui Suite). Surface pits have been dug down to 0.4 m b.s. at two

positions (vegetated vs. bare) in the middle level of the floodplain (Figure 4-14a, b).



Figure 4-14 Profiles L14-15 and L14-16 at the Zimov'e modern floodplain in (a) and (b) overview images and (c) and (d) detailed profile images.

Unfrozen samples were taken for OSL analyses at depths of 0.05 (L14-15-OSL1), 0.1 (L14-16-OSL1) and 0.15 m b.s. (L14-16-OSL2) (Figure 4-14c, d). The floodplain deposits were composed of light brown, grey-brown, and dark grey silt layers alternating with yellowish sand and pebble layers. Orange zones marked the contact between the grey to brown silt and the yellowish sand and pebbles. Some black organic bands were intercalated and a black organic-rich zone occurred in the lower part of profile L14-16 at about 0.25 to 0.3 m b.s. In profile 14-15 fine roots concentrated at surface (modern vegetation).

5 SOIL ORGANIC MATTER STUDIES

Josefine Walz, Georg Schwamborn, Sebastian Wetterich

5.1 Introduction

Soils and soil processes in permafrost-affected landscapes are strongly influenced by the predominant cold temperatures and often water-logged conditions, resulting in slow carbon turnover rates. Further, freeze-thaw processes such as cryoturbation incorporates soil organic matter into deeper soil layers (Bockheim, 2007), where it is protected from microbial decomposition. Thus, permafrost-affected soils and sediments have accumulated substantial amounts of organic matter. Within a warming climate, however, soils could be subjected to increased microbial decomposition and add to the greenhouse gas concentration in the atmosphere. It remains unclear, how much and how fast organic matter can be mineralized upon permafrost thaw (Beer, 2008).

To study near-surface processes and possible changes in soil organic matter dynamics on Bol'shoy Lyakhovsky, five representative geomorphological units were sampled during the summer campaign, i.e. (1) the Yedoma Ice Complex, (2) thermo-erosional valleys and their log deposits, (3) thermo-cirques, (4) Alas deposits, and (5) floodplain deposits from the Zimov'e River valley (Figure 5-1). Samples were taken for the purpose of assessing potential greenhouse gas release from permafrost degradation and active layer deepening. Incubation experiments with soils from the different geomorphological units may reveal differences in organic matter decomposability, expressed by CO₂ and CH₄ production rates under aerobic and anaerobic conditions (Figure 5-2).

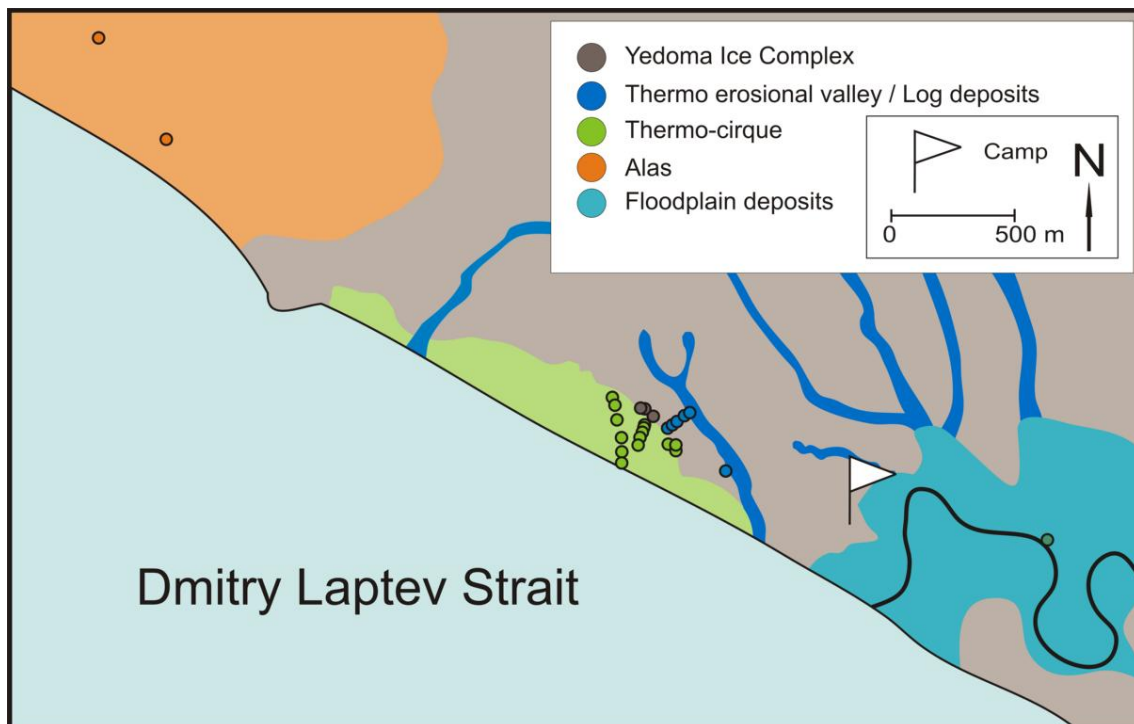


Figure 5-1 Sample locations on the southern coast of Bol'shoy Lyakhovsky.

To obtain samples, soil pits were dug to the permafrost table and samples were taken horizon-wise from the thawed active layer. If a location was water-saturated, a soil monolith was excavated. Additional permafrost samples were taken from the thermo-cirque and the floodplain of the Zimov'e River. Frozen samples were obtained manually using an axe and hammer. After soil profile descriptions, sub-samples were taken from the identified soil layers and individually packed in plastic bags or glass containers and kept frozen in an ice cellar (lednik - ледник in Russian). Samples have been kept frozen until further analysis in the laboratory.

Soil descriptions and classifications were made according to the World References Base (WRB) for Soil Resources (IUSS, 2014), which is based on the identification of diagnostic horizons, properties, and materials. After WRB, all sampled soils are classified as Cryosols (CR), since they have a cryic horizon starting within 100 cm of the soil surface. Further differentiation in the field can be made between soils with organic rich histic horizons (hi), mainly found in wet, water-logged areas, turbic (tu) soils with marked features of cryoturbation, and soils with gleyic properties (gl). A finer differentiation will be made in the laboratory with additional soil parameters; e.g. carbon and nitrogen contents, pH, electrical conductivity, grain size.

In the following chapter, soils sampled in the five identified geomorphological units are described and some characteristic soil profiles are shown. Sample depths are given in cm below soil surface. A complete sample list with basic descriptions is given in Appendix 5-1.

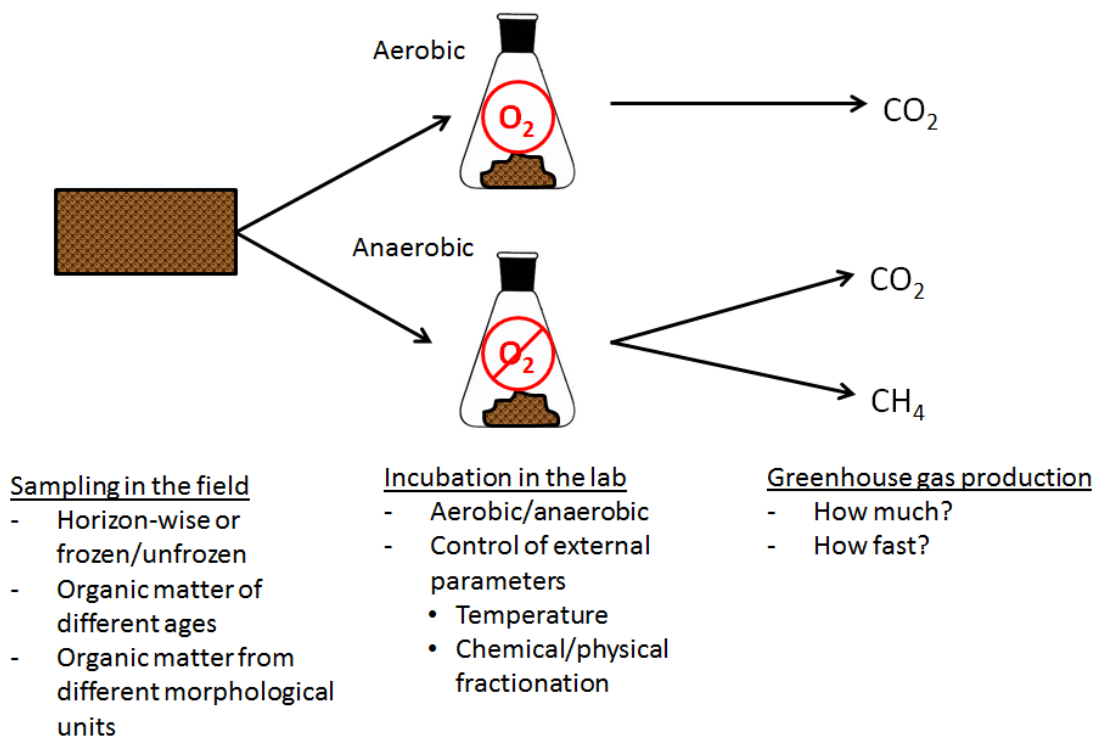


Figure 5-2 Incubation experiment design.

5.2 Yedoma

The surface of the Yedoma Ice Complex is characterized by the occurrence of baidzerakhs. These 1-2 m high thaw mounds are left elevated from the surrounding terrain when the ice wedges of the former ice wedge polygonal tundra melted. Soils directly within baidzerakhs (Figure 5-3) did not differ greatly from soils from the lower surroundings. Soils had generally very thin (<2 cm - max. 5 cm) topsoil layers. Most of the soil columns were brownish in color, with signs of cryoturbation and the incorporation of peaty lenses into deeper soil layers. Above the permafrost table, soils from both the baidzerakh as well as the surrounding areas showed weak to moderate development of gleyic properties. Differences were observed in thaw depth. Dry, well-drained baidzerakh were generally thawed deeper (up to 60 cm) than the moister surrounding area (30-45 cm).

Turbic Cryosol (gleyic)

CR-tu--gl

Yedoma Ice Complex (17.08.2014)

N 73°20.169' E 141°19.667'

Horizon	Depth cm	Texture	Roots
Ah	0-5	silt	many
Bhg@	5-35	silt	many
Bg@	35-55	silt	common

A cryoturbated soil with a thin topsoil layer enriched in organic matter (Ah) overlying mineral subsoil with distinct mottling. The upper B horizon is marked by brownish color with greyish mottles (Bhg), while the lower B horizon is marked by greyish color with brownish-orange mottles. The @ stands for signs of cryoturbation.

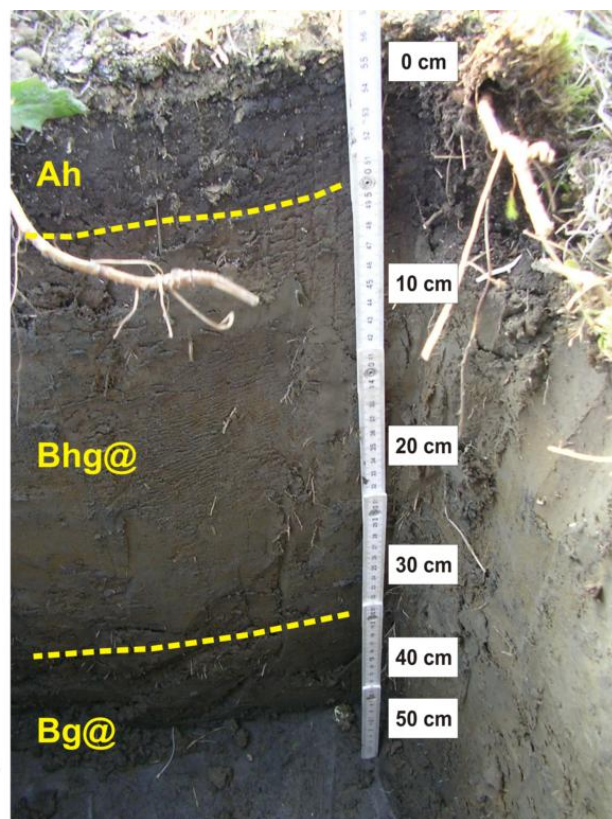


Figure 5-3 Soil profile from the Yedoma Ice Complex (sample code JW14 BL22).

5.3 Thermo-erosional valley / Log deposits

Several thermo-erosional valleys transect the surface of the Yedoma Ice Complex. They are presumably underlain by thawing ice wedges and have no baidzerakh at the surface. These smaller tributary valleys drain into larger log valleys. A transect with five points (sample codes JW14 BL13 P1-5) has been sampled along one of these valleys from the edge of a steep exposed ice wall bordering a thermo-cirque towards the center of a water-saturated log valley. Hydromorphic properties were generally developed more strongly in the wetter lower parts towards the log valley than in the drier, better drained upper parts near the ice edge. The drier soils showed very little horizon development and were mainly of brownish color. Right above the permafrost table, reducing

conditions resulted in a more greyish color, often in combination with orange mottles mostly near roots. The upper parts of the soils often lacked the accumulation of partly decomposed organic matter typical for topsoil layers. Only the sample point located in the central part of the log valley clearly developed a diagnostic histic horizon (sample code JW14 BL13 P5). The resulting soil is classified as a Histic Reductaquic Cryosol, where a thick histic layer of slightly to moderately decomposed organic matter overlies a gleyic mineral layer (Figure 5-4).

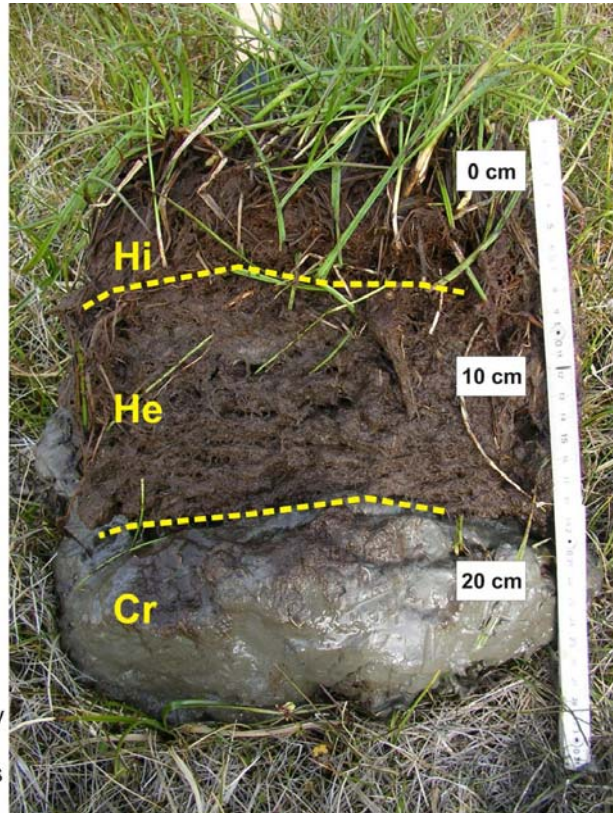
Histic Reductaquic Cryosol

CR-ra.hi

Log valley deposits (03.08.2014)

N 73°20.165' E 141°19.959'

Horizon	Depth cm	Texture	Roots
Hi	0-6	fibric	many
He	6-18	fibric	many
Cr	18-36	silt	none



A organic-rich water-saturated soil with a thick histic horizon consisting of an organic horizon with slightly decomposed organic material near the surface (Hi) and moderately decomposed organic material below (He), overlying a C horizon with reducing conditions and no other pedogenetic change (Cr).

Figure 5-4 Soil profile of log deposits (sample code JW14 BL13 P5).

5.4 Thermo terrace (thermo-cirque)

Several thermo-cirques mark the southern coast of Bol'shoy Lyakhovsky. Steep walls (up to 20 m) of ice-rich Yedoma deposits are exposed along several hundred meters. As the ice melts and the walls retreat, sediment and soil packages are thawed out and left as baidzerakh forming the thermo-cirques.

Two transects with five baidzerakh each were sampled across the largest thermo-cirque. Incubation studies of the sampled baidzerakh will be conducted in the laboratory to study the effect and timing of thawing out on remobilization of previously frozen carbon and reactivation of microbial decomposition of soil organic matter. The first transect went from the northwestern edge of the thermo-cirque towards the central drainage channel (sample codes JW14 BL3-7). Five baidzerakh with prominent topography (2-3 m height) and varying degrees of vegetation have been sampled. Samples were always taken in pairs; one sample from the unfrozen top part of each baidzerakh and one from the frozen lower part. The second transect went from the bottom of the ice wall in

the central part of the thermo-cirque towards the center drainage valley (sample codes JW14 BL8-12). Compared to the first transect, baidzerakh from the second transect were smaller and to a greater extent eroded. Along the second transect, only samples from the thawed part were taken.

The most prominent feature of soils from the thermo-cirque was the development of gleyic properties, represented by alternating oxidizing and reducing conditions within the soil profile (Figure 5-5). The depth and strength of these properties, however, varied between the individual baidzerakh and were strongly dependent on micro-topography and drainage. The strongest reducing conditions with clear signs of mottling were found along the second transect with little topography and drainage. Most soils showed signs of cryoturbation. The resulting soil is classified as a Turbic Cryosol (Gleyic).

Turbic Cryosol (Gleyic)

CR-tu--gl

Thermo cirque (02.08.2014)

N 73°20.119' E 141°19.611'

Horizon	Depth cm	Texture	Roots
Bgh@	0-26	silt	common
Bh@	26-33	silt	few
Bg@	33-55	silt	few

A cryoturbated soil with changing redoximorphic characteristics. The uppermost B horizon shows gleyic properties and an accumulation of organic matter (Bgh). The middle B horizon is enriched in organic matter (Bh) and lacks a clear gleyic color pattern. The lower most B horizon is marked by distinct pattern of greyish and orange mottles. The @ stands for signs of cryoturbation (evident here by the uneven boundaries between layers and incorporation of organic matter into deeper soil layers).

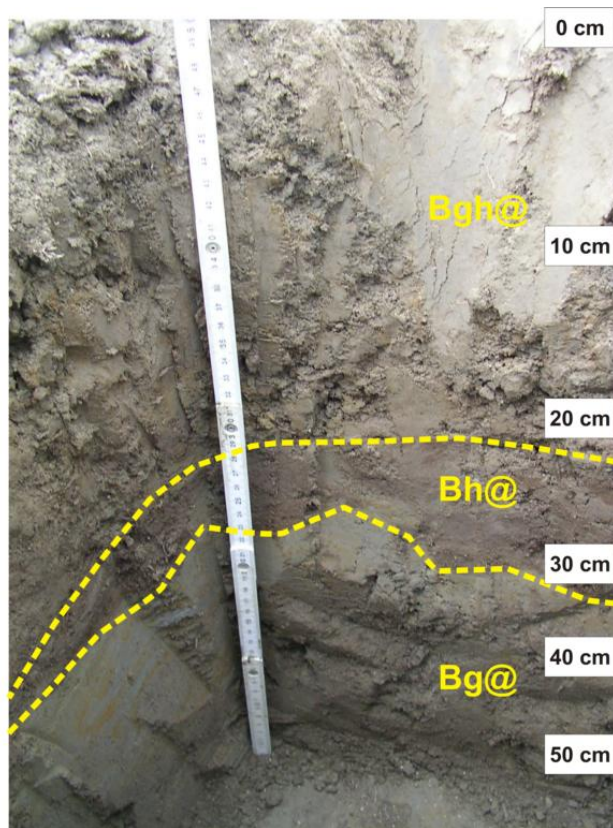


Figure 5-5 Soil profile from the thermo-cirque (sample code JW14 BL11).

5.5 Alas

A large Alas is located about 4 km west of the Zimov'e River. The Alas is intersected by several large water-filled gullies and the surface is characterized by high-centered polygons. Within the Alas, two locations were chosen for representative surface samples. The first location was located in the drier central part of the Alas, several tens of meters away from larger gullies. The sample location is grass-dominated (mainly *Carex* sp.) with few mosses. The thaw depth at the day of sampling (11.08.2014) was only 13 cm; it was the shallowest thaw depth from all observed sample locations during the field campaign. Cryoturbation resulted in uneven layer boundaries and the permafrost table impeded drainage, resulting in the development of gleyic

properties (Figure 5-6). The resulting soil is classified as a Turbic Cryosol (Gleyic).

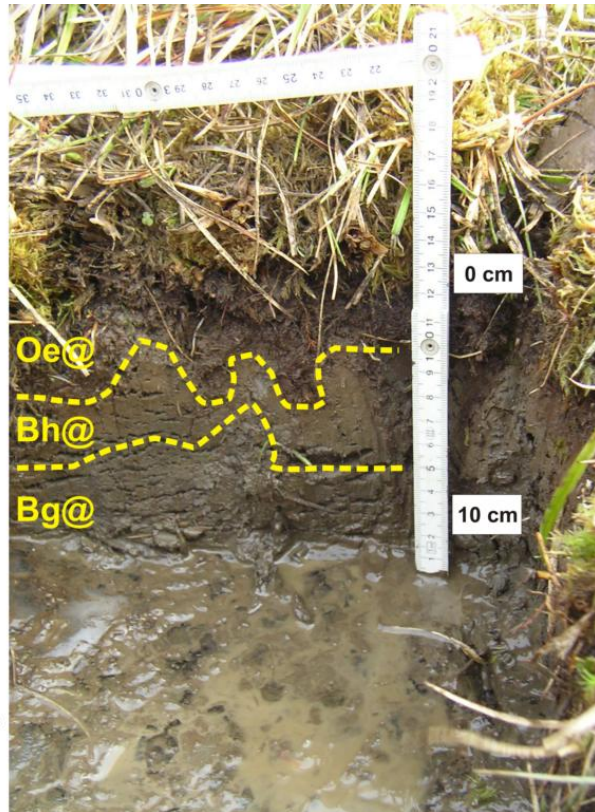
Turbic Cryosol (Gleyic)

CR-tu--gl

Holocene Alas deposits (11.08.2014)

N 73°21.513' E 141°14.806'

Horizon	Depth cm	Texture	Roots
Oe@	0-3	fibric	many
Bh@	3-8	silt loam	few
Bg@	8-13	silt loam	few



A cryoturbated permafrost-affected soil with a thin organic horizon with moderately decomposed organic material (Oe) overlying two B horizons with an accumulation of organic matter in the top layer (Bh) and reducing conditions below (Bg). The @ stands for signs of cryoturbation (evident here by the uneven boundaries between soil layers).

Figure 5-6 Soil profile of Alas deposits from a drier grass-dominated site (sample code JW14 BL15).

The second location was located in the wetter eastern part of the Alas. The sample location is moss-dominated (*Sphagnum* sp. and *Calliergon* sp.) with few grasses and a water table at the soil surface. These conditions are favorable for the development of histic horizons with partly decomposed mosses covering deeper gleyic mineral soil layers (Figure 5-7). The resulting soil is classified as a Histic Reductaquic Cryosol.

Histic reductaquic Cryosol

CR-ra.hi

Holocene Alas deposits (11.08.2014)

N 73°20.865' E 141°15.525'

Horizon	Depth cm	Texture	Roots
Oe	0-16	fibric	many
Bhr	16-31	silt loam	common

A organic-rich water-saturated soil with a thick histic horizon consisting of an organic horizon with moderately decomposed moos (Oe) overlying a B horizon with reducing conditions and accumulation of organic matter (Bhr).

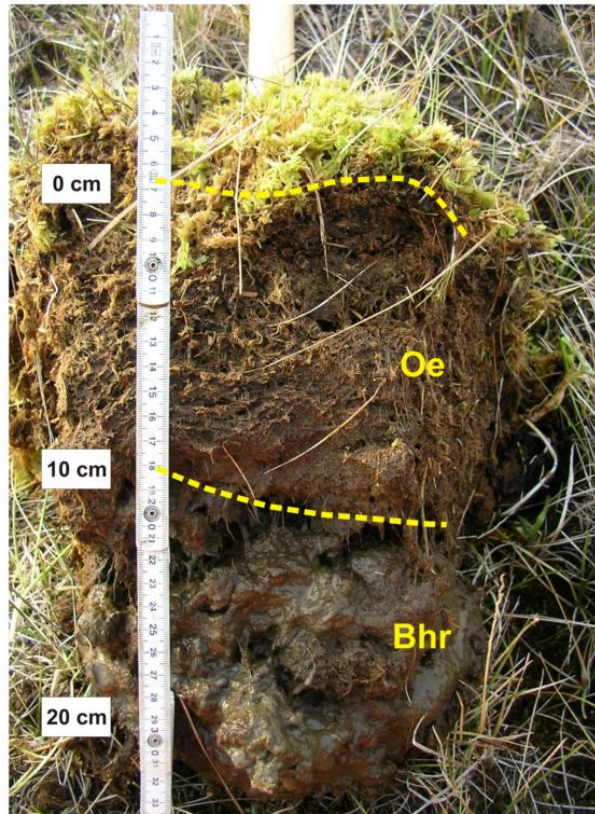


Figure 5-7 Soil profile of Alas deposits from a wet moss-dominated site (sample code JW14 BL16).

5.6 Modern floodplain deposits of the Zimov'e River

Floodplain deposits of the Zimov'e River were sampled at an outcrop about 2 km upstream from the river mouth. The deposits were layered with alternating light sandy and darker colored silty layers and with interbedded organic material (mostly fragments of drift wood). Layer thicknesses varied between a few mm to 2-3 cm. Sporadically thicker layers showed internal finer layers (Figure 5-8).

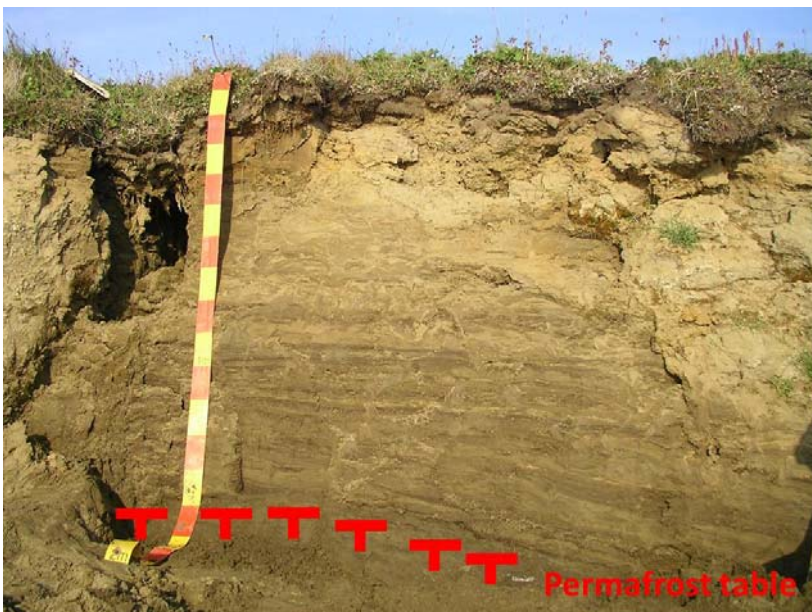


Figure 5-8 Floodplain deposits of the Zimov'e River (sample code JW14 BL14).

5.7 Summary

Soils at the southern coast of Bol'shoy Lyakhovsky were generally poorly developed. Marked difference occurred in the presence of hydromorphic patterns (e.g. gleyic properties) and some variation in soil color between different profiles and within profiles with depth. All soils had a cryic horizon within 100 cm from the soil surface and classified as Cryosols after WRB. In the field, soils were mainly classified as Turbic Cryosols or as Histic Reductaquic Cryosols. Turbic Cryosols with clear signs of cryoturbation occurred mainly in drier parts and developed strong gleyic properties above the permafrost table. Histic Reductaquic Cryosols occurred only in water-saturated depressions, where thin peat layers overlie gleyic mineral layers. Further analytical measurements of soil parameters in the laboratory will likely give more information about soil development stages and greenhouse gas production potentials at the different locations.

6 TACHYMETRY AND KITE AERIAL PHOTOGRAPHY

Stephan Schennen, Niklas Allroggen, Sebastian Wetterich, Jens Tronicke

Accurate positioning is an important prerequisite to integrate and compare different field datasets, especially, if acquired by different methods or at different spatial scales. Thus, geodetic surveying is a crucial part of a multidisciplinary field campaign. In addition, kite aerial photography is an easy to deploy and cost-efficient method to obtain basic remote sensing data. Here, we used this method for gathering supplementary information regarding our field sites and their surroundings as needed, for example, for field site documentation and a detailed interpretation of geophysical data and models.

6.1 Tachymetry

In both the spring and the summer expedition, we used a self-tracking total station for surveying exposures, boreholes etc. and for positioning geophysical data points. In total, we set up five local coordinate systems (one per morphology). An additional coordinate system was used to relate four coordinate systems (located between coring location L14-04 and Zimov'e River mouth, see Figure 3-1) to sea level and to establish a link between datasets recorded at the different morphologies.

At each site, we used at least four fixpoints for the initial setup of a local coordinate system. These fixpoints were marked in the field by ground pegs. Thus, we were able to relocate within an already defined coordinate system and to interrupt and resume data acquisition on different days.

We used a Leica TCP 1203 Total Station (Figure 6-1) with auto-tracking capability. This feature was also used for kinematic geophysical data acquisition such as 2D and 3D GPR surveying (see chapter 7).



Figure 6-1 Geodetic surveying equipment used for positioning: self-tracking total station (left) and prism (right).

6.2 Kite Aerial Photography

A kite aerial photography (KAP) system consists basically of a kite and a camera. The camera is placed in a camera rig (fixed at the kite's rope; Figure 6-2) for leveling and to sustain a constant shooting angle. It is either triggered manually by a remote control or automatically with a constant shooting interval.



Figure 6-2 Kite aerial photography system that was used as supplementary low-cost remote sensing tool. Left: Field impression of data acquisition. Right: Close up of kite and camera-equipped rig.

During the summer campaign, we collected ~400 photographic images with our KAP system (Figure 6-2). We used a HQ Power Sled L 3.0 with an area of 3 m², suitable for wind speed of 2-5 bft (according to the manufacturer). A 200 m rope was equipped with a self-constructed rig to keep a common compact camera as horizontal as possible. In Siberia, we used the commercially available cameras Canon Ixus 130 and Canon PowerShot A2500 employing an auto shooting mode with one image every 10 seconds. We acquired pictures in a height of approximately 40 to 150 m and covered in total an area of approximately 50 ha (according to preliminary georeferenced data). As an example, Figure 6-3 shows a composite image of the Zimov'e River mouth.

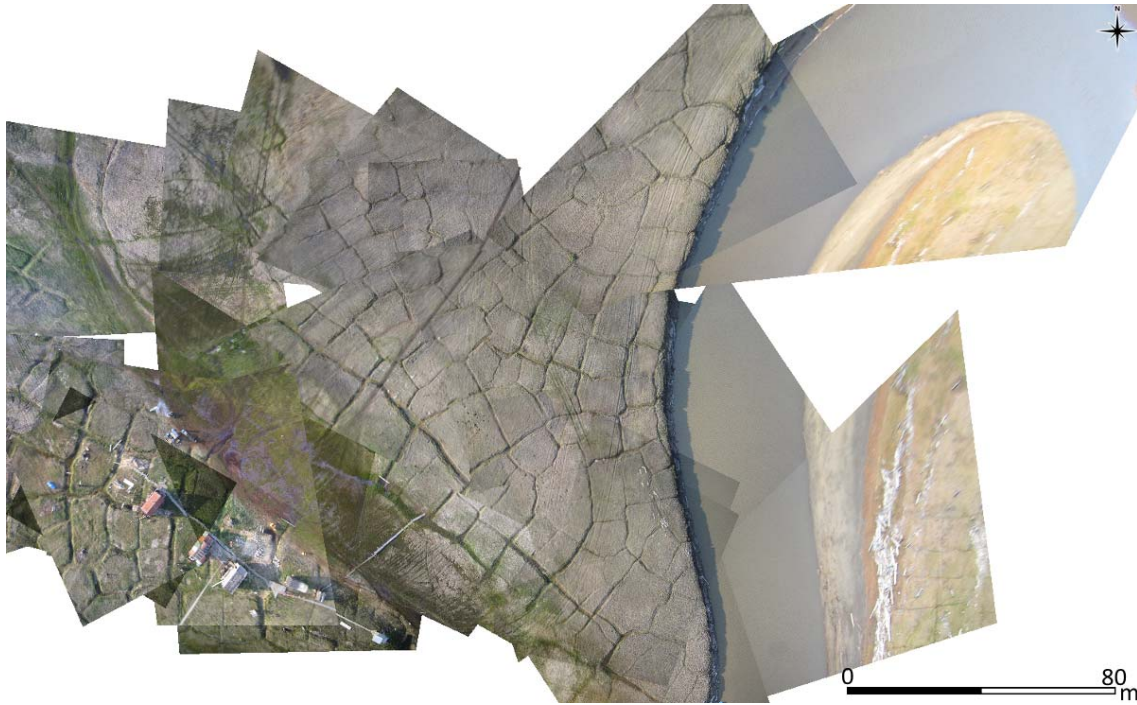


Figure 6-3 Example of a preliminary processed orthomosaic of KAP data acquired at the Zimov'e River mouth. The composite image shows our camp (lower left corner), which was located next to a polygonally patterned floodplain (central part of the image) of the Zimov'e River (right part of the image).

7 NEAR SURFACE GEOPHYSICS

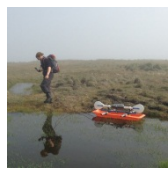
Stephan Schennen, Niklas Allroggen, Jens Tronicke

The main objective of geophysical surveying is to image and examine subsurface structures in the vicinity of sample locations such as coring sites (Table 7-1). Thus, we intend to provide detailed subsurface models to upscale multidisciplinary results that are obtained on core samples.

The employed near surface geophysical methods such as ground-penetrating radar (GPR), electromagnetic induction (EMI) and electrical resistivity tomography (ERT) provide the opportunity to image and characterize the subsurface based on physical properties such as electrical resistivity or dielectric permittivity. All three methods are non-invasive and provide data at different spatial resolution and penetration depth and, thus, provide complementary information suitable for an integrated interpretation and to diminish ambiguities when interpreting individual datasets.

In the following, we briefly review the employed geophysical techniques and provide information regarding the used hardware, the employed surveying geometries, and other important technical parameters. After that, we provide some typical data examples (preliminary results) for each field site surveyed during the two field campaigns in spring and summer. Table 7-1 provides a simplified summary of applied surveying methods for each survey site.

Table 7-1 Overview regarding geophysical surveying (GPR, EMI, and ERT) on Bol'shoy Lyakhovsky in 2014. "x" on gray background denotes data acquisition in spring, whereas "x" on green background denotes data acquisition in summer. KAP data acquisition is shown additionally.

Survey site								
	GPR		EMI		ERT		KAP	
Zimov'e River mouth	x	x	x	x		x		x
Thermo terrace	x							x
Yedoma	x	x	x	x		x		x
Thermo-erosional valley		x		x		x		x
Alas	x	x				x		x

7.1 Employed geophysical techniques

A **ground penetrating radar** (GPR) system is based on two antennas, which are connected to a data acquisition unit. The transmitting antenna excites an electromagnetic wave field, which is recorded by a second antenna (receiving antenna) placed at a certain distance (offset) to the transmitter. The radiated waveform exhibits a broad frequency range around a dominant frequency primarily depending on the design of the antennas (common dominant

frequencies are between 50 MHz and 1 GHz). The waveform is modified (e.g., in its frequency content and amplitude) along its travel path through the subsurface depending on the electromagnetic properties of the media.

Concerning common geomaterials electromagnetic energy propagates the fastest in air (~0.30 m/ns) and the slowest in liquid water (~0.03 m/ns). Attenuation of the electromagnetic wave depends on the electrical resistivity of the medium. High resistive media (such as frozen soils or ice) are transparent for electromagnetic waves while liquid water typically reduces the resistivity and, thus, results in higher attenuation. Thus, GPR can be considered as suitable tool to investigate permafrost environments.

Here, we used a Sensors and Software Inc. pulseEkko Pro System with three pairs of unshielded antennas (nominal center frequencies of 50, 100, and 200 MHz). In common offset (CO) mode, antennas were generally mounted in a fixed distance of 1 m on a special surveying platform. Positioning was performed with a self-tracking Leica Total Station TCP 1203 (see also chapter 6) which automatically tracked a prism mounted above the center of the sledge (Figure 7-1). Furthermore, we acquired several common-midpoint (CMP) datasets to derive 1D velocity models at selected locations. These velocity models are critical for processing and interpreting our CO datasets. When acquiring CMP data, we uniformly increased the offset between the antennas (typically in increments of 10 cm), while the midpoint between was fixed. Maximum CMP offsets are listed in the Appendix 7-1 to 7-5.



Figure 7-1 Impression of common-offset GPR data acquisition on Bol'shoy Lyakhovsky. GPR transmitter (denoted by red rhomb) and receiver (denoted by blue rhomb) are fixed on a sledge. The sledge is equipped with a prism and pulled along several closely spaced (< 0.5 m) survey lines across the field site. GPR data are acquired with a constant trigger frequency ("freerun" mode). During data acquisition, a total station tracks the prism automatically and provides coordinates for each trigger position with cm accuracy.

Electromagnetic induction (EMI) surveying is a near-surface geophysical method based on the induction of eddy currents in the subsurface. Survey instruments basically consist of two coils and a data acquisition unit. A transmitter coil excites a primary magnetic field at a fixed frequency, which induces electrical currents in the conducting underground. These eddy currents excite another, secondary magnetic field, which can be recorded using the receiver coil. Sensitivity to a certain depth interval depends on coil orientation,

coil spacing and excitation frequency.

Here, we used a GSSI Profiler equipped with two coplanar coils at a fixed distance of 1.21 m. As a rough estimate, our response was dominated by the subsurface conductivity of the uppermost 2 m. However, preliminary data investigation and test surveys provided evidence for technical problems (drift problems), which was the major reason to focus on GPR and ERT data acquisition later on. Depending on the field conditions, the GSSI profiler was mounted on a pulka (Figure 7-2) or carried by hand.



Figure 7-2 Impression of EM data acquisition on Bol'shoy Lyakhovsky. The EMI device is mounted on a pulka and pulled across the survey site. A manually carried data logger triggers data acquisition with a constant time interval. Positioning is either performed by a self-tracking total station or with an internal GPS of the data logger.

Electrical resistivity tomography (ERT) is mainly used to infer a 2D resistivity model of the subsurface along a survey line. Our ERT system consists of fifty electrodes, a multi-core cable, control unit with integrated power supply, and a field computer for survey setup and control as well as storing the data (Figure 7-3). A slowly alternating direct current is injected into the ground at two electrodes (A and B). Two other electrodes (M and N) are used to measure the potential difference. Taking values and the geometry (positions of electrodes A, B, M, and N) into account, an apparent resistivity can be calculated. Successive combination of all electrodes in groups of four electrodes (A, B, M and N) results in a so-called pseudosection, which contains data for different depth levels along the survey line.



Figure 7-3 Impression of ERT data acquisition on Bol'shoy Lyakhovsky. Our survey lines consist of 50 electrodes that are connected by a multi-core cable to a control unit with integrated power supply. A laptop is used for data acquisition.

For all survey lines, we used two classical electrode configurations known as Wenner and Dipole-Dipole configurations (more details can be found in common textbooks), which are known for their robustness and high lateral resolution, respectively. In a final step, apparent resistivity data are inverted to reconstruct a 2D resistivity model of the subsurface. We expected that resistivity variations in the active layer are mainly caused by soil moisture changes. Thus, we also acquired supplementary Time Domain Reflectometry (TDR) data along most of our ERT profiles to estimate soil moisture content within the uppermost soil layers.

7.2 Zimov'e River mouth

In spring and summer, the surroundings of our camp at the Zimov'e River mouth (see Figure 3-1 for location and Figure 7-4 for a photograph) were used to test the functionality of our geophysical equipment and to select optimum survey configurations. In spring, we acquired GPR data along two 290 m long traverses (Figure 7-5, Annotation A1). We used three antenna pairs with nominal center frequencies of 50, 100, and 200 MHz. In all datasets, penetration depth was comparable (~200 ns). However, taking penetration depth, data quality, resolution, and handling into account, we considered the 100 MHz antenna pair for most of our field sites surveyed later on. Furthermore, we acquired a supplementary profile (Figure 7-5, profile A2) across the floodplain and a multi-offset profile along traverse A3. An example of 100 MHz GPR common offset data is shown in Figure 7-6.

In summer, we collected additional GPR, ERT, TDR, and EMI data. We tested successfully GPR antennas with center frequencies of 100 and 200 MHz along profile B1. Furthermore, we acquired TDR and ERT data along profile B2. We collected EMI data on profile B1, B3, and B4. The latter two are located on the floodplain and intersected with the 100 MHz GPR profiles acquired in spring.



Figure 7-4 Impression of GPR data acquisition on the western part of profile A1 (see Figure 7-5) in spring. The eastern part of the profile can be seen in foreground. Northernmost point of both profiles is located on the crest at the horizon.

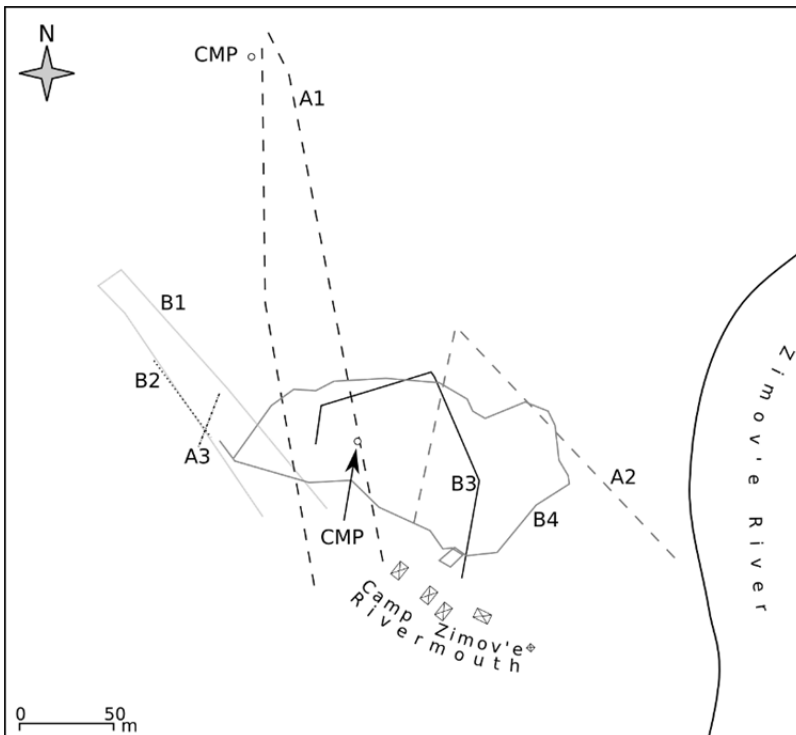


Figure 7-5 Map illustrating the locations of geophysical datasets at the field site Zimov'e River mouth. Profiles A1, A2, and A3 were acquired in spring and profiles B1, B2, B3, and B4 in summer. Annotations are explained in more detail in Appendix 7-1. The location of Zimov'e River mouth is shown in Figure 3-1.

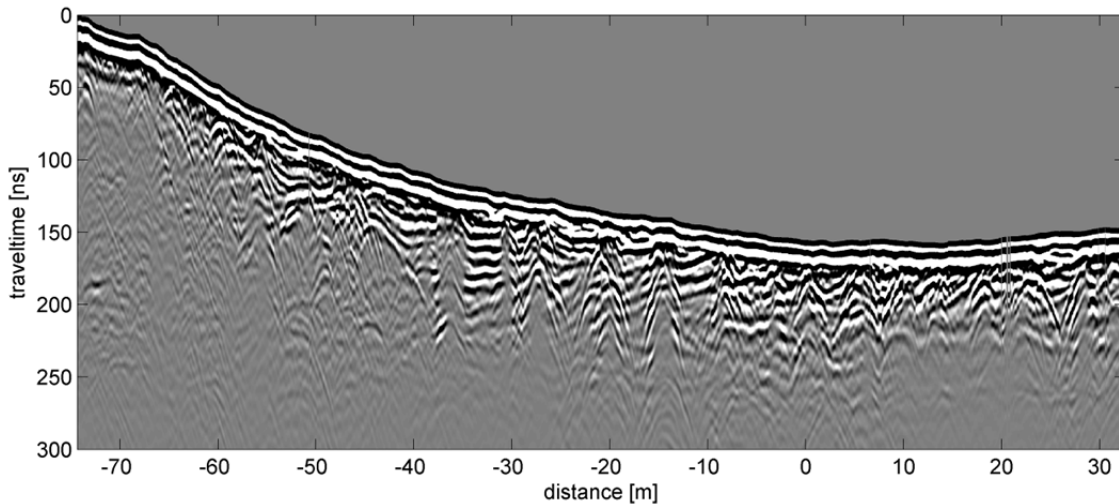


Figure 7-6 Example of 100 MHz GPR field data acquired on the eastern branch of profile A1. Data processing included time-zero correction, bandpass filtering, amplitude scaling (t^2 amplitude scaling), and topographical correction. Preliminary results of a nearby CMP suggest a propagation velocity of 0.17 m/ns. Based on this velocity, the penetration depth along this profile is approximately 10-20 m. The GPR data show a complex pattern of subhorizontal reflectors (e.g., at distances between -35 m and -10 m), which are intersected by diffraction hyperbolas. Both features are probably related to the typical polygonal patterns consisting of ice wedges and sediments.

7.3 Thermo terrace

Our first 3D GPR dataset was acquired in spring on the thermo terrace (see Figure 3-1 for location and Figure 7-8 for a photograph). The survey covers an area of roughly 40 m x 20 m, which exhibits a total topographic variation of ~4.60 m. Sediment samples are available at the borehole location L14-03 (Figure 7-7). We set up the total station within a group of baidzerakhs close to the survey area for calm positioning conditions (Figure 7-8). However, we had to interrupt data acquisition several times to protect our equipment from harsh weather conditions such as snow storms and, thus, data acquisition lasted five days in total. A drawback of the sheltered position within the baidzerakhs was a restricted view to the survey site. As a consequence, we skipped a small inaccessible area in the eastern part of the survey site (see shaded area in Figure 7-8).

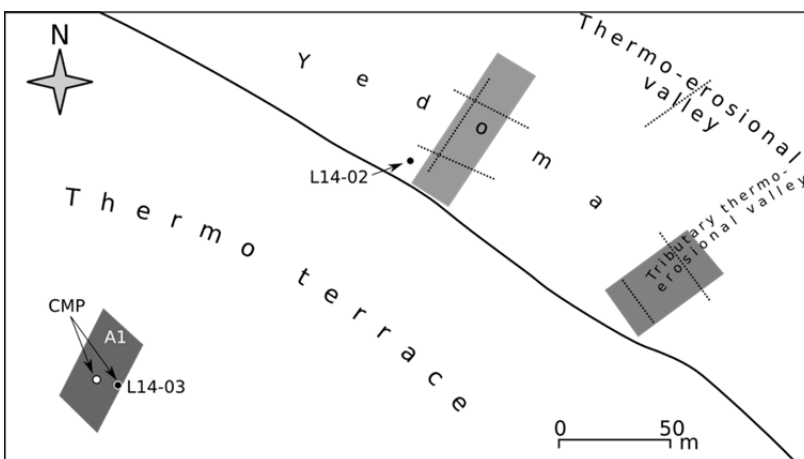


Figure 7-7 Map illustrating the locations of geophysical datasets at the field site thermo terrace (lower left part of the figure) and adjacent survey sites. Annotations are explained in more detail in Appendix 7-2. Survey profiles and areas of adjacent sites are annotated in Figure 7-10 and 7-14.

Although surveying at this site was challenging in terms of meteorological and topographical conditions (snow fall, changing topography below snow cover), we sustained a dense dataset with generally five or more data traces per 20 cm x 20 cm. Spatial gaps within the dataset are generally small compared to the observed wave length of approximately 1.60 m.

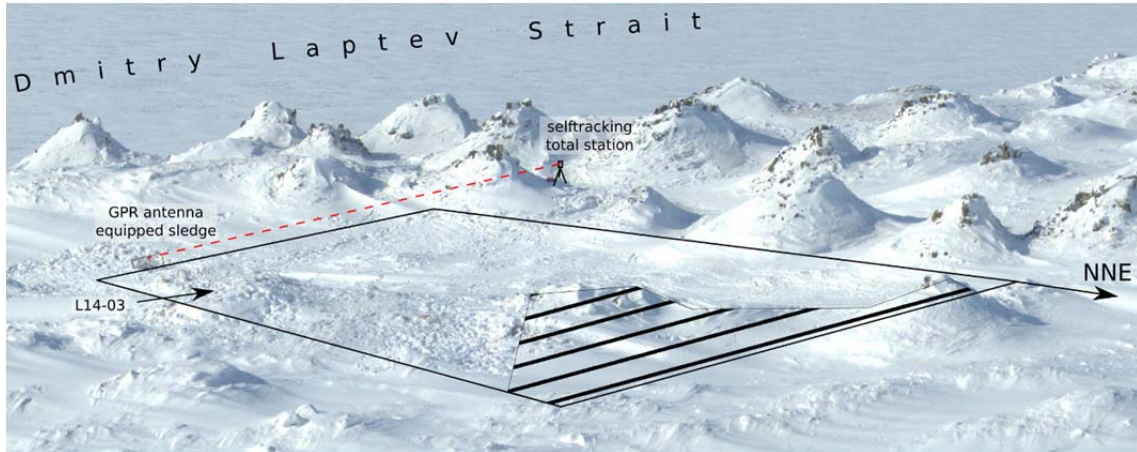


Figure 7-8 Impression of survey area A1 at site thermo terrace in spring. The sketched survey area covers ~40 m x ~20 m. The shaded area in lower part of the figure masks a topographical depression that was inaccessible from total station position.

Our topographic model of preliminary processed data (Figure 7-9) is smooth in most areas of the survey area A1, indicating a high positioning accuracy. However, we observe some sharp features (e.g. at $x = 34$ m, $y = 6$ m). These features probably result from an increase in snow thickness between two acquisition days. The white line in Figure 7-9 denotes a 2D profile that is extracted from our 100 MHz GPR 3D data as an example (Figure 7-9). Major features in our data are hyperbolas, probably related to point diffractors from off-profile positions and high energetic, chaotic reflections below a baidzerakh. We observe a maximum penetration depth of approximately 250 ns for data recorded above the baidzerakh. At this surveying site, CMP surveys indicate a velocity of ~ 0.16 m/ns resulting in a maximum penetration depth of approximately 20 m.

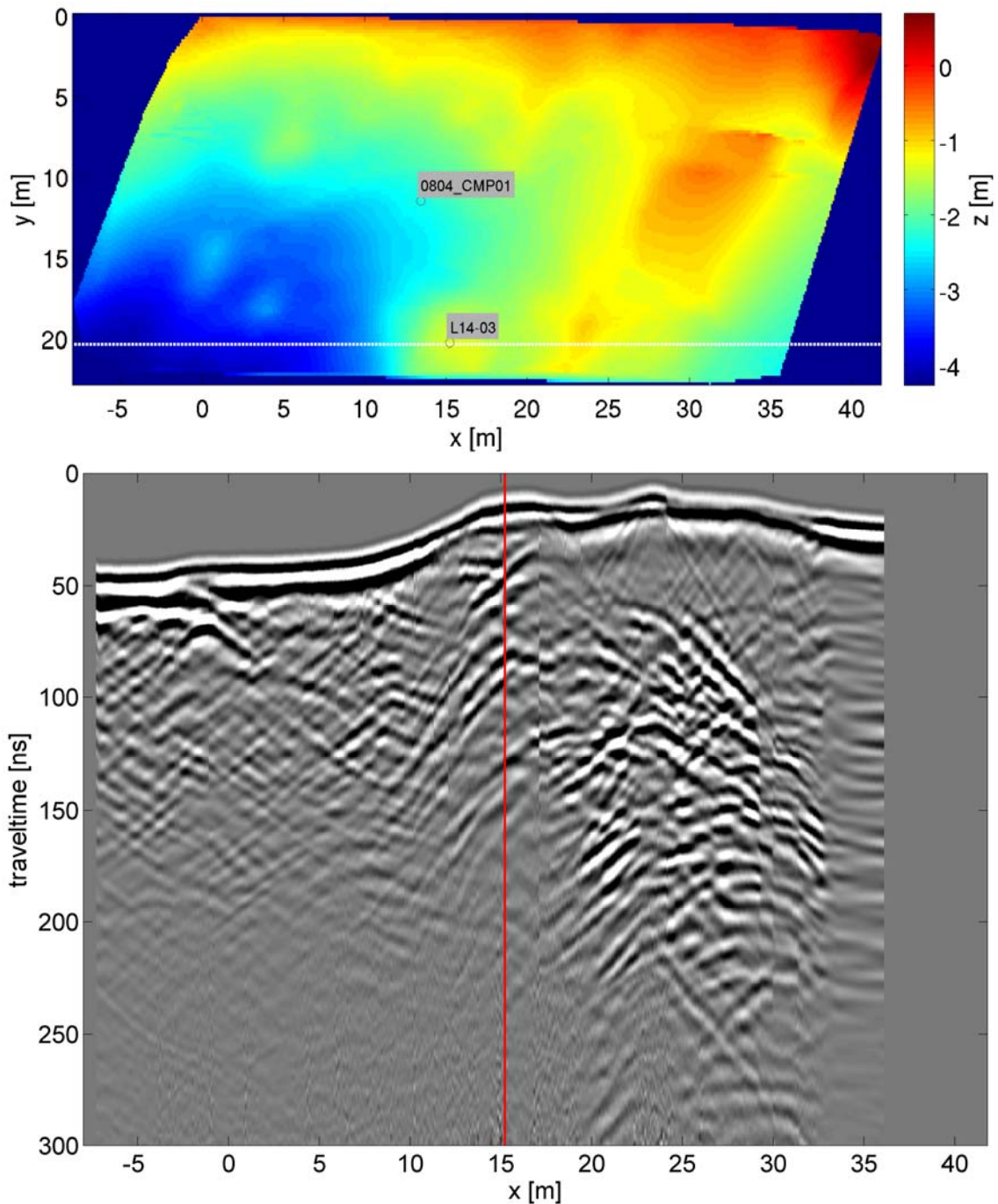


Figure 7-9 Top: Digital terrain model (DTM) of survey area A1 (for locations see Figure 7-7). The reference value for elevation (0 m) is at the location of the total station. Bottom: Example of 100 MHz GPR data on survey area A1. Data processing included time-zero correction, bandpass filtering, amplitude scaling (t^2 amplitude scaling) and topographical correction. Red vertical line at $x = \sim 15$ m indicates the coring location L14-03. Data exhibits a maximum penetration depth of approximately 250 ns (e.g., around profile position $x = \sim 27$ m). The shown preliminary processed data show chaotic, high energetic reflections interfering with diffracted energy probably originating off-line (e.g., around profile position $x = \sim 27$ m, $t = \sim 150$ ns).

7.4 Yedoma

We acquired geophysical data on the Yedoma survey site (see Figure 3-1 for location and Figure 7-10 for a photograph) during both spring and summer expeditions. A map illustrating the location of all acquired datasets is shown in

Figure 7-10 a). In spring, we acquired 3D GPR data using antennas with a center frequency of 100 MHz (survey area A1 covering ~25 m x ~40 m) and 200 MHz (survey area A2 covering ~9 m x ~16 m). A2 was centered on a baidzerakh close to drilling location L14-02. In summer we continued 3D GPR data acquisition on area B1 (~19 m x ~48 m) with 100 MHz antennas and also acquired an additional 3D 200 MHz GPR centered on a baidzerakh (survey area B2 covering ~8 m x ~11 m). Furthermore, we recorded two CMP datasets in spring and six CMP datasets in summer to estimate subsurface velocities at selected points.

In addition to GPR data, we recorded 2D ERT data along three selected profiles (B3, B4, B5; see Figure 7-10). ERT profile B3 is aligned in the direction of GPR data acquisition and follows the topographic gradient for 49 m from Yedoma top towards the thermo-erosional valley in the foreground of Figure 7-10. ERT profiles B4 and B5 were aligned perpendicular to the direction of GPR data acquisition and exhibit a length of 37 m each. All electrode positions of each ERT profile were additionally sampled using TDR and surveyed using a total station.

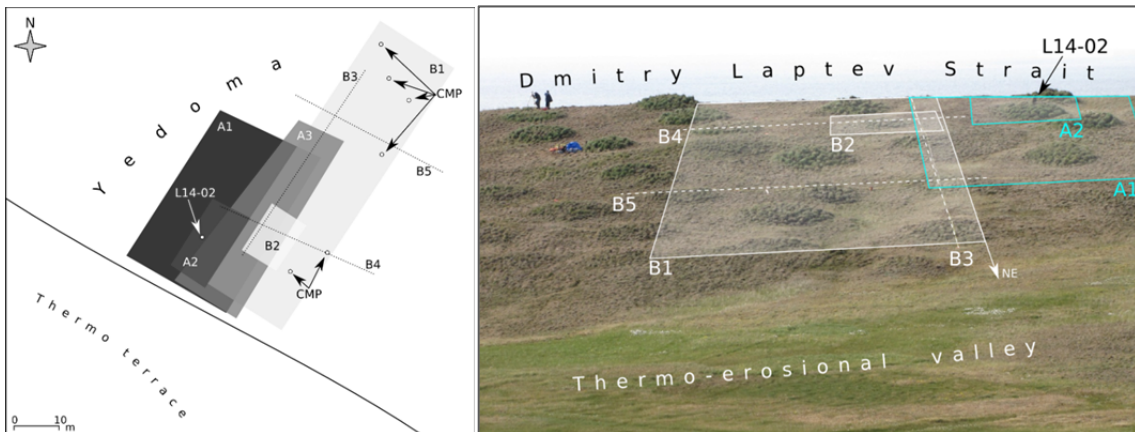


Figure 7-10 Left: Simplified map of geophysical datasets acquired at survey site Yedoma. Further details of the particular datasets can be found in Appendix 7-3. Right: Impression of survey site Yedoma with overlain sketches of survey areas and profiles. Note persons in upper left corner for scale and be aware of perspective distortion.

In spring, we recorded a 3D GPR dataset using 100 MHz antennas within three days, covering an area of ~24 m x ~41 m (survey area A1; Figure 7-11). Acquisition conditions were more favorable than at our survey site Thermo terrace, resulting, for example, in a more uniform data acquisition with a typical data density of four to six traces per 20 cm x 20 cm. As an example, Figure 7-11 shows a 2D profile extracted from the resulting GPR data cube. Our data indicate structure underneath baidzerakhs, where we observe reflections until a traveltimes of up to 100 ns. Areas between baidzerakhs are dominated by high energetic hyperbolas. These are observed for several tens of meters and interpreted as diffracted energy as indicated by timeslices and adjacent profiles.

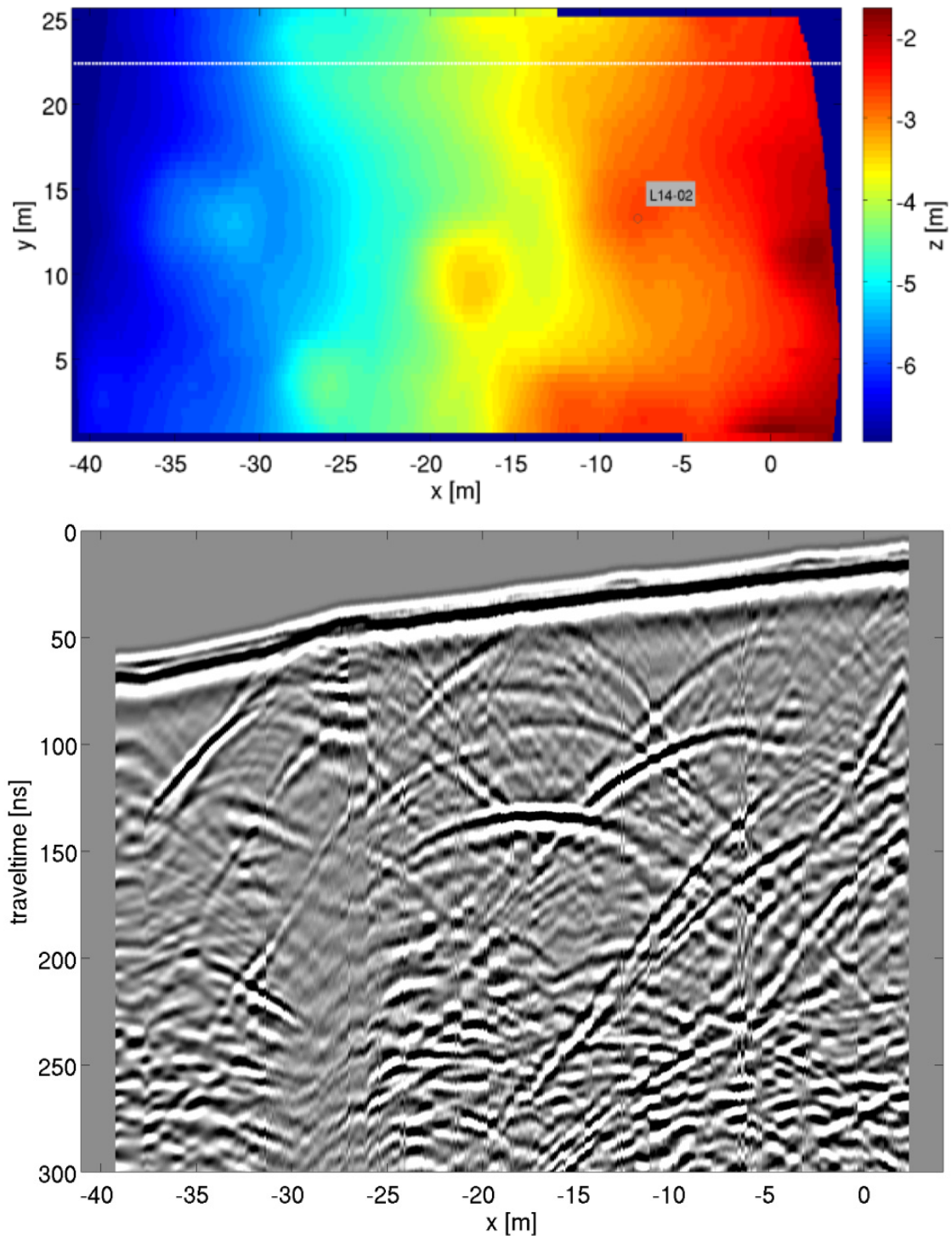


Figure 7-11 Top: Digital terrain model of survey area A1. The reference value for elevation (0 m) is at the location of the total station. Smooth topography indicates high position accuracy. The white line denotes the location of a 2D GPR profile shown below. Bottom: Example of 100 MHz GPR data acquired on survey A1. Data processing included time-zero correction, bandpass filtering, scaling (t^2 amplitude scaling), and topographical correction. Our 2D profile shows a distinct pattern of high energetic hyperbolas. However we relate these in most cases to scattering from adjacent baidzerakh and not to subsurface features from the recorded profile. We observe high energetic reflections just below baidzerakhs (e.g., between profile position $x = -32$ and $x = -27$) up to a traveltime of approximately 70 ns (~6 m depth according to preliminary evaluated CMP data). For comparison, Figure 7-12 shows GPR data acquired along the same profile in summer.

In summer, we acquired another 3D 100 MHz GPR dataset on the Yedoma (survey site B1). The survey area was extended in downslope direction towards the transition to a thermo-erosional valley. The dataset covers an area of $\sim 19\text{ m} \times \sim 48\text{ m}$ (Figure 7-12) in total and was recorded within two days. For comparison, this survey overlaps with survey A2 recorded in spring. In Figure 7-12), we show a 2D profile extracted from the summer 3D dataset which corresponds to profile shown in Figure 7-11). Compared to the spring data (same profile, same center frequency of 100 MHz), the penetration depth underneath baidzerakhs is reduced in summer (compare Figures 7-11 and 7-12). However, we observed a distinct shallow reflection (probably originating from the base of the active layer) not visible in spring. Furthermore, we found early-time amplitude variations that are consistent with qualitative field observations of soil moisture. Another dominant feature in our summer data are hyperbolas, which can be easily identified at comparable position as in spring data (e.g. around profile position $x = \sim -19\text{ m}$, $t = \sim 150\text{ ns}$). This further indicates the high quality of our GPR and positioning data.

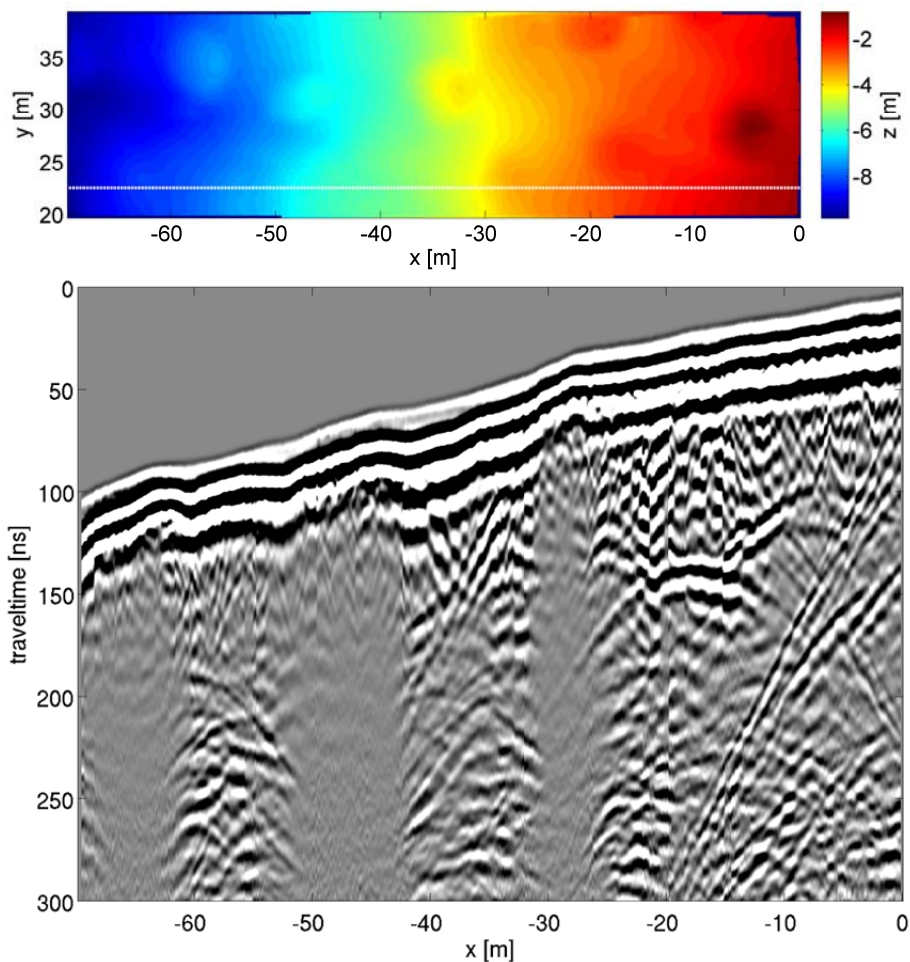


Figure 7-12 Top: Digital terrain model of survey area B1. The reference value for elevation (0 m) is at the location of the total station. The white line denotes the location of the 2D GPR profile shown in the bottom figure. It is aligned along profile B3, where we recorded additional ERT data (inverted ERT data is shown in Figure 7-13). Bottom: Example of 100 MHz GPR data that are extracted from our 3D dataset recorded at survey area B1. Data processing included time-zero correction, scaling (t^2 amplitude scaling), and topographical correction. Dominant features are high energetic hyperbolas, active layer reflection, and regions of distinct attenuation below baidzerakhs.

As a typical example for our ERT data, we show the preliminary inversion result of ERT data acquired along profile B3 (Figure 7-13). Resistivity variations span three orders of magnitude and the shown model indicates a layered underground, where the upper layer (up to depths of ~1 m) is interpreted as the active layer with resistivity values between 100 and 500 Ohm m. In this layer, low resistivity values correspond to areas, where increased soil moisture was observed in the field. However, active layer thicknesses seem to be overestimated. Underneath the active layer, increased resistivities are imaged as expected for ice and frozen sediments, respectively.

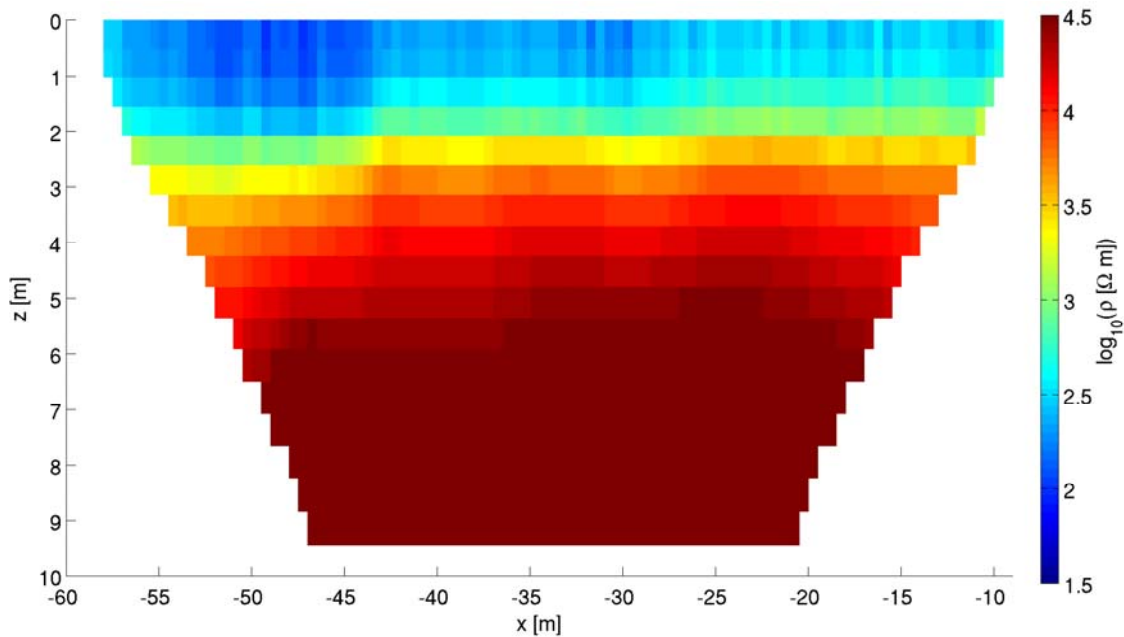


Figure 7-13 Exemplary, preliminary resistivity model based on inversion of data acquired along profile B3. We observe a distinct contrast in resistivity at a depth of ~1 m, which is interpreted as interface between thawed active layer and frozen ground. Thus, active layer thickness is likely overestimated. Furthermore, we observe lateral variation in resistivity of the active layer. Here, low resistive regions coincide with field observations of increased soil moisture content.

7.5 Thermo-erosional valley

Only in summer, geophysical data were recorded in the thermo-erosional valleys. Here, we collected ERT data along the 37 m profile B5 centered across the axis of a thermo-erosional valley (Figure 7-14). Furthermore, we examined a smaller, tributary thermo-erosional valley. Here, we collected a 3D 200 MHz GPR dataset covering ~44 m x ~24 (survey area B1) and four CMP datasets for estimating GPR velocities. Our GPR survey area B1 was intersected by two ERT profiles (profiles B3 and B4 in Figures 7-14 and 7-15), which were centered on the axis of the tributary thermo-erosional valley. B3 was located in the topographically upper part of the GPR survey area and exhibited a length of 24 m, whereas B4 was located in the topographically lower part with a length of 37 m. Furthermore, we acquired EM data on survey area B2, which includes also B1, B3, and B4.

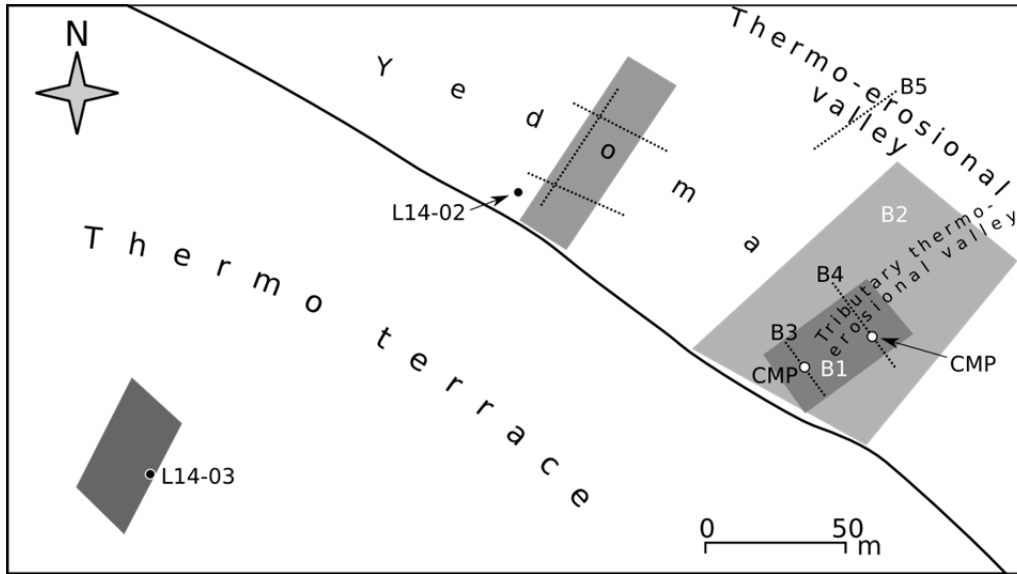


Figure 7-14 Simplified map of geophysical datasets acquired in a tributary and a major thermo-erosional valley. Annotations are explained in more detail in Appendix 7-4. Adjacent survey sites Yedoma and Thermo terrace are shown for orientation. Survey profiles and areas at these sites are annotated in Figure 7-7 and Figure 7-10.

In Figure 7-15 a), we provide a more detailed impression regarding the survey site located in the tributary thermo-erosional valley. Figure 7-15c) shows an example of 200 MHz GPR data acquired in the upper part of the tributary thermo-erosional valley (Figures 7-15a and 7-15b). Dominant features in our GPR data are observed within the first 100 ns. Here, in addition to direct waves, we observe shallow reflections and multiple reflections indicating sedimentary filling of the valley.

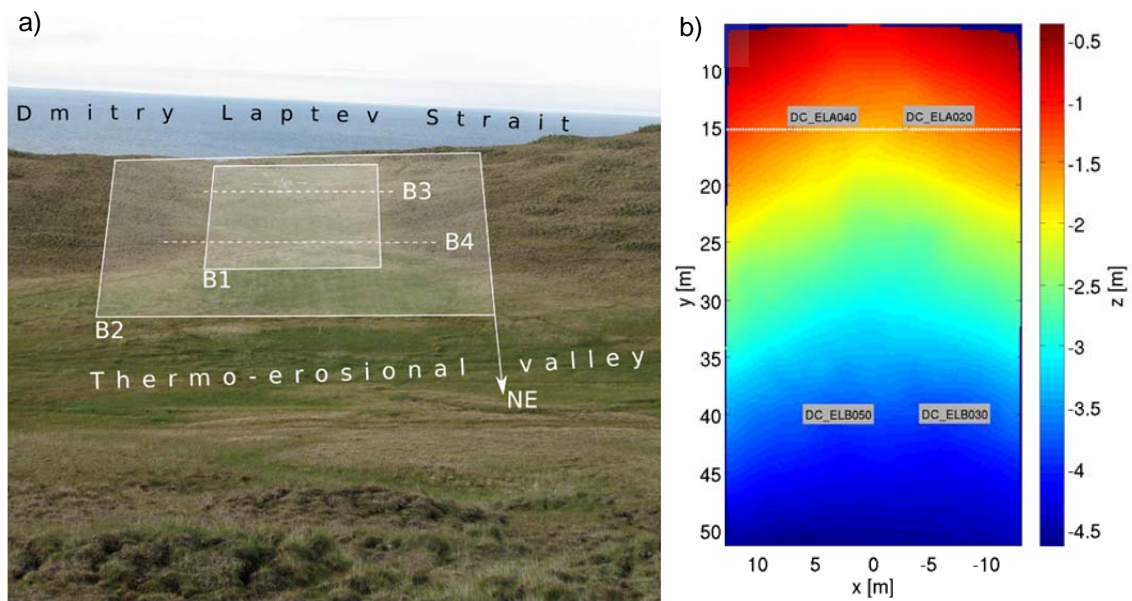


Figure 7-15 (continued on next page)

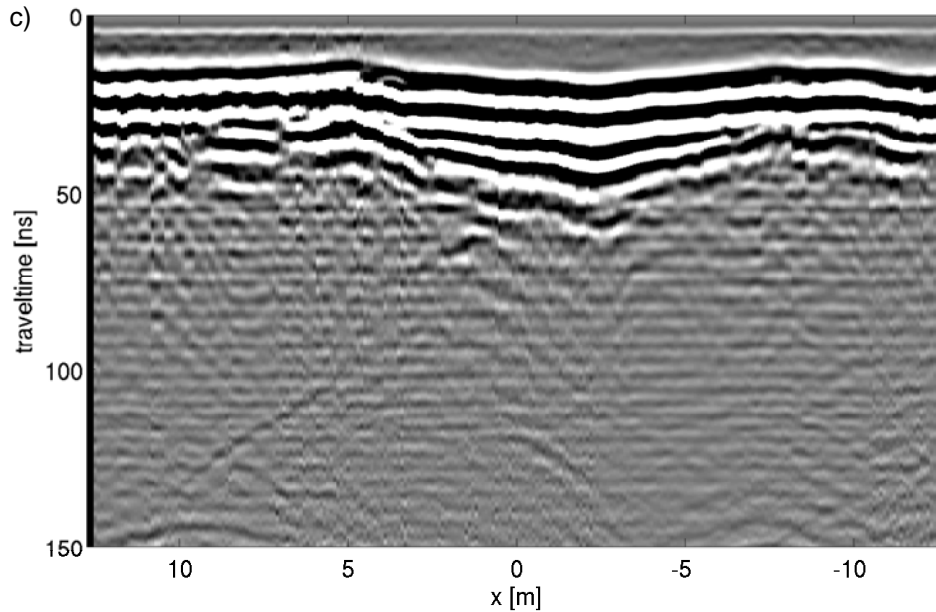


Figure 7-15 a) Field impression of the site tributary thermo-erosional valley (see previous page). b) Digital terrain model of survey area B1. The reference value for elevation (0 m) is at the location of the total station (see previous page). c) Example of 200 MHz GPR data acquired on survey area B1. Data processing included time-zero correction and scaling (t^2 amplitude scaling). Dominant feature is an early-time GPR interference pattern consisting of air waves, ground waves, a shallow reflector, and multiples. Hyperbolas and reflectors occurring at larger traveltimes exhibit a distinct lower level in energy. They are observed until ~ 200 ns and can be highlighted by processing techniques such as amplitude envelope scaling.

7.6 Alas

In spring, we acquired several 2D 100 MHz GPR profiles at the survey site Alas (see Figure 3-1 for location and Figure 7-16). Here, GPR antennas were carried manually using a PVC rig. Furthermore, we recorded CMP data at an orthogonal intersection of two profiles. Dominant features in spring data (not shown) are high energetic hyperbolas, which intersect with horizontal to subhorizontal reflectors. We observe in some profiles a typical lateral unit of ~ 15 m and relate these features to a polygonal pattern of ice wedges and sediment columns (similar to 2D GPR data acquired at Zimov'e River mouth, see Figure 7-1). CMP data indicate a typical penetration depth of ~ 7.5 m.

In summer, we recorded a 3D 200 MHz GPR dataset at survey area B1 (~ 25 m x ~ 26 m) and two CMP datasets. Furthermore, we acquired ERT and TDR data along profile B2 (37 m), which crossed the GPR survey area. Dominant features in extracted 2D GPR data (not shown) are shallow reflections, which originate probably from the base of the active layer. Furthermore, we observe an attenuation pattern, which can be observed both in penetration depth (~ 5 m to ~ 10 m, estimated using CMP velocity estimates) and early-time GPR amplitude. Figure 7-17 c) shows a timeslice at 12.2 ns to demonstrate these changes in amplitude. Data were time-zero corrected and extracted from our 3D 200 MHz GPR dataset. We observe a polygonal amplitude pattern that is related to the position of ice wedges as also indicated by the digital terrain model (Figure 7-17a) and the rectified aerial photography (Figure 7-17b).

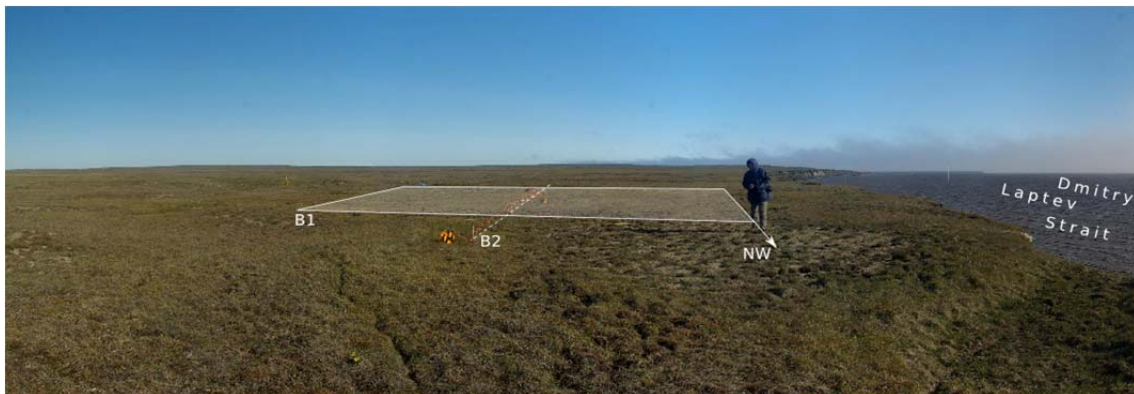
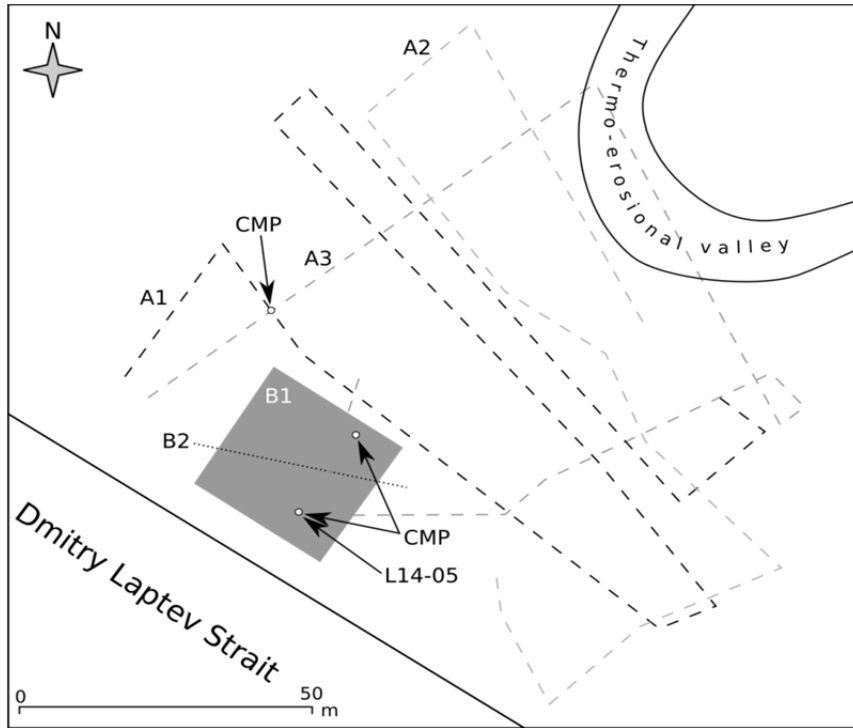


Figure 7-16 Top: Field impression of survey site Alas with overlain sketches of survey area B1 (~25 m x ~26 m) and profile B2 (~37 m). Note person for scale and be aware of perspective distortion. Bottom: Simplified map of geophysical datasets acquired at survey site Alas. Annotations are explained in more detail in Appendix 7-5.

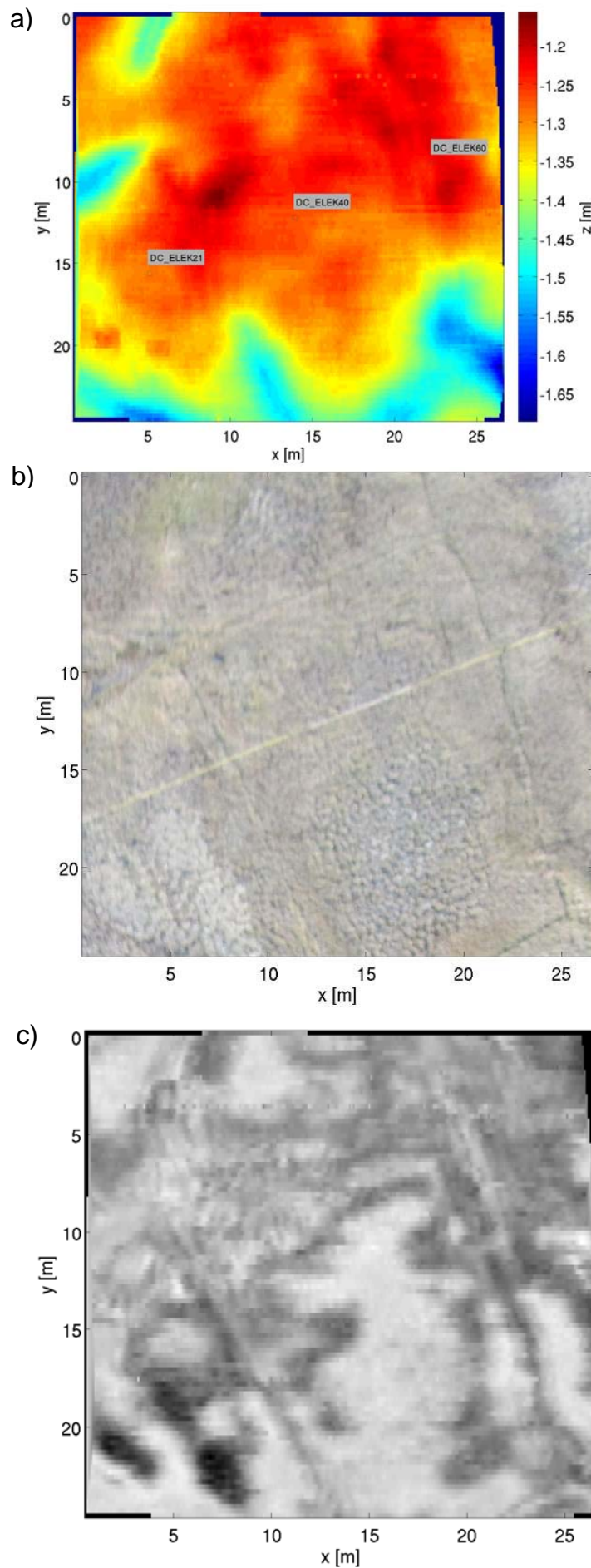


Figure 7-17 Data examples acquired at survey area B1. a) Digital terrain model. The reference value for elevation (0 m) is at the location of the total station. b) Preliminary processed aerial photograph. c) Timeslice at 12.2 ns extracted from our 3D 200 MHz GPR dataset. The amplitude pattern of our GPR timeslice exhibits a polygonal structure, which is consistent with the margin of a high-centered polygon as also seen in the terrain model and the aerial photography. Therefore, we relate our polygonal GPR amplitude pattern to the position of ice wedges.

8 REFERENCES

- Andreev, A.A., Grosse, G., Schirrmeister, L., Kuzmina, S.A., Novenko, E.Yu., Bobrov, A.A., Tarasov, P.E., Kuznetsova, T.V., Krbetschek, M., Meyer, H., Kunitsky, V.V., 2004. Late Saalian and Eemian palaeoenvironmental history of the Bol'shoy Lyakhovsky Island (Laptev Sea region, Arctic Siberia). *Boreas* 33, 319-348.
- Andreev, A.A., Grosse, G., Schirrmeister, L., Kuznetsova, T.V., Kuzmina, S.A., Bobrov, A.A., Tarasov, P.E., Novenko, E.Yu., Meyer, H., Derevyagin, A.Yu., Kienast, F., Bryantseva, A., Kunitsky, V.V., 2009. Weichselian and Holocene palaeoenvironmental history of the Bol'shoy Lyakhovsky Island, New Siberian Archipelago, Arctic Siberia. *Boreas* 38, 72-110.
- Andreev, A., Schirrmeister, L., Tarasov, P.E., Ganopolski, A., Brovkin, V., Siegert, C., Wetterich, S., Hubberten, H.-W., 2011. Vegetation and climate history in the Laptev Sea region (Arctic Siberia) during late Quaternary inferred from pollen records. *Quaternary Science Reviews* 30, 2182-2199.
- Beer, C., 2008. Soil science: The Arctic carbon count. *Nature Geoscience* 1, 569-570.
- Bockheim, J., 2007. Importance of cryoturbation in redistributing organic carbon in permafrost-affected soils. *Soil Science Society of America Journal* 71, 1335-1342.
- Kienast, F., Tarasov, P., Schirrmeister, L., Grosse, G. and Andreev, A.A., 2008. Continental climate in the East Siberian Arctic during the last interglacial: Implications from palaeobotanical records. *Global and Planetary Change* 60, 535-562.
- Kyz'michev, A.B., Soloviev, A.V., Gonikberg, V.E., Shapiro, M.N., Zamzhitskii, O.V. 2006. Mesozoic syncollision siliciclastic sediments of the Bol'shoi Lyakhov Island (New Siberian Islands). *Stratigraphy and Geological Correlation* 14, 30-48.
- Ilyashuk, B.P., Andreev, A.A., Bobrov, A.A., Tumskoy, V.E., Ilyashuk, E.A., 2006. Interglacial history of a palaeo-lake and regional environment: a multi-proxy study of a permafrost deposit from Bol'shoy Lyakhovsky Island, Arctic Siberia. *Journal of Paleolimnology* 35, 855-872.
- IUSS, W., 2014. World Reference Base for Soil Resources. International soil classification system for naming soils and creating legends for soil maps, FAO, Rome.
- Meyer, H., Dereviagin, A., Syromyatnikov, I. 2000. In: Expeditions in Siberia in 1999, ed. V. Rachold, Ber. Polarforschung 354, p. 139.
- Meyer, H., Dereviagin, A. Yu., Siegert, C., Schirrmeister, L., Hubberten, H.-W. 2002. Paleoclimate reconstruction on Big Lyakhovsky Island, North Siberia - Hydrogen and oxygen isotopes in ice wedges, Permafrost and Periglacial Processes 13, 91-105.
- Schirrmeister, L., Grosse, G., Kunitsky, V., 2000. Paleoclimate signals of ice-rich permafrost deposits - Cryolithological and sedimentological studies. *Berichte zur Polar und Meeresforschung* 354, 126-131.
- Schirrmeister, L., Oezen, D., Geyh, M.A. 2002: ²³⁰Th/U dating of frozen peat, Bol'shoy Lyakhovsky Island (North Siberia). *Quaternary Research* 57, 253-258.

- Schirrmeister, L., Wetterich, S., Tumskoy, V., Dobrynin, D., 2008. Palaeoenvironmental studies on Bol'shoy Lyakhovsky Island. *Berichte zur Polar und Meeresforschung* 584, 51-84.
- Tumskoy V.E., 2012. Osobennosti kriolitogeneza otlozhenii severnoi Yakutii v srednem Neopleistotsene - Golotsene (Peculiarities of cryolithogenesis in northern Yakutia from the Middle Neopleistocene to the Holocene). *Kriosfera Zemli (Earth's Cryosphere)* 16, 12-21 (in Russian)
- Wetterich, S., Schirrmeister, L., Andreev, A.A., Pudenz, M., Plessen, B., Meyer, H., Kunitsky, V.V., 2009. Eemian and Late Glacial/Holocene palaeoenvironmental records from permafrost sequences at the Dmitry Laptev Strait (NE Siberia, Russia). *Paleogeography, Paleoclimatology, Paleoecology* 279, 73-95.
- Wetterich, S., Rudaya, N., Meyer, H., Opel, T., Schirrmeister, L., 2011. Last Glacial Maximum records in permafrost of the East Siberian Arctic. *Quaternary Science Reviews* 30, 3139-3151.
- Wetterich, S., Tumskoy, V., Rudaya, N., Andreev, A.A., Opel, T., Meyer, H., Schirrmeister, L., 2014. Ice Complex formation in arctic East Siberia during the MIS3 Interstadial. *Quaternary Science Reviews* 84, 39-55.

APPENDIX

Appendix 3-1 to 3-6; drill and log protocols	67
Appendix 4-1; exposure samples	83
Appendix 5-1; soil organic matter samples	91
Appendix 7-1 to 7-5; geophysical datasets	97

The appendix numbering refers to the relevant chapters.

Appendix 3-2

Log protocol of core L14-01.

Log protocol																				
Science personnel: G. Schwaborn (GS) / L. Schirrmelster (LS) Site: L14-01 (N 73.33616°; E 141.32776°) .. Hole: test drilling close to cabin, half distance of GPR profile (CMP site) Date: 07.04.14 (test drilling) Core ø: 132 mm (drill bit) R(g: KMB-3-15M) Box #: 7051																				
Depth	Rock type		Ground ice fabric				Notes	Digital Pictures	↑ ↓ ← → ↖ ↗											
	From (m)	To (m)	ice cement	lens-like	reticulate	massive					layered	Contact to bottom: sharp / transit	Additional observations (plant remains, gas bubbles, fossils...)							
0.00	0.58	CT = cryotexture, LL = lense-like																		
0.58	0.82	Silt, layered, 2 mm thick each, brown spots, fine CT Silt, non-layered, narrow horizontal micro CT, at 0.66 m coarse lenses building horizontal layer		x x					Grass-rooted, cm-long roots No visible organics borehole suspended due to loss of core tube in the ground (froze in).											yes
Sampling: m Samples:  ground ice  substrate																				

Log protocol of core L14-02 continued.

Log protocol												
Science personnel: GS / LS / YK		Site: L14-02 (N 73.33616°; E 141.32776°)		Hole: 32 m asl, 19 m to edge of thermo terrace; 150 m to L7-18		Rig: KMB-3-15M		Box #: 7051				
Date: 09.04.14 (10.45-18.00h)		Core ø: 132; 112 mm (drill bit)										
Depth	Rock type		Ground ice fabric					Notes	Digital Pictures			
	From (m)	To (m)	Colour	Contact to bottom: sharp / transit	ice cement	lens-like	reticulate			massive	layered	Contact to bottom: sharp / transit
3.77	4.27	CT = cryotexture, LL = lense-like	grey			x						
4.27	5.03	Silt, CT irregular, at 3.77 m ice-rich, at 4.00 m vertical ice vein 2 cm thick, at 4.10 m ice band with silty inclusion and gas bubbles, at 4.10-4.27 m silt with subvertical orientation Silt, fine CT at 4.27-4.37 m, at 4.67 m and 4.82 m coarse LL to blocky CT			x							
5.03	5.67	Silt, alternation of fine and coarse LL CT, ice band at 5.63-5.67 m				x						
5.67	6.23	Silt, horizontal coarse LL CT										
Sampling: m												
Samples:  ground ice  substrate												

Log protocol of core L14-02 continued.

Log protocol												
Science personnel: GS / LS / YK		Site: L14-02 (N 73.33616°; E 141.32776°)		Hole: 32 m asl, 19 m to edge of thermo terrace; 150 m to L7-18		Rig: KMB-3-15M		Box #: 7052				
Date: 11.04.14 (10.15-18.30h)		Core ø: 112; 93 mm (drill bit)										
Depth (m)	From (m)	To (m)	Rock type		Ground ice fabric						Notes	Digital Pictures
			Colour	Contact to bottom: sharp / transit	ice cement	lens-like	reticulate	massive	layered	Contact to bottom: sharp / transit		
10.92	11.17	11.17	Diagonal contact between silty sediment and massive ice at 10.92 m, massive ice from 11.02 m, ice is milky and has sediment, diagonal LL CT Milky ice as above	grey	s		x				Interpretation: contact to ice wedge	yes
11.17	11.26	11.26					x				Change to drill bit "saw teeth". air bubbles ø 1-2 mm	
11.26	11.78	11.78	Ice with air bubbles, some silty streaks				x				Change to smaller drill bit ø 93 mm.	
11.78	12.35	12.35	Ice (crushed)				x				11.78-12.18 m: mixed sample, 12.18-12.35 m: regular sample, air bubbles ø 2-3 mm	
12.35	12.97	12.97	see above				x				single chips refrozen in core	
12.97	13.52	13.52	see above				x					
13.52	13.72	13.72	see above, bottom 7 cm become darker, more massive				x					
13.72	14.22	14.22	see above				x					
14.22	14.71	14.71	see above				x					
14.71	15.15	15.15	see above				x					
15.15	15.28	15.28	see above				x					
15.28	15.91	15.91	see above				x					
15.91	16.48	16.48	see above				x					
16.48	16.94	16.94	see above				x					
Sampling: m		
Samples:  ground ice												
											 substrate	

Log protocol of core L14-02 continued.

Log protocol										
Science personnel: GS / LS / YK Site: L14-02 (N 73.33616°; E 141.32776°) Hole: 32 m asl, 19 m to edge of thermo terrace; 150 m to L7-18 Date: 13.04.14 (10.15-18.30h) Core ø: 93; 76 mm (drill bit) Rig: KMB-3-15M Box #: 7052										
Depth	Rock type		Ground ice fabric					Notes	Digital Pictures	
	From (m)	To (m)	ice cement	lens-like	reticulate	massive	layered			Contact to bottom: sharp / transit
16.94										
17.50		CT = cryotexture, LL = lense-like								
17.84	17.50	see above				x				
18.07	17.84	see above				x				
18.67	18.07	see above				x				
18.67	18.95	see above, very bottom has dark massive ice				x			Single ice wedge chips refrozen in core	yes
18.95	19.20	see above, very bottom has dark massive ice				x			Change to drill bit "sawteeth".	
19.20	19.41	see above, very bottom has dark massive ice				x			Very bottom has dark massive ice; drill artefact?	
19.41	19.64	see above				x			Mixed sample in bag	
19.64	19.83	see above, very bottom has dark massive ice				x			Very bottom has dark massive ice; drill artefact?	
19.83	20.02	see above, very bottom has dark massive ice				x			Mixed sample in bag	
									Partly clean ice with air bubbles, very bottom has dark massive ice; drill artefact?	
									Very bottom has dark massive ice; drill artefact?	
									Mixed sample in bag	
									Very bottom has dark massive ice; drill artefact?	
									Mixed sample in bag	
Sampling: m Samples:  ground ice  substrate										

Appendix 3-4

Log protocol of core L14-03.

Log protocol												
Science personnel: GS / LS / YK Site: L14-033B (N 73.33538°, E 141.32337°) Hole: 17 m asl, thermo terrace with underlying Kuchchugui Date: 14.04.14 (11.00-19.00h) Core ø: 132; 112 mm (drill bit) Rig: KMB-3-15M Box #: 7065												
Depth	Rock type		Ground ice fabric					Notes	Digital Pictures			
	From (m)	To (m)	Colour	Contact to bottom: sharp / transit	ice cement	lens-like	reticulate			massive	layered	Contact to bottom: sharp / transit
0.00	0.50	Loamy silt and fine sand, vertical mm-thick, cm-long cracks with Fe-oxides, spotted orange-grey-brown, no CT, free of ice and thawed during drilling	brown-grey								Core unfrozen due to core barrel recovery, upper 2 cm with plants and rooting interpretation: active layer	yes
0.50	0.95	Loamy silt and fine sand, 00.50-00.54 m SAB; active layer see above, spotted orange-brown Fe-oxides, 0.54-0.95 m coarse LL to blocky CT, diagonal ice veins, > mm thin, cm-long, ice bands mm-thick, cm-long 3x at 0.59-0.62 m, 0.77-0.80 m, 0.86 m, 0.91		x							interpretation: active layer to 0.54 m no visible plant remains scattered organic spots	
0.95	1.18	see above, at 1.13 m white ice band (frozen snow layer?), blocky to coarse LL CT		x							Loss of core tube due to freeze-in - continuation as hole 03B, new borehole has ø 112 mm.	
0.00	0.65	same as hole 03: coarse LL horizontal CT	brown-grey								Interpretation: active layer depth 0.5 m, central part remained frozen when coring	
0.65	0.90	Silt, ice-rich, coarse LL horizontal CT		x							scattered plant remains	
1.12	1.45	Silt, coarse LL horizontal CT, vertical ice veins, ice bands cm-thick milky to clear ice at shortly at 1.30 m, color change from dark to light brown / grey at 1.37 m	dark to light	x	x						Core segment measures 33 cm instead of 21 cm .	
1.45	1.66	Silt, blocky to coarse LL, ice band at bottom 2 cm		x							plant remains scattered	
1.66	1.98	Silt, blocky (upper 8 cm) then coarse LL, ice-rich, ice bands at 2 cm; 17 cm; 22 cm; 30 cm		x								
1.98	2.42	see above		x								
Sampling: m Samples:  ground ice  substrate												

Log protocol of core L14-03 continued.

Log protocol									
Science personnel: GS / LS / YK		Site: L14-033B (N 73.33538°, E 141.32337°).....		Hole: 17 m asl, thermo terrace with underlying Kuchchugui		Rig: KMB-3-15M.....		Box #: 7058 / 7062.....	
Date: 15.04.14 (10.15-17.30h).....		Core ø: 112 mm (drill bit)							
Depth	Rock type	Ground ice fabric				Notes	Digital Pictures		
		ice cement	lens-like	reticulate	massive			layered	Contact to bottom: sharp / transit
From (m)	To (m)	Colour	Contact to bottom: sharp / transit	Contact to bottom: sharp / transit	Contact to bottom: sharp / transit	Additional observations (plant remains, gas bubbles, fossils...)	Digital Pictures		
6.67	7.35	CT = cryotexture, LL = lense-like							
7.35	8.13	see above; polosaliki incl. fine lamellae of diagonal CT							
8.13	8.51	see above; polosaliki, massive ice at 50-60 cm							
8.51	9.34	see above; ice-rich at 30-45 cm							
9.34	9.89	see above; polosaliki upper 11 cm, sharp contact to layered fine sand to silt, layering mm to cm, pebble layer 60-62 cm, fine sand structureless 60-80 cm	s						
9.89	10.44	fine sand to 25 cm, it has simple gravels, angular 1-2 cm ø, sharp contact to polosaliki at 25 cm	s						
10.44	10.89	see above; polosaliki, bended layers become bigger							
10.89	11.60	see above; polosaliki, single gravel scattered at 25-35 cm							
11.60	12.10	see above; polosaliki							
12.10	12.82	see above; polosaliki upper 55 cm, single gravel swimming at 35 cm, gravel portion increases at 55 cm							
12.82	13.02	gravel , ice-rich, ice-bonded, clasts subangular and up to 4 cm (see at 55 cm)							
13.02	13.70	see above; clear ice, cm-sized crystals, partly in lenses, air bubbles occur							
13.70	14.43	see above; Fe-oxide spots at 50 cm to bottom, subangular clasts <3 cm							
14.43	15.10	sand (without layering), Fe-oxide colours, ice-poor at 50-80 cm, gravel to sand at bottom							
		gravel , ice-poor upper 40 cm, sand 40-60 cm, single stone at 62-63 cm							
Sampling:							m		
Samples:							ground ice substrate		

Log protocol of core L14-3 continued.

Log protocol

Science personnel: GS / LS / YK Site: **L14-033B** (N 73.33538°, E 141.32337°) Hole: 17 m asl, thermo terrace with underlying Kuchchugui
 Date: 16.04.14 (10.15-13.00h) Core ø: 112 mm (drill bit) Rig: KMB-3-15M Box #: 7062

Depth	Rock type	Ground ice fabric					Notes	Digital Pictures
		ice cement	lens-like	reticulate	massive	layered		
From (m)								
To (m)	CT = cryotexture, LL = lense-like	ice cement	lens-like	reticulate	massive	layered	Additional observations (plant remains, gas bubbles, fossils...)	
		Contact to bottom: sharp / transit					Replacement of drill bit; the day before the drill bit lost one tooth before last run; after last run three more teeth were lost.	yes
15.10	Sand 0-15 cm, gravel 15-31 cm, clasts <3 cm ø, subangular, component supported						thawed during recovery from core!	
15.41	Stony gravel						Borehole finished due to stony ground.	
							(Lost core barrel from first day is retrieved by drilling circles around and loosening it.)	
Sampling: m								
Samples:  ground ice  substrate								

Appendix 3-5

Log protocol of core L14-4.

Log protocol											
Depth		Rock type		Ground ice fabric					Notes	Digital Pictures	
From (m)	To (m)	CT = cryotexture, LL = lense-like	Colour	Contact to bottom: sharp / transit	ice cement	lens-like	reticulate	massive	layered	Contact to bottom: sharp / transit	Additional observations (plant remains, gas bubbles, fossils...)
00.00	00.67	fine sand , ice-poor to micro LL CT 0 to 43 cm, silt, blocky to coarse LL CT to vertical ice veins 43-67 cm	grey			x					scattered plant remains
0.67	0.89	silt , ice-rich, ice lenses, white-milky vertical ice lenses or veins <1 mm thick, 2-4 cm long				x					Interpretation possibly reworked on thermo terrace
0.89	1.12	see above									peaty inclusion
1.12	1.52	see above, ice-rich silt with lamellar, reticulate CT structure					x				Interpretation possibly reworked on thermo terrace
1.52	1.71	see above, camouflage -structured									no visible organics
1.71	2.00	see above									organic spots at 2.40 m
2.00	2.50	see above, angular isolated clasts in icy matrix									organic spots at 3.00 m, 3.10 m
2.50	2.95	see above									change to thermobox 7074
2.95	3.50	see above, angular blocky CT upper 5 cm, vertical banded layered silt at 5-15 cm									brownish (organic?) spot at 40 cm
3.50	4.06	see above, ice-rich, blocky CT						x			Interpretation: ice wedge ice
4.06	4.24	see above						x			ice wedge ice
4.24	4.50	ice incl. mm-sized bubbles						x			ice wedge ice, single ice chips refrozen in core
4.50	4.64	ice incl. mm-sized bubbles						x			
4.64	4.89	ice incl. mm-sized bubbles						x			
4.89	5.07	ice incl. mm-sized bubbles, upper 5 cm with big crystals						x			
Sampling: m											
Samples:  ground ice  substrate											

Science personnel: GS / LS / YK Site: **L14-04** (N 73.34100°, E 141.28586°) Hole: 12 m asl, thermo terrace with underlying Eemian deposits
 Date: 17.04.14 (11.00-18.00h) Core ø: 112 mm (drill bit) Rig: KMB-3-15M Box #: 7067 / 7074

Appendix 3-6

Log protocol of core L14-5.

Log protocol										
Science personnel: GS / LS / YK Site: L14-05 (N 73.34994°, E 141.24156°) Hole: 05 (11 m asl / Alas) Date: 19.04.14 (11.15-11.45h) Core ø: 112 mm (drill bit) Rig: KMB-3-15M Box #: 7053										
Depth	Rock type	Colour	Contact to bottom: sharp / transit	Ground ice fabric					Notes	Digital Pictures
				ice cement	lens-like	reticulate	massive	layered		
From (m)	CT = cryotexture, LL = lense-like							Additional observations (plant remains, gas bubbles, fossils...)		
0.00	Tundra surface, silt, Fe-oxide colours at 0-20 cm, massive, ice-poor at 20-36 cm,	grey						Drilling stops due to damage of last coring head joint (part between engine and metal rods).	yes	
0.6	Silt, grey to brown, coarse to LL CT, organic inclusions							Additional samples taken from the nearby coastal bluff (see Figure 3-10; note change between m depth and m asl in figure)		
0.9	Ice wedge ice, silty streaks in line to layering, numerous bubbles <1 mm									
1.1	Silt, LL to latice, slightly lighter grey, some organics scattered							Shells from ostracods		
1.3	Grey silt, Fe-oxide patches, coarse LL to reticulate, some organics scattered									
1.7	See above Fe-oxide patches, coarse LL to reticulate							Wood remains Organic layers Wood remains		
2.5	Silty sand, Fe-oxid patches, coarse LL reticulated, no visible organics									
3.6	mid grey silty sand, Fe-oxide along horizontal ice veins, shell remains (possibly more remains from ostracods visible), some diagonal ice veins make latice-like CT									
5.5	grey silt, latice-like CT, wood remains									
6.5	see above, organic layers in the middle part									
7.2	see above, prominent macro wood remain, faintly layered, ice-poor, massive CT									
7.8	grey silt, massive CT, Fe-oxide patches, organics									
Sampling: m Samples:  ground ice  substrate										

Log protocol of core L14-5 continued.

Log protocol												
Depth		Rock type	Colour	Contact to bottom: sharp / transit	Ground ice fabric					Notes	↑ ↓ pressured air	Digital Pictures
From (m)	To (m)				ice cement	lens-like	reticulate	massive	layered	Contact to bottom: sharp / transit	Additional observations (plant remains, gas bubbles, fossils...)	
0.00	0.33	lundra surface soil upper 5 cm; silt, Fe-oxide colours at 0-20 cm, massive CT at 5-18 cm, silt, reticulate CT at 18-33 cm	brown grey light grey dark grey light grey					x			rich in organics and roots	yes
0.33	0.65	silt, coarse lattice-like CT									no visible organics	
0.65	0.85	see above, coarser lattice-like CT to bottom part									Change of drill bit to ø93 mm	
0.85	1.04	see above, lattice-like CT, some lenses in upper 5 cm									organic patches visible at 20 cm	
1.04	1.39	see above, Fe-oxides in the bottom 10 cm										
1.39	1.95	see above, ice-richer, Fe-oxides, LL CT, ice bands at 8, 13, 36 cm										
1.95	2.45	LL to coarse LL, rich in Fe-oxides										
2.45	3.25	silt, 0-50 cm, transition in colour between 50-65 cm to silt, 65-80 cm, faintly layered indicated by Fe-oxides, horizontal LL to occasionally coarse LL CT	brown-grey dark grey									
3.25	3.35	see above, silt, horizontal LL CT, punctuated by some Fe-oxides, i.e. at 75 cm	dark grey									
3.35	4.35	see above, transition to brown Fe-oxide bearing layers, horizontal LL CT at 75 cm	brown grey									
4.35	5.30	see above, organic layer at 15 cm									some organics scattered and organic layer at 15 cm	
5.30	5.44	silt, ice-rich, LL CT	dark grey								Core segment measures 85 cm instead of 10 cm! change to thermobox 7063	
Sampling: m												
Samples:  ground ice substrate												

Science personnel: GS / LS / YK Site: L14-05 (N 73.34994°, E 141.24156°) Hole: 05 new (11 m asl, Alas)
 Date: 21.04.14 (10.30-18.30h) Core ø: 112 / 93 mm (drill bit) Rig: KMB-3-15M Box #: 7026 / 7063

Log protocol of core L14-5 continued.

Log protocol											
Depth		Rock type		Ground ice fabric					Notes	Digital Pictures	
From (m)	To (m)	CT = cryotexture, LL = lense-like	Colour	Contact to bottom: sharp / transit	ice cement	lens-like	reticulate	massive	layered	Contact to bottom: sharp / transit	Additional observations (plant remains, gas bubbles, fossils...)
5.44	6.71	see above									
6.71	7.26	see above, silt, horizontal LL CT, ice-poor at bottom	middle grey			x					
7.26	7.89	see above, LL CT				x					Core segment measures 77 cm instead of 127 cm layered organic inclusions at 24, 41, 52 cm prominent organic (-peaty) spot at 20-25 cm; more spots at bottom organic remains scattered Borehole suspended due to damaged joint.
Sampling: m Samples:  ground ice substrate 											

Appendix 4-1

Sample list and field descriptions of the exposure profiles studied in summer 2014. The following abbreviations are used: OSL - Optically-Stimulated Luminescence, ref - reference sample for gamma spectrometry, BK – Bodenkunde, PG – Paläogenetik, 14C – Radiocarbon, N / E / H / A - North / East / Height / Accuracy, IC - Ice Complex, b.s. – below surface, a.s.l. – above sea level.

Sample	Description	Depth	Height	Wet-based ice content [wt%]	Dry-based ice content [wt%]
		[m b.s.]	[m a.s.l.]		
Profile L14-14 / pre-Quaternary, Vetvistyj River (tributary of Zimov'e River) (L7-17 reference)					
N 73°20,831', E 141°24,035', H 12m, A 5m (river shore)					
13.08.2014					
not sampled					
Profile L14-11 / Yukagir IC peat (L7-01 reference)					
N 73°20,080', E 141°19,277', H 0m, A 5m (beach, sea level)					
04.08. and 08.08.2014					
L14-11-PG1	light-brown (sometimes green) moss peat with fine ice lenses and rather coarse vertical and subvertical ice veins (20 mm thick and 200 to 300 mm long)		3.5	89.7	872.3
L14-11-Th/U	see L14-11-PG1		3.5	89.8	881.8
L14-11-BK4	see L14-11-PG1		3.5	88.3	757.1
L14-11-4	greenish-grey fine-grained sands with coarse reticulated ice lenses (2 mm thick and 20 to 50 mm long) and ice bands (up to 20 mm thick), pebbles and peat lenses (50x50 to 100x100 mm)		2.5		
L14-11-5	see L14-11-4		2.2		
L14-11-BK7	see L14-11-4		2	49.9 47.2 64.2	99.5 89.4 179.3

Sample	Description	Depth [m b.s.]	Height [m a.s.l.]	Wet-based ice content [wt%]	Dry-based ice content [wt%]
Profile L14-10 / Yukagir IC to Kuchchegui at beach (L7-01, L7-02, L7-03, L7-04 reference) N 73°20,081', E 141°19,236', H -3m, A 3m (beach) / N 73°20,087', E 141°19,252', H 5m, A 4m (wall top) 03.08. and 04.08.2014					
L14-10-OSL1	brown-yellowish silt and fine sand, relatively homogeneous with slightly horizontal layering (visible in thawed surface), only some parts medium-scale waved (~0.5m length), fine roots and some organic inclusions (<1cm), only fine ice lenses or massive cryostructures	1.9	5.1	25.6	34.5
L14-10-OSL1 gamma (frozen)	see L14-10-OSL1	1.9	5.1		
L14-10-OSL2	see L14-10-OSL1; OSL core close to ice-rich sediment	1.9	5.1	26.0	35.2
L14-10-OSL2 gamma (frozen)	see L14-10-OSL1	1.9	5.1		
L14-10-OSL2 gamma (ice)	material taken from ice-rich sediment next to OSL2 core	1.9	5.1		
L14-10-OSL1/2 gamma (ref)	see L14-10-OSL1	1.9	5.1		
L14-10-BK3	see L14-10-OSL1	1.9	2.5	43.6	77.5
L14-10-OSL3	brown-yellowish silt and fine sand enriched with coarse sand to pebbles (<2cm, max. 5cm), not rounded and clustered in 'pockets' indicating cryoturbation (paleo active layer), brown to slightly orange (gravel-pockets),	2.4	4.6	22.3	28.6

Sample	Description	Depth [m b.s.]	Height [m a.s.l.]	Wet-based ice content [wt%]	Dry-based ice content [wt%]
	less roots compared to L14-10-OSL1, only fine ice lenses or massive cryostructures				
L14-10-OSL3 gamma (frozen)	see L14-10-OSL3	2.4	4.6		
L14-10-OSL4	see L14-10-OSL3	2.5	4.5	22.1	28.4
L14-10-OSL4 gamma (frozen)	see L14-10-OSL3	2.5	4.5		
L14-10-OSL3/4 gamma (ref)	see L14-10-OSL3	2.5-2.4	4.5-4.6		
L14-10-PG1	see L14-11-PG1	4.1	2.5	80.2	404.6
L14-10-Th/U	see L14-11-PG1	4.1	2.5	65.7	191.6

Profile L14-17 / Kuchchegui to Yedomia contact

N 73°20,111', E 141°19,042', H 12m, A 5m (beach level)

16.08.2014

not sampled

Profile L14-12 / Krest Yuryakh (Last Interglacial lake) (L14-04a, b, c reference)

N 73°20,433', E 141°17,099', H 9m, A 3m (wall top) / N 73°20,429', E 141°17,096', H 1m, A 3m

06.08.2014

L14-12-BK6	grey-bluish silt loam with many large (2-5 cm) peat lenses, ice cemented	0.5	7.5		
L14-12-14C	Wood and root fragments (<i>Betula</i> or <i>Salix?</i>), in matrix of grey-bluish silt with horizontal to subhorizontal ice lenses (mm thick, cm long) and many scattered organic fragments (mainly wood)	1	7		
L14-12-OSL1	grey-bluish silt and fine sand, only slightly layered with several horizontal (50 - >100 mm length) and few vertical ice bands	3.5	4.5	22.5	29.0

Sample	Description	Depth [m b.s.]	Height [m a.s.l.]	Wet-based ice content [wt%]	Dry-based ice content [wt%]
	surrounded by yellowish-orange-brown zones, few shorter horizontal ice lenses without yellowish contact zones, black spots (<1cm, few <2cm) of organics often with "helix" (bigger black circle)				
L14-12-OSL1 gamma (frozen)	see L14-12-OSL1	3.5	4.5		
L14-12-OSL2	see L14-12-OSL1	3.5	4.5	23.6	30.9
L14-12-OSL2 gamma (frozen)	see L14-12-OSL1	3.5	4.5		
L14-12-OSL2 gamma (ref)	see L14-12-OSL1	3.5	4.5		
L14-12-BK5	see L14-12-OSL1	3.5	4.5	23.3 22.2	30.4 28.5
L14-12-OSL4	grey-bluish silt and fine sand with pebbles (slightly clustered (>2 mm up to 30 mm in diameter), black spots (2 to 5 mm in diameter) of degraded organic occurred in clusters, whitish fine sand layers (ca. 1 mm thick and 20 to 50 mm long), massive cryostructure	5.2	2.8	22.4	28.9
L14-12-OSL4 gamma (frozen)	see L14-12-OSL4	5.2	2.8		
L14-12-OSL3/4 gamma (ref)	see L14-12-OSL4	5.2	2.8		
L14-12-Kies	see L14-12-OSL4	5.2	2.8		
L14-12-OSL3	see L14-12-OSL4	5.3	2.7	19.8	24.6
L14-12-OSL3 gamma (frozen)	see L14-12-OSL4	5.3	2.7		

Profile L14-09 / Molotkov (Yedoma) IC on thermo terrace (L14-03 reference)
N 73°20,120', E 141°19,402', H 17m, A 5m (baidzherakh top)

Sample	Description	Depth [m b.s.]	Height [m a.s.l.]	Wet-based ice content [wt%]	Dry-based ice content [wt%]
01.08. and 02.08.2014					
L14-09-OSL1	grey silt and few fine sand with single pebbles and organic lenses (50x50 mm), horizontal lens-like to coarse lens-like (1 to >1 mm thick and 10 to 50 mm long)	1	16	35.0	53.9
L14-09-OSL1 gamma (frozen)	see L14-09-OSL1	1	16		
L14-09-OSL1 gamma (unfrozen)	see L14-09-OSL1	1	16		
L14-09-OSL1 gamma (ice)	ice-rich material sampled directly below L14-09-OSL1	1	16		
L14-09-OSL2	see L14-09-OSL1	1	16	32.5	48.2
L14-09-OSL2 gamma (frozen)	see L14-09-OSL1	1	16		
L14-09-OSL3	see L14-09-OSL1	1	16	35.1	54.1
Profile L14-08 / Molotkov (Yedoma) IC on thermo terrace (L14-02, L7-18 reference)					
N 73°20,170', E 141°19,600', H 26m, A 5m (wall bottom) / N 73°20,172', E 141°19,622', H 29m, A 4m (wall top)					
01.08.2014					
L14-08-OSL1	light brown-greyish silt and few fine sand with fine grass roots clustered in several areas and single dark-brown organic spots (10x10 mm), fine lens-like (<1 mm thick and 2 to 10 mm long) in different pattern (mainly horizontal partly reticulated, partly ataxic) or massive	1.5	23.5	22.7	29.4
L14-08-OSL1 gamma (frozen)	see L14-08-OSL1	1.5	23.5		
L14-08-OSL2	see L14-08-OSL1	1.5	23.5	27.8	38.5

Sample	Description	Depth	Height	Wet-based ice content [wt%]	Dry-based ice content [wt%]
		[m b.s.]	[m a.s.l.]		
L14-08-OSL2 gamma (frozen)	see L14-08-OSL1	1.5	23.5		
L14-08-BK8	see L14-08-OSL1	2	23		
Profile L14-13 / Molotkov (Yedoma) IW below thermo terrace					
N 73°19,948', E 141°20,334', H 11m, A 6m (wall top) 17.08.2014					
L14-13 36Cl A	syngenetic ice-wedge ice	1			
L14-13 36Cl B	syngenetic ice-wedge ice	1			
L14-13 36Cl C	syngenetic ice-wedge ice	1			
Profile L14-07 / Sartan IC at Zimov'e River mouth (L7-07 reference)					
N 73°19,857', E 141°20,674', H 1m, A 5m (beach) / N 73°19,862', E 141°20,705', H 12m, A 5m (wall top) 30.07., 31.07. and 17.08.2014					
L14-07-OSL1	light brown silt with few grass-roots and organic lenses, fine horizontal and subhorizontal cryostructure (<1mm thick and 2 to 5 mm long) between ice bands (every 5 to 10 cm) which were oriented towards the ice wedge. In places, single vertical ice veins (1 to 2 mm thick and 50 to 100 mm long).	1.5	7.5	21.7	27.7
L14-07-OSL1 gamma (frozen)	see L14-07-OSL1	1.5	7.5		
L14-07-OSL2	see L14-07-OSL1	1.5	7.5	29.3	41.5
L14-07-BK1	see L14-07-OSL1	1.5	7.5	32.9	49.0
L14-07-14C	fresh(greenish) peat	2	7		
L14-07-bone#1, #2, #3	<i>in-situ</i> bone fragments	2	7		
L14-07 36Cl	syngenetic ice-wedge ice	2	7		
L14-07 DOC	syngenetic ice-wedge ice	2	7		
L14-07-PG1	brown peat in a silty grey reddish spotted matrix	2.3	6.7		

Sample	Description	Depth [m b.s.]	Height [m a.s.l.]	Wet-based ice content [wt%]	Dry-based ice content [wt%]
L14-07-BK2	with numerous coarse plant remains, fine lens-like cryostructure with horizontal and subhorizontal single lenses (<1mm thick and 2 to 5 mm long) see L14-07-PG1	2.5	6.5	44.8	81.2

Profile L14-15 / Modern floodplain of Zimov'e River
N 73°19,986', E 141°22,043', H 2m, A 5m (floodplain surface)
14.08.2014

L14-15-OSL1	unfrozen, alternations of light brown, grey-brown, and dark grey silt layers and yellowish sand and pebble layers, black organic bands, fine roots concentrated at surface	0.05		24.5	32.4
L14-15-OSL1 gamma (unfrozen)	see L14-15-OSL1	0.05			
L14-15-OSL1 gamma (ref)	see L14-15-OSL1	0-0.1			

Profile L14-16 / Modern floodplain of Zimov'e River
N 73°19,991', E 141°22,070', H -4m, A 2m (floodplain surface)
14.08.2014

L14-16-OSL1	unfrozen, alternations of grey silt layers with yellowish-brown, orange sand layers, black organic bands	0.1		28.4	39.6
L14-16-OSL1 gamma (unfrozen)	see L14-16-OSL1	0.1			
L14-16-OSL2	see L14-16-OSL1	0.15			
L14-16-OSL2 gamma (unfrozen)	see L14-16-OSL1	0.15			

Surface samples L14-rock and mineral soil
14.08.2014

Sample	Description	Depth	Height	Wet-based ice content	Dry-based ice content
		[m b.s.]	[m a.s.l.]	[wt%]	[wt%]
1-Beach	hand piece	N 73°20.277'	E 141°18.028'		
2-Beach	hand piece	N 73°20.233'	E 141°18.259'		
3-Beach	hand piece	N 73°20.172'	E 141°18.648'		
4-Beach	hand piece	N 73°20.145'	E 141°18.827'		
5-Beach	hand piece	N 73°20.277'	E 141°18.028'		
6-Beach	hand piece	N 73°20.233'	E 141°18.259'		
7-Beach	hand piece	N 73°20.172'	E 141°18.648'		
8-Beach	hand piece	N 73°20.145'	E 141°18.827'		
9-Beach	hand piece	N 73°20.277'	E 141°18.028'		
1-Yukagir	mineral soil	N 73°20.080'	E 141°19.277'		
2-Yukagir	mineral soil	N 73°20.080'	E 141°19.277'		
1-Zimov'e	pebble strata	N 73°20.429'	E 141°17.096'		
2-Zimov'e	modern floodplain	N 73°19.849'	E 141°22.755'		

Appendix 5-1

Surface samples for soil organic matter studies. Sample depths are given in cm below soil surface (b.s.s.).

#	GPS	Day of sampling	Sample	Sub-sample	Depth		Description
					upper	lower	
Yedoma Ice Complex							
Vegetation ^{a)} : <i>Peltigera aphthosa</i> , <i>Thamnolia vermicularis</i> , <i>Dactylina arctica</i> , <i>Calliergon</i> sp., <i>Carex</i> sp., <i>Saxifraga</i> sp., <i>Salix</i> sp., <i>Betula nana</i> , <i>Eriophorum scheuchzeri</i> , <i>Dryas punctata</i> , <i>Alopecurus alpinus</i> , <i>Novosiversia glacialis</i> , <i>Arenaria serpyllifolia</i>							
1	N 73°20.174' E 141°19.646'	30.07.14	JW14 BL1	P1	0	10	Dark brownish silt, loosely packed, many roots
				P2	10	20	Dark brownish silt, soil loosely packed, many roots, below 14 cm increased amounts of organic inclusions (plant and/ or moss fibers/roots) signs of cryoturbation
				P3	20	28	Greyish-brown silt with some clay, few roots, weakly developed gleyic/stagnic properties, scattered Fe-oxide mottles, signs of cryoturbation
				P4	30	34	Brownish-grey silt with some clay, clearly developed gleyic/stagnic properties, signs of cryoturbation
2	N 73°20.179' E 141°19.644'	30.07.14	JW14 BL2	P1	0	10	Dark brownish silt, soil loosely packed, many roots
				P2	10	20	Dark brownish silt, many roots, soil loosely packed, increased amounts of organic inclusions (plant and/ or moss fibers/roots) signs of cryoturbation
				P3	20	30	Greyish-brown silt, fine roots common, signs of cryoturbation
				P4	30	37	Grey silt with some clay, few fine roots, reducing conditions, pit filling with water
3	N 73°20.174' E 141°19.646'	30.07.14	Soil-2014-A	0-0.1	0	10	See JW14 BL1 P1
				0.1-0.2	10	20	See JW14 BL1 P2
				0.2-0.3	20	28	See JW14 BL1 P3
				0.3-0.4	30	34	See JW14 BL1 P4

#	GPS	Day of sampling	Sample	Sub-sample	Depth		Description
					upper	lower	
					[cm b.s.s.]		
4	N 73°20.179' E 141°19.644'	30.07.14	Soil-2014-B	0-0.1	0	10	See JW14 BL2 P1
				0.1-0.2	10	20	See JW14 BL2 P2
				0.2-0.3	20	30	See JW14 BL2 P3
				0.3-0.4	30	37	See JW14 BL2 P4
5	N 73°20.169' E 141°19.667'	17.08.14	JW14 BL22	P1	1	5	Dark blackish heavily decomposed plant/moss material, many roots
				P2	15	25	Brownish silt with greyish mottles, many roots
				P3	50	55	Greyish silt with brownish-orange mottles, some roots

Thermo-erosional valley / Log deposits

Vegetation^{a)}: *Peltigera aphthosa*, *Thamnia vermicularis*, *Dactylina arctica*, *Calliergon* sp., *Sphagnum* sp., *Carex* sp., *Saxifraga* sp., *Salix* sp., *Eriophorum scheuchzeri*, *Dryas punctata*, *Caltha palustris*, *Alopecurus alpinus*

6	N 73°20.137' E 141°19.812'	03.08.14	JW14 BL13	P1.1	0	10	Brownish silt with very little clay, many roots
				P1.2	10	40	Brownish silt with greyish mottles, orange mottles near roots
7	N 73°20.145' E 141°19.849'	03.08.14	JW14 BL13	P2.1	0	10	Brownish silt with very little clay, many roots
				P.2	10	40	Brownish silt with greyish mottles, orange mottles near roots
8	N 73°20.151' E 141°19.882'	03.08.14	JW14 BL13	P3	0	25	Brownish silt loam, some roots
9	N 73°20.158' E 141°19.920'	03.08.14	JW14 BL13	P4.1	0	10	Brownish silt with some clay, some accumulation of organic matter
				P4.2	10	25	Grey silt with orange mottles near roots
10	N 73°20.165' E 141°19.959'	03.08.14	JW14 BL13	P5.1	6	18	Light brownish moderately decomposed plant material, many roots, water-saturated
				P5.2	18	22	Grey silt, no roots, reducing conditions, water-saturated
11	N 73°20.151' E 141°19.882'	12.08.14	JW14 BL16	SB	3	8	See JW14 BL13 P3
12	N 73°20.027 E 141°20.251	15.08.14	JW14 BL18	AK1	-2	0	Sphagnum moss
				AK2	-2	0	Sphagnum moss

#	GPS	Day of sampling	Sample	Sub-sample	Depth		Description
					upper	lower	
Thermo-cirque							
Vegetation ^{a)} : <i>Peltigera aphthosa</i> , <i>Thamnolia vermicularis</i> , <i>Dactylina arctica</i> , <i>Calliergon</i> sp., <i>Carex</i> sp., <i>Saxifraga</i> sp., <i>Salix</i> sp., <i>Eriophorum scheuchzeri</i> , <i>Dryas punctata</i> , <i>Alopecurus alpinus</i>							
13	N 73°20.210' E 141°19.388'	01.08.14	JW14 BL3	P1	5	15	Brownish silt with some clay, many fine roots, very dry
				P2	40	100	Brownish silt with some clay, weak mottling
13	N 73°20.210' E 141°19.388'	01.08.14	JW14 BL3	P3	150	160	Blackish-grey silt with fine sand, scattered orange mottles, few fine roots, scattered plant macro rests, horizontal to sub-horizontal slightly waved ice lenses (3 mm thick, 2 cm long), prominent ice veins above and below sample depth
14	N 73°20.193' E 141°19.408'	01.08.14	JW14 BL4	P1	10	20	Brownish-grey silt, scattered dark brown peaty lenses, many fine roots
				P2	120	130	Greyish silt matrix with scattered brownish peaty lenses, ice cemented, above and below sample depth prominent ice veins
15	N 73°20.159' E 141°19.430'	01.08.14	JW14 BL5	P1	25	35	Brownish silt, may fine roots, very dry
				P2	315	325	Greyish-brown silt loam, some fine roots, ice cement with few randomly scattered horizontal ice lenses (1 mm thick, 3 cm long), plant macro rest, scattered mottles of dark blackish organic rich material

#	GPS	Day of sampling	Sample	Sub-sample	Depth		Description
					upper	lower	
					[cm b.s.s.]		
16	N 73°20.117' E 141°19.465'	01.08.14	JW14 BL6	P1	25	35	Dark greyish-brown silt, some orange mottles, many roots, scattered pebbles at lower boundary
				P2	115	125	Greenish-grey silt, some fine roots, ice cemented, prominent ice vein below sample depth
17	N 73°20.830' E 141°19.464'	01.08.14	JW14 BL7	P1	15	25	Brownish-grey silt, few fine roots, some dark blackish peaty lenses
				P2	105	115	Greyish silt with orange mottles, few fine roots, ice cemented with few scattered very fine ice lenses
18	N 73°20.147' E 141°19.651'	02.08.14	JW14 BL8	P1	4	15	Brownish silt loam, many roots
				P2	23	33	Greyish silt with orange mottles near roots, scattered peaty lenses
19	N 73°20.143' E 141°19.644'	02.08.14	JW14 BL9	P1	15	25	Greenish-brown silt loam, mottles of greyish silt, scattered peaty lenses, many roots
				P2	40	45	Greyish silt with orange mottles, few roots
20	N 73°20.132' E 141°19.631'	02.08.14	JW14 BL10	P1	10	20	Greenish-brown silt with some clay, many roots, weakly developed orange mottles, few scattered peaty lenses
21	N 73°20.119' E 141°19.611'	02.08.14	JW14 BL11	P1	10	20	Brownish silt, loosely packed, some peaty lenses, some roots, weakly developed orange mottles
				P2	40	50	Greyish silt with orange mottles, few roots
22	N 73°20.100' E 141°19.594'	02.08.14	JW14 BL12	P1	10	35	Brownish silt loam, many roots, weakly developed orange mottles
				P2	50	55	Greenish-brown silt loam with orange mottles, few roots
23	N 73°20.105' E 141°19.942'	02.08.14	JW14 BL19	P1	15	25	Light greyish-brown silt, weakly developed mottles, many roots
				P2	95	100	Greyish silt with some clay, scattered spots of blackish organic material

#	GPS	Day of sampling	Sample	Sub-sample	Depth		Description
					upper	lower	
				P3	135	145	Similar to JW14BL19 P2, but frozen and fewer blackish spots
24	N 73°20.103' E 141°19.916'	02.08.14	JW14 BL20	P1	20	45	Greyish silt, few roots, some scattered blackish organic material
				P2	80	100	Similar to JW14 BL20 P1 but frozen
25	N 73°20.111' E 141°19.872'	02.08.14	JW14 BL21	P1	15	30	Greyish silt, few roots, some scattered blackish organic material
				P2	105	120	Similar to JW14 BL21 P1 but frozen
26	N 73°20.60' E 141°19.471'	02.08.14	JW14 BL23	P1	0	15	Greyish silt, water saturated

Alas

Vegetation^{a)}: *Peltigera aphthosa*, *Thamnolia vermicularis*, *Dactylina arctica*, *Calliergon* sp., *Sphagnum* sp., *Carex* sp., *Salix* sp., *Eriophorum scheuchzeri*, *Dryas punctata*, *Alopecurus alpinus*, *Ranunculus glacialis*

27	N 73°21.153' E 141°14.806'	11.08.14	JW14 BL15	P1	0	3	Dark blackish moderately decomposed mosses and plant material, many plant fibers and roots present, signs of cryoturbation
				P2	3	8	Brownish silt loam, few plant fibers or fine roots present, signs of cryoturbation
				P3	8	13	Greyish-brown silt loam, stagnic conditions, few plant fibers or fine roots present, signs of cryoturbation
28	N 73°21.153' E 141°14.806'	11.08.14	JW14 BL15	SB			see JW14 BL15 P3
29	N 73°20.865' E 141°15.525'	11.08.14	JW14 BL16	P1	-2	0	Green Sphagnum mosses
				P2	0	16	Light brownish moderately decomposed mosses. water-saturated
				P3	16	31	Dark brownish silt loam with a lot of plant fibers and roots present, water-saturated, reducing conditions

#	GPS	Day of sampling	Sample	Sub-sample	Depth		Description
					upper	lower	
Floodplain deposits							
Vegetation ^{a)} : <i>Peltigera aphthosa</i> , <i>Thamnolia vermicularis</i> , <i>Dactylina arctica</i> , <i>Calliergon</i> sp., <i>Sphagnum</i> sp., <i>Carex</i> sp., <i>Salix</i> sp., <i>Betula nana</i> , <i>Eriophorum scheuchzeri</i> , <i>Dryas punctata</i> , <i>Alopecurus alpinus</i>							
30	N 73°19.849' E 141°22.755'	10.08.14	JW14 BL14	P1	90	110	Layered deposits with alternating light sandy and darker colored silty layers with interbedded organic material (mostly fragments of drift wood). Layer thicknesses varied between a few mm to 2-3 cm, thicker layers sometimes showed finer layering within
				P2	140	150	
31	N 73°19.848' E 141°22.770'	12.08.14	JW14 BL17	P1	10	20	Brownish silt loam, many roots, mottling
				P2	30	40	Greyish silt loam, roots common, mottling, signs of cryoturbation

a) Not a complete vegetation survey

Appendix 7-1

Geophysical datasets acquired at site Zimov'e River mouth.

Location, Profile	Method	Frequency	Acquisition Date
A1 (2 x 290 m)	GPR	50, 100, 200 MHz	05.04.14
	EMI	1, 4, 16 kHz	05.04.14
A2 (280 m)	GPR	100 MHz	22.04.14
A3 (50 m)	GPR	100 MHz	22.04.14
CMP (max. offset 16 m)	GPR	100, 200 MHz	06.04.14
B1 (2 x 180 m)	GPR	100, 200 MHz	30.07.14
	EMI	1, 4, 12, 16 kHz	31.07.14
B2 (50 m)	ERT		31.07.14
	TDR		31.07.14

Appendix 7-2

Geophysical datasets acquired at survey site thermo terrace.

Location, Profile	Method	Frequency	Acquisition Date
A1 (23 x 42 m)	GPR	100 MHz	09.-13.04.14, 18.04.14
CMP (max. offset 22 m)	GPR	100 MHz	20.04.14

Appendix 7-3

Geophysical datasets that were acquired at survey site Yedomá.

Location, Profile	Method	Frequency	Acquisition Date
A1 (25 m x 41 m)	GPR	100 MHz	14.-16.04.14
A2 (9 m x 16 m)	GPR	200 MHz	21.04.14
CMP (max. offset >10 m)	GPR	100 MHz	20.04.14
A3 (10 m x 45 m)	EMI	1, 4, 12 kHz	21.04.14
B1 (19 m x 48 m)	GPR	100 MHz	01.-02.08.14
B2 (8 m x 11 m)	GPR	200 MHz	05.08.14
	ERT		04.-05.08.14
	TDR		04.08.14
	TDR		05.08.14
B3 (49 m)	TDR		06.08.14
	ERT		03.-04.08.14
	TDR		04.08.14
B4 (37 m)	ERT		06.08.14
	TDR		05.08.14
B5 (37 m)	ERT		03.08.14
	GPR	200 MHz	05.08.14

	TDR	04.08.14
	TDR	05.08.14
	TDR	06.08.14

Appendix 7-4

Geophysical datasets acquired at survey site thermo-erosional valley.

Location, Profile	Method	Frequency	Acquisition Date
B1 (44 m x 24 m)	GPR	200 MHz	07.-08.08.14
CMP (max. offset 8 m)	GPR	200 MHz	03.08.14
B2 (100 m x 75 m)	EM	12 kHz	04.08.14
B3 (24 m)	ERT		09.08.14
B4 (37 m)	ERT		10.08.14
B5 (37 m)	ERT		10.08.14

Appendix 7-5

Geophysical datasets acquired at survey site Alas.

Location, Profile	Method	Frequency	Acquisition Date
A1 (397 m)	GPR	100 MHz	19.04.14
A2 (270 m)	GPR	100 MHz	19.04.14
A3 (287 m)	GPR	100 MHz	19.04.14
CMP (max. offset 8 m)	GPR	100 MHz	19.04.14
B1 (25 x 26 m)	GPR	200 MHz	11.-12.08.14
CMP (max. offset 8 m)	GPR	200 MHz	12.08.14
B2 (37 m)	ERT		13.08.14
	TDR		13.08.14

Die **Berichte zur Polar- und Meeresforschung** (ISSN 1866-3192) werden beginnend mit dem Band 569 (2008) als Open-Access-Publikation herausgegeben. Ein Verzeichnis aller Bände einschließlich der Druckausgaben (ISSN 1618-3193, Band 377-568, von 2000 bis 2008) sowie der früheren **Berichte zur Polarforschung** (ISSN 0176-5027, Band 1-376, von 1981 bis 2000) befindet sich im electronic Publication Information Center (**ePIC**) des Alfred-Wegener-Instituts, Helmholtz-Zentrum für Polar- und Meeresforschung (AWI); see <http://epic.awi.de>. Durch Auswahl "Reports on Polar- and Marine Research" (via "browse"/"type") wird eine Liste der Publikationen, sortiert nach Bandnummer, innerhalb der absteigenden chronologischen Reihenfolge der Jahrgänge mit Verweis auf das jeweilige pdf-Symbol zum Herunterladen angezeigt.

The **Reports on Polar and Marine Research** (ISSN 1866-3192) are available as open access publications since 2008. A table of all volumes including the printed issues (ISSN 1618-3193, Vol. 1-376, from 2000 until 2008), as well as the earlier **Reports on Polar Research** (ISSN 0176-5027, Vol. 1-376, from 1981 until 2000) is provided by the electronic Publication Information Center (**ePIC**) of the Alfred Wegener Institute, Helmholtz Centre for Polar and Marine Research (AWI); see URL <http://epic.awi.de>. To generate a list of all Reports, use the URL <http://epic.awi.de> and select "browse"/ "type" to browse "Reports on Polar and Marine Research". A chronological list in declining order will be presented, and pdf icons displayed for downloading.

Zuletzt erschienene Ausgaben:

Recently published issues:

- 686 (2015)** Russian-German Cooperation CARBOPERM: Field campaigns to Bol'shoy Lyakhovsky Island in 2014, edited by Georg Schwamborn and Sebastian Wetterich
- 685 (2015)** The Expedition PS86 of the Research Vessel POLARSTERN to the Arctic Ocean in 2014, edited by Antje Boetius
- 684 (2015)** Russian-German Cooperation SYSTEM LAPTEV SEA: The Expedition Lena 2012, edited by Thomas Opel
- 683 (2014)** The Expedition PS83 of the Research Vessel POLARSTERN to the Atlantic Ocean in 2014, edited by Hartwig Deneke
- 682 (2014)** Handschriftliche Bemerkungen in Alfred Wegeners Exemplar von: Die Entstehung der Kontinente und Ozeane, 1. Auflage 1915, herausgegeben von Reinhard A. Krause
- 681 (2014)** Und sie bewegen sich doch ...Alfred Wegener (1880 – 1930): 100 Jahre Theorie der Kontinentverschiebung – eine Reflexion, von Reinhard A. Krause
- 680 (2014)** The Expedition PS82 of the Research Vessel POLARSTERN to the southern Weddell Sea in 2013/2014, edited by Rainer Knust and Michael Schröder
- 679 (2014)** The Expedition of the Research Vessel 'Polarstern' to the Antarctic in 2013 (ANT-XXIX/6), edited by Peter Lemke
- 678 (2014)** Effects of cold glacier ice crystal anisotropy on seismic data, by Anja Diez
- 677 (2014)** The Expedition of the Research Vessel "Sonne" to the Mozambique Ridge in 2014 (SO232), edited by Gabriele Uenzelmann-Neben
- 676 (2014)** The Expedition of the Research Vessel "Sonne" to the Mozambique Basin in 2014 (SO230), edited by Wilfried Jokat



ALFRED-WEGENER-INSTITUT
HELMHOLTZ-ZENTRUM FÜR POLAR-
UND MEERESFORSCHUNG

BREMERHAVEN

Am Handelshafen 12
27570 Bremerhaven
Telefon 0471 4831-0
Telefax 0471 4831-1149
www.awi.de

